AN ABSTRACT OF THE DISSERTATION OF

Xiangming Wu for the degree of Doctor of Philosophy in Chemical Engineering
presented on February 26, 2014.

Title: Molecular Origins of Peptide Entrapment in Polyethylene Oxide Layers

Abstract approved:

_____

Joseph McGuire Karl F. Schilke

A more quantitative understanding of peptide entrapment and elution from otherwise protein-repellent polyethylene oxide (PEO) brush layers will provide direction for development of new strategies for drug storage and delivery. Here we describe criteria for peptide integration and structural change within the PEO brush, and discuss the reversibility of peptide entrapment with changing solvent conditions. For this purpose, three cationic peptides were used: the arginine-rich amphiphilic peptide WLBU2, the chemically identical but scrambled peptide S-WLBU2, and the non-amphiphilic homopolymer poly-*L*-arginine (PLR). Circular dichroism (CD) was used to record the adsorption and conformational changes of (amphiphilic) WLBU2 and S-WLBU2, and (non-amphiphilic) polyarginine peptides, at uncoated (hydrophobic) and PEO-coated silica nanoparticles. UV spectroscopy and a quartz crystal microbalance with dissipation monitoring (QCM-D) were used to quantify changes in the extent of peptide elution. Peptide conformation was controlled between disordered and α-helical forms by varying the concentration of perchlorate ion. We show an initially more ordered (α-helical) structure promotes peptide adsorption into the PEO layer. Further, a partially helical

peptide undergoes an increase in helicity after entry, likely due to concomitant loss of capacity for peptide-solvent hydrogen bonding. Peptide interaction with the PEO chains resulted in entrapment and conformational change that was irreversible to elution with changing solution conditions in the case of the amphiphilic peptide. In contrast, the adsorption and conformational change of the non-amphiphilic peptide was reversible. We also evaluated the effects of peptide surface density on the conformational changes caused by peptide-peptide interactions, and using CD, QCM-D, and UV spectroscopy, showed that these phenomena substantially affect the rate and extent of peptide elution from PEO brush layers. Specifically, for amphiphilic peptides at sufficiently high surface density, peptide-peptide interactions result in conformational changes which compromise their resistance to elution. In contrast, elution of a non-amphiphilic peptide is substantially independent of its surface density, presumably due to the absence of peptide-peptide interactions.

The sequential and competitive adsorption behavior of WLBU2, S-WLBU2 and PLR at pendant PEO layers was studied by optical waveguide lightmode spectroscopy (OWLS), time-of-flight secondary ion mass spectrometry (TOF-SIMS), CD and UV spectroscopy. Results strongly indicate that amphiphilic peptides are able to displace non-amphiphilic peptides that are adsorbed in PEO layers, while non-amphiphilic peptides cannot displace amphiphilic ones. In summary, peptides of high amphiphilicity are expected to dominate the competitive adsorption with less amphiphilic peptides in PEO layers.

Molecular Origins of Peptide Entrapment in Polyethylene Oxide Layers

by

Xiangming Wu

A DISSERTATION

submitted to

Oregon State University

in partial fulfillment of
the requirements for the
degree of

Doctor of Philosophy

Presented February 26, 2014

Commencement June 2014

Doctor of Philosophy dissertation of Xiangming Wu presented on February 26, 2014

APPROVED:

_____

Co-Major Professor, representing Chemical Engineering

_____

Co-Major Professor, representing Chemical Engineering

_____

Head of the School of Chemical, Biological, and Environmental Engineering

_____

Dean of the Graduate School

I understand that my dissertation will become part of the permanent collection of Oregon State University libraries. My signature below authorizes release of my dissertation to any reader upon request.

_____

Xiangming Wu, Author

ACKNOWLEDGMENTS

I would like to express my appreciation to all the people who contributed to the successful completion of this dissertation. My advisors, Dr. Joseph McGuire and Dr. Karl Schilke, deserve a very special acknowledgement for their guidance during this research. When I joined OSU in fall 2011, I found Joe's research was most closely related to my background in the department and I was so glad that he accepted me as a graduate student. In the past two and half years, Joe always supported, encouraged and made every effort to help me on every problem I ran into. To me, he is more like family. Dr. Schilke, aka rat, served as an encyclopedia during the entire course of my research. When there is a questions about experiment, there is an answer in that encyclopedia. It is my honor to work with both of them.

I am thankful to my committee members, Dr. Kerry McPhail, Dr. Victor Hsu and Dr. Claudia Maier for all the valuable discussion about my research and for their patience in reviewing the dissertation.

My sincere thanks to Matt Ryder, Greg McKelvey, Gershon Starr, Fallon Fumasi, Dan Cheung, Will Denton, Miranda Raper and Ashaen Patel in the McGuire and Schilke Lab. They provided tremendous help on this work. It was always a great time working with them and I am sure I will miss that.

I would like to express my deepest gratitude towards my wife Ying Zhang for her love, encouragement and unconditional support on every decision I made. She is also currently a graduate student in OSU and I always benefited from her strong bioanalytical

background. It was her experience on circular dichroism helped me to quickly start up my research. In addition, I cannot remember how many times she smiled lovely and said “You know what, I have used that before”, after telling her what instrument I would be using for the next step of my research. I love you so much.

Finally, I would like to thank my parents, whose infinite love and moral support made it possible for me to complete my study in OSU.

CONTRIBUTION OF AUTHORS

Portions of the text and figures in chapter 1 were developed by Matt Ryder, whom I collaborated with extensively during my tenure here at Oregon State University, and whose contributions appear in chapters 2 and 3 primarily through his work and analysis of quartz crystal microbalance with dissipation monitoring (QCM-D) and time-of-flight secondary ion mass spectrometry (TOF-SIMS).

TABLE OF CONTENTS

TABLE OF CONTENTS (Continued)

LIST OF FIGURES

LIST OF FIGURES (Continued)

LIST OF APPENDIX FIGURES

LIST OF APPENDIX FIGURES (Continued)

LIST OF APPENDIX FIGURES (Continued)

LIST OF APPENDIX FIGURES (Continued)

LIST OF APPENDIX TABLES

DEDICATION

This work is dedicated to our beautiful daughter Reine.

To borrow a phrase:

‘without her help, it would have been written in half the time’!

MOLECULAR ORIGINS OF PEPTIDE ENTRAPMENT IN POLYETHYLENE OXIDE LAYERS

CHAPTER 1

INTRODUCTION

The non-fouling properties of material surfaces presenting pendant PEO chains are well established, and considerable effort continues to be made to improve our quantitative understanding of the protein repellent mechanisms of PEO coatings. On the other hand, there are few reports in the literature comparing the adsorption of proteins of different sizes to a given PEO layer, and even fewer that describe the adsorption of small proteins or synthetic peptides at pendant PEO layers. Despite the fact that the adsorption of sufficiently small proteins to pendant PEO brush layers is predicted theoretically, prior to completing the work described here we had little experimentally-based, quantitative understanding of the adsorption and function of sufficiently small peptides/proteins at otherwise protein-repellent PEO layers.

Better understanding of the mechanisms of peptide "entrapment" within PEO layers is very much needed, as it will provide direction for the storage and controlled release of a variety of bioactive agents from a new array of biocompatible, functional surface coatings. Our overall objective with this research was to begin to quantify the molecular origins of small peptide adsorption and entrapment in surface-bound, pendant PEO layers.

In this dissertation, Chapter 2 describes criteria for integration and structural change of peptides within the PEO brush, and discusses the reversibility of peptide entrapment with changing solvent conditions for amphiphilic and non-amphiphilic motifs. For this

purpose, circular dichroism (CD) was used to record the adsorption and conformational changes of poly-*L*-arginine (PLR) and WLBU2 at bare (hydrophobic) and PEO-coated silica nanoparticles. In order to elucidate the effect of structure on peptide interaction with the PEO brushes, the solution conformation of PLR and WLBU2 peptides was controlled between the disordered and α-helical forms by varying the solution conditions.

Chapter 3 decribes work providing an improved understanding of surface density effects on peptide elution from PEO layers, through discussion of evidence of concentration-dependent, peptide-peptide interactions likely contributing to those effects. The adsorption behavior of three peptides was evaluated for this purpose, including, in addition to WLBU2 and PLR, a peptide chemically identical to WLBU2 but of scrambled sequence (S-WLBU2).

Chapter 4 explores the sequential and competitive adsorption behavior of PLR, WLBU2 and S-WLBU2 at pendant PEO layers. Solution depletion methods and CD were used to evaluate competitive peptide exchange and peptide conformational change at PEO-coated silica nanoparticles. OWLS and TOF-SIMS were used to directly detect peptide sequential and competitive adsorption on covalently-immobilized PEO layers.

The major conclusions made in this overall study are summarized in Chapter 5.

ADSORPTION, STRUCTURAL ALTERATION AND ELUTION OF PEPTIDES AT PENDANT PEO LAYERS

Xiangming Wu, Matthew P. Ryder, Joseph McGuire, Karl F. Schilke

School of Chemical, Biological and Environmental Engineering, Oregon State University, Corvallis, OR 97331

Colloids and Surfaces B: Biointerfaces
http://www.sciencedirect.com/science/journal/09277765
Volume 112, Pages 23-29

CHAPTER 2

ADSORPTION, STRUCTURAL ALTERATION AND ELUTION OF PEPTIDES AT PENDANT PEO LAYERS

Abstract

An experimentally based, quantitative understanding of the entrapment and function of small peptides within PEO brush layers does not currently exist. Earlier work provided a rationale for expecting that an ordered, compact peptide will enter the PEO phase more readily than a peptide of similar size that adopts a less ordered, less compact form, and that amphiphilicity will promote peptide retention within the hydrophobic region of the PEO brush. Here we more deliberately describe criteria for peptide integration and structural change within the PEO brush, and discuss the reversibility of peptide entrapment with changing solvent conditions. For this purpose, circular dichroism (CD) was used to record the adsorption and conformational changes of (amphiphilic) WLBU2 and (non-amphiphilic) polyarginine peptides at uncoated (hydrophobic) and PEO-coated silica nanoparticles. Peptide conformation was controlled between disordered and α-helical forms by varying the concentration of perchlorate ion. We show an initially more ordered (α-helical) structure promotes peptide adsorption into the PEO layer. Further, a partially helical peptide undergoes an increase in helicity after entry, likely due to concomitant loss of capacity for peptide-solvent hydrogen bonding. Peptide interaction with the PEO chains resulted in entrapment and conformational change that was irreversible to elution with changing solution conditions in the case of the amphiphilic peptide. In contrast, the adsorption and conformational change of the non-amphiphilic

peptide was reversible. These results indicate that responsive drug delivery systems based on peptide-loaded PEO layers can be controlled by modulation of solution conditions and peptide amphiphilicity.

Key words: peptide integration; PEO brush; WLBU2; cationic amphiphilic peptides (CAPs); polyarginine; circular dichroism (CD)

2.1. Introduction

In an earlier paper, we suggested the potential for surface coatings based on entrapment of bioactive agents into PEO brush layers for short-term medical device applications [1]. In particular, strategies featuring drug-loaded but otherwise nonfouling coatings for blood contact hold promise for enhancing the performance of medical devices, ranging from anti-infective catheters to hemoperfusion modules with microscale flow features. Lampi et al. [1] used optical waveguide lightmode spectroscopy (OWLS) to describe the adsorption of poly-*L*-glutamic acid and the cationic amphiphilic peptide WLBU2 at polyethylene oxide (PEO) brush layers. Circular dichroism (CD) was also used to describe the structures of poly-*L*-lysine and WLBU2 at solid, hydrophobic surfaces, and in the PEO brush. The solution structure of each peptide was controlled between disordered and more ordered (α-helical) forms by varying the salt concentration in the peptide solutions. Although protein adsorption at sparse PEO brush layers is predicted and observed in practice [2-4], an experimentally based, quantitative understanding of the adsorption and function of small peptides at PEO brush layers does not currently exist. The results of our previous work [1] provide a rationale for expecting that a more ordered and compact (e.g. α-helical) peptide will enter the PEO phase more readily than a peptide of similar size that adopts a less ordered, less compact form. Furthermore, because a hydrophobic inner core is predicted to exist in PEO brushes [5], it is expected that amphiphilicity will promote the retention of peptides within this region of the PEO brush.

WLBU2 (RRWVRRVRRWVRRVVRVVRRWVRR) is an engineered, 24-residue cationic amphiphilic peptide (CAP), with 13 positively charged arginine residues, and 11

nonpolar valine or tryptophan residues. It shows substantial promise for clinical applications, due to its wide spectrum antimicrobial activity against both Gram-negative and Gram-positive bacteria under physiological conditions. Segregation of the positively-charged Arg and hydrophobic Val/Trp groups onto opposing faces of an α-helix confers the ability to disrupt bacterial cell membranes, even when immobilized [6-12]. While the hydrophobic residues in WLBU2 make it a highly amphiphilic peptide, poly-*L*-arginine (PLR) is chemically homogeneous and not amphiphilic, and thus serves as an excellent control for the effects of amphiphilicity on peptide adsorption and entrapment in PEO brush layers. When dissolved in water under neutral pH, PLR adopts a combination of random and extended (e.g. polyproline-II and 2.51 helix) structures, while WLBU2 shows little appreciable stable structure [1, 6-9, 13-17]. However, in the presence of perchlorate ion (ClO_4^-), both peptides will adopt a rigid α-helical structure [16].

In this paper, we more deliberately describe criteria for integration and structural changes of peptides within the PEO brush, and discuss the reversibility of peptide entrapment with changing solvent conditions for amphiphilic and non-amphiphilic motifs. For this purpose, circular dichroism (CD) was used to record the adsorption and conformational changes of PLR and WLBU2 at bare (hydrophobic) and PEO-coated silica nanoparticles. In order to elucidate the effect of structure on peptide interaction with the PEO brushes, the solution conformation of PLR and WLBU2 peptides was controlled between the disordered and α-helical forms by varying the concentration of perchlorate ion.

2.2. Materials and Methods

Peptides and materials. Lyophilized 30-residue average (4.7 kDa, PDI < 1.20) synthetic poly-*L*-arginine hydrochloride (PLR) was purchased from Alamanda Polymers (Huntsville, AL). PLR was dissolved at 5.0 mg/mL in HPLC water, and separated into 1.0 mL aliquots that were frozen and thawed prior to each experiment. The 5.0 mg/mL PLR stock was diluted to 0.2 mg/mL in HPLC water, or with 0.05 M or 0.5 M perchloric acid ($HClO_4$), to invoke either disordered or helical conformations, respectively. Similarly, lyophilized WLBU2 (3.4 kDa) was purchased from GenScript (Piscataway, NJ), and dissolved at 5 mg/mL in HPLC water and frozen in 1 mL aliquots. The WLBU2 stock solution was thawed prior to use, and diluted to 0.2 mg/mL in HPLC water, or with 0.2 M or 0.5 M $HClO_4$. All peptides were used as supplied, without further purification. Diluted peptide solutions were degassed for 40 min under vacuum immediately before use.

Self-assembled PEO brush layers were formed by suspension of hydrophobic silica nanoparticles (R816, Degussa, 190 m^2/g, 10-12 nm) in Pluronic® F108 (BASF) in HPLC water for 10 h on a rotator. About 3.3 mg/m^2 of F108 are required for complete surface coverage [18]; a 5x excess of F108 over this amount was used to ensure good coverage of the silica nanoparticles. Uncoated and F108-coated nanoparticles were then incubated with PLR or WLBU2 at 0.2 mg/mL under different solvent conditions, for a desired period of time (2h to 7 d) at 20 ℃. Nanoparticle concentrations (2 mg/mL and 10mg/mL) were selected based on previous OWLS results [1], and provided either sufficient surface

area for complete adsorption of the peptide, or a 5x excess surface area for adsorption (to minimize peptide-peptide interactions).

Evaluation of peptide secondary structure. Peptide secondary structure in the presence or absence of nanoparticles was evaluated in triplicate by circular dichroism (CD) using a Jasco J-815 spectropolarimeter (Easton, MD) at 25 ℃. The spectra from each of the three replicates for each sample were nearly identical, with only slight (~5%) differences in signal intensity; representative spectra are shown throughout. The instrument was calibrated using 0.6 mg/mL *D*(+)–camphorsulfonic acid. Spectra were recorded in a cylindrical cuvette (0.1 cm pathlength) from 185 to 260 nm in 0.5 nm increments, and 10 scans were averaged in order to increase the signal-to-noise ratio. The 0.2 mg/mL peptide samples prepared as outlined above were filtered (0.20 μm) prior to contact with nanoparticles and recording of CD spectra. Nanoparticles were rinsed by centrifugation (10,000 rpm, 20 min) and removal of the supernatant, after which the pellet was resuspended in water or $HClO_4$ of desired concentrations, and the process repeated a total of three times. All CD spectra were blanked against peptide-free solutions or NP suspensions.

Stabilization of F108 coatings on OWLS waveguides. SiO_2-coated OW2400c OWLS sensors were purchased from MicroVacuum (Budapest, Hungary). Sensors were cleaned using 3% aqueous SDS (30 min) followed by 10 min wash in 5:1:1 mixture of H_2O:HCl:H_2O_2 solution at 80 ℃ for 10 min. After cleaning, surfaces were rinsed with water, and dried under a stream of nitrogen. The sensor surfaces were then modified by vapor deposition of trichlorovinylsilane (TCVS, TCI America, Portland, OR). 200 μL of

TCVS was evaporated at 20 ℃ into a stream of dry nitrogen carrier gas, which was directed over the waveguide surfaces for 4 hrs. The silanized waveguides were then immersed in a solution of 5% w/v Pluronic® F108 in water, and were rotated in solution overnight. After incubation, samples were γ-irradiated with a ^{60}Co source to a total dose of 3 kGy to covalently the F108 to the surface [19, 20]. The irradiated waveguides were rinsed with water, dried with N_2, and stored desiccated under N_2 in the dark until used.

Measurement of the rate and extent of peptide adsorption. Peptide adsorption was measured with an OWLS 210 instrument (MicroVacuum, Budapest, Hungary). A Rheodyne manual sample injector was used to inject sample solutions through a flow loop (~4.0 mL) into the OWLS flow cell. Flow rates were maintained at 50 μL/min for 40 minutes of sample adsorption time, and solution temperature was kept at 20 ℃ by the internal TC heater/cooler unit. Incident angle scans were performed from -5 °to 5 °at a step size of 0.01 °. Both peaks of each of the transverse electric and magnetic modes were measured to determine the relative refractive index of the surface adlayer. OWLS experiments began with a baseline of peptide-free water or perchloric acid, followed by injection of 0.1 mg/mL peptide in either water or perchloric acid, and a subsequent rinse with either perchloric acid or water. A single OWLS experiment was performed for each adsorption/rinse condition. Reproducibility of OWLS measurements is high, typically with less than 5% variation in the plateau adsorbed mass at each adsorption/rinse step [21, 22].

2.2. Results and Discussion

Effect of perchlorate ions on structure of PLR. Polyarginine (PLR) exhibits a "disordered" (polyproline-II) structure in water under pH < 12, and an α-helical structure under pH > 12 [14]. However, pH could not be used in this study to influence peptide structure, as the silica nanoparticles used for CD would be hydrolyzed at basic pH [23]. Instead, perchlorate ions (ClO_4^-) were used to induce the α-helical conformation of PLR [16]. Circular dichroism spectra of PLR show it to be disordered in water, but the peptide becomes more helical with increased concentration of perchloric acid (Figure 2.1, left). This structural change is indicated by the change in the spectrum from a characteristic "random coil" to "α-helix" form, as well as an increase in ellipticity at 222 nm [24-26]. Deconvolution of representative CD spectra with Dichroweb [27, 28] indicate that the helicity of PLR increases from approximately 2% in water to 31% in 0.05 M HClO4, and reaches 61% α-helix in 0.5 M $HClO_4$.

Effect of perchlorate ions on structure of WLBU2. While WLBU2 is almost completely disordered in water [9], it exhibits a high α-helix content in $HClO_4$, increasing from 3% in water to 15% in 0.2 M or 30% in 0.5 M $HClO_4$, respectively (Figure 2.1, right). The lower α-helix content observed for WLBU2, when compared to PLR at equivalent $HClO_4$ concentrations, may be due to the lower arginine content (13 of 24 amino acids) of WLBU2. However, computed "absolute" helicity values are dependent upon the model implemented in the software, and should only be used for comparative purposes [24, 28].

$HClO_4$ concentrations above 0.5 M did not further increase the calculated helicity of either PLR or WLBU2 in an aqueous milieu (data not shown), although WLBU2 is reported to reach 81% α-helix in a membrane-mimetic solvent (20% trifluoroethanol) [9]. No conformational change was observed for either PLR or WLBU2 in aqueous solutions of PEO (data not shown), indicating that peptide conformation is largely unaffected by the presence of free PEO chains. This implies that any structural change observed in the presence of a PEO brush is due to the unusual environment of the brush layer, and cannot be attributed to individual PEO-peptide interactions.

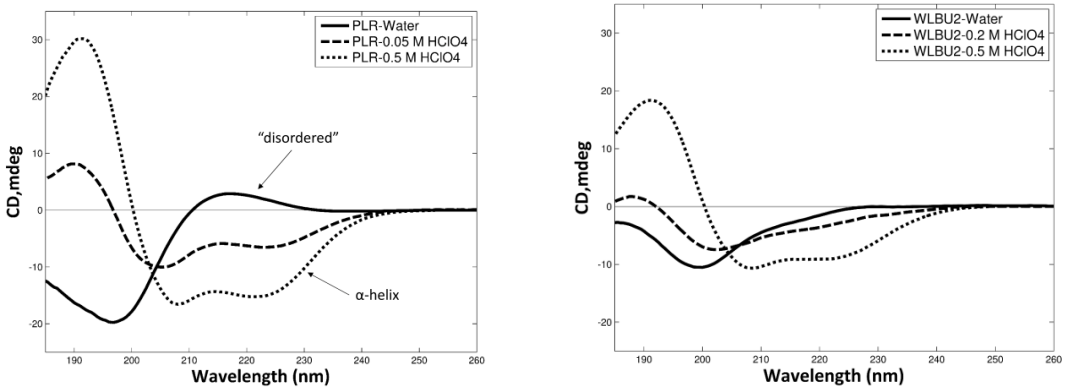

Figure 2.1. CD spectra of PLR (left) in water, 0.05 M $HClO_4$, 0.5 M $HClO_4$ and WLBU2 (right) in water, 0.2 M $HClO_4$, 0.5 M $HClO_4$. Characteristic spectra for peptides in "disordered" (random coil) and α-helix conformations are labeled.

Adsorption of disordered PLR and WLBU2. Both WLBU2 and PLR show substantially disordered structure when dissolved in water (Figure 2.1). Our previous OWLS and CD experiments showed that disordered poly-*L*-lysine (PLL) and WLBU2 have little affinity for F108-coated surfaces [1]. Here, we applied CD to the evaluation of PLR and WLBU2 structure in the presence and absence of uncoated (hydrophobic) and F108-coated

nanoparticles. Spectra recorded for disordered PLR in the presence of uncoated and F108-coated nanoparticles are quite similar (Figure 2.2). The CD signal is greatly decreased after washing the bare or coated nanoparticles one time with water. This result indicates that the disordered peptides do not interact strongly with the nanoparticles, and are easily eluted from bare or F108-coated surfaces. Similar behavior has been observed for disordered PLL at hydrophobic and F108-coated OWLS sensors [1]. Presumably, the large solution volume of the swollen, "disordered" peptide prevents penetration and integration into the PEO brush. Slightly more PLR was retained on the bare nanoparticles, presumably through electrostatic interactions between the positively charged guanidinium groups and negatively charged uncoated nanoparticle surface. However, this interaction with the bare surface is apparently too weak to cause any substantial conformational changes in the PLR [29].

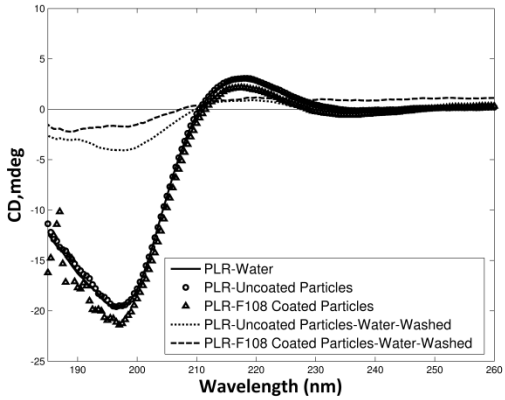

Figure 2.2. CD spectra of PLR in water, and in suspension with uncoated and F108-coated nanoparticles before and after washing.

As with PLR, the “disordered” conformation of WLBU2 in water is similar and independent of the presence or absence of F108-coated nanoparticles. The loss of CD signal indicates that the peptide was almost completely removed after washing with water (Figure 2.3).

However, a substantial conformational difference was observed for WLBU2 in water and in suspension with bare, hydrophobic nanoparticles. Unlike PLR, WLBU2 is amphiphilic and its hydrophobic groups have great affinity for the uncoated hydrophobic surface. We speculate that initial adsorption of the hydrophobic side-chains (which are ordered along one face of the helical form of the amphipathic peptide) favors the formation of a partially α-helical structure on the surface. The CD signal is only partially reduced by washing with water, indicating that a large population of adsorbed and non-elutable peptides remains on the nanoparticles. Figure 2.3 also suggests that the wash preferentially removes loosely-bound “disordered” peptides, as the remaining adsorbed peptides produce a weak yet characteristic α-helical spectrum.

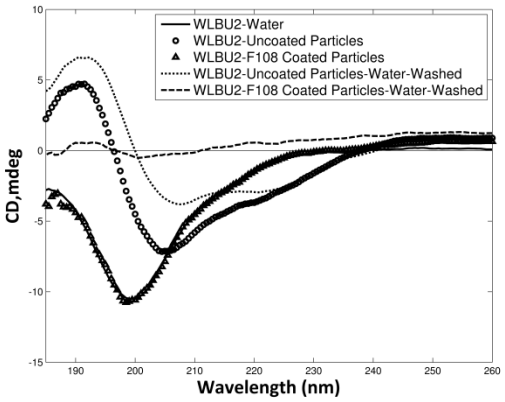

Figure 2.3. CD spectra of WLBU2 in water, and in suspension with uncoated and F108-coated nanoparticles before and after washing.

Adsorption of α-helical PLR and WLBU2. As discussed above, both PLR and WLBU2 are substantially α-helical (61% and 30%) in 0.5M $HClO_4$. The α-helix conformation of PLR in 0.5M $HClO_4$ was mostly independent of the presence of uncoated hydrophobic nanoparticles (Figure 2.4, left). However, the helicity of PLR increased slightly, from 61% to 82%, in the presence of F108-coated nanoparticles. This phenomena is more obvious in Figure 2.4 (right), in which PLR of a lower helicity (31% in 0.05 M $HClO_4$) was added to suspensions of uncoated and F108-coated nanoparticles. Again, no conformational change occurred in the presence of the uncoated nanoparticles, but an increase in helicity (from 31% to 49%) was observed in the presence of the F108-coated nanoparticles. These results suggest that interactions between the peptide and the hydrophobic core of the PEO brush, in which a peptide with a small amount of initial α-helix conformation becomes more helical as a result of contact with the brush. In contrast, a completely disordered peptide is completely excluded from the brush and undergoes no conformational change.

Perchlorate ions stabilize a peptide's α-helical structure by competing with water molecules which would normally solvate the peptide, causing a loss of hydration and promoting the intra-peptide hydrogen-binding characteristic of the α-helix conformation [30]. Theoretical and experimental evidence suggests that a hydrophobic region that is favorable for protein adsorption exists in the interior of a PEO brush [4, 5, 31]. A similar effect is expected when a partially dehydrated, helical peptide penetrates into the hydrophobic inner region of the PEO brush, promoting the peptide's further dehydration and increasing its helicity. Similar conformational changes in response to the

hydrophobic cell membrane are thought to be responsible for PLR's cell-penetrating and cytotoxic properties [32].

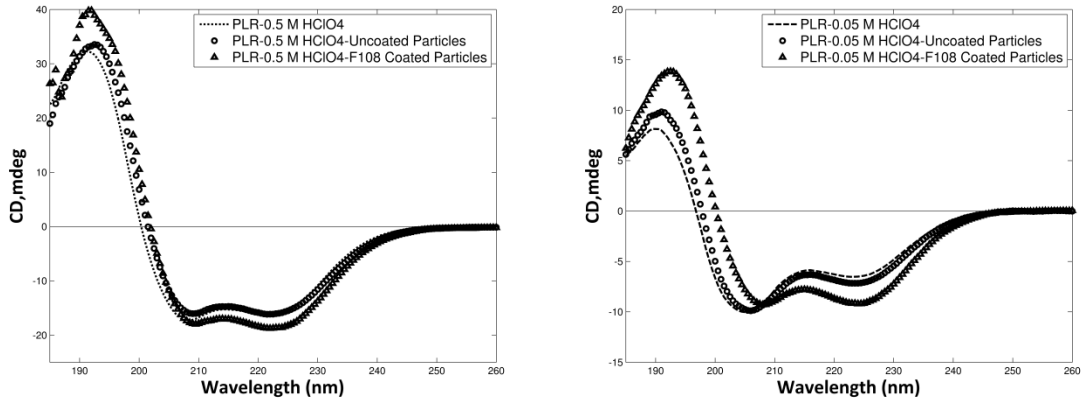

Figure 2.4. CD spectra of: (left) PLR in 0.5 M $HClO_4$, and in suspension with uncoated and F108-coated nanoparticles, (right) PLR in 0.05 M $HClO_4$, and in suspension with uncoated and F108-coated nanoparticles.

Stability of peptides at nanoparticle surfaces. The data presented thus far suggest that an increase in α-helix conformation is associated with integration of the peptides into F108 brushes. If so, these peptides should be more resistant to elution than would peptides which were conformationally changed but merely loosely-bound or unassociated with the brush. Uncoated and F108-coated nanoparticles were incubated with α-helical PLR in 0.5 M $HClO_4$ solution, and then washed twice with 0.5 M $HClO_4$ (maintaining conditions which promote α-helix structure). The partial decrease in CD signal after each wash with 0.5 M $HClO_4$ (Figure 2.5) is consistent with some loss of peptide with each rinse. However, the residual CD signal after washing indicates that considerable α-helical peptide remained on both surfaces after rinsing them with $HClO_4$. Importantly, the

spectra are nearly identical in the presence or absence of F108, suggesting that the interactions of the helical peptide with the hydrophobic surface are closely mimicked by the apolar conditions which are expected to exist within the F108 brush [4, 5].

In contrast, however, when the nanoparticle suspensions were contacted with α-helical PLR in $HClO_4$ and then washed with water, the peptide was nearly completely eluted from both F108-coated and uncoated surfaces (Figure 2.5), although a small residual signal suggests some ordered helical form for the remaining peptides. Remarkably similar behavior was observed for nanoparticles contacted with "disordered" peptides in water (Figure 2.2). The bulk concentration of perchlorate ion would be greatly reduced during washing, thus eliminating the helix-stabilizing microenvironment and allowing the peptide to resume a "disordered" conformation. Taken together, these results suggest that elution of peptides from the F108 brush is at once governed and controllable by bulk solution conditions.

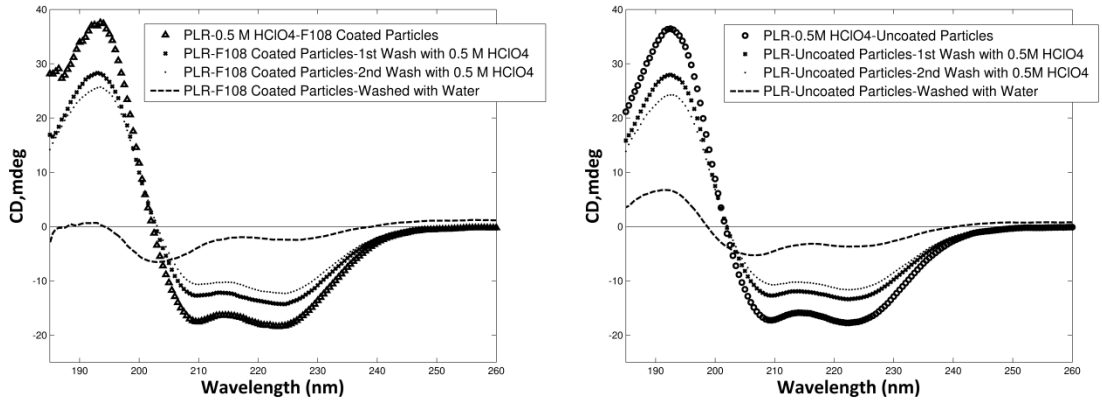

Figure 2.5. CD spectra of: PLR in $HClO_4$, and in suspension with F108-coated (left) and uncoated (right) nanoparticles before and after washing with $HClO_4$ or water.

Optical waveguide lightmode spectroscopy (OWLS). OWLS experiments were carried out to verify that α-helical peptides are stably adsorbed on F108-coated surfaces, and their rate of elution is primarily determined by solution conditions (Figure 2.6). One obvious criticism of the CD experiments is that the F108 is not covalently linked to the nanoparticle surface, and thus some results might be interpreted as competitive displacement of the triblocks by the peptides (especially the inherently amphiphilic WLBU2). Although no obvious desorption of triblocks by nisin (a CAP of similar size to WLBU2) was observed in previous work [18, 33], we investigated peptide adsorption at immobilized F108 brushes using TCVS-modified OWLS waveguides on which we covalently immobilized F108 using γ-irradiation [18, 19]. Results with PLR in water (Figure 2.6) are entirely consistent with those in this work: contact of the F108-coated waveguide with disordered PLR resulted in negligible adsorption, while ordered peptide adsorbed strongly. As suggested above, the adsorbed α-helical peptide was relatively resistant to elution under helix-promoting solution conditions, but was quickly and completely desorbed when eluted with water (which favors the "disordered" form of the peptide, Figure 2.5).

Changes in peptide structure in F108 brushes. WLBU2 in 0.5 M $HClO_4$ (initially 30% helical) achieves considerable α-helix content (39%) after adsorption onto a bare hydrophobic surface (Figure 2.7, left) and into a PEO layer (43% helical). The increase in helicity is more obvious in Figure 2.7 (right), when WLBU2 is in 0.2 M $HClO_4$ (initially 15% α-helical), its helicity increases to 43% after entrapment into the PEO layer. Importantly, regardless of the initial helicity, the final α-helix content of the adsorbed

WLBU2 is the same (43%) after adsorption into a PEO layer. This is different from the behavior of PLR (Figure 2.4), suggesting a conformational change due to the strong interaction between hydrophobic groups on the peptide and the hydrophobic inner region of PEO layer. Figure 2.7 also suggests that the interaction between WLBU2 and the PEO brush, while strong, allows for good molecular flexibility, since the final helicity of partially-ordered WLBU2 in the PEO brush is greater than on the bare surface (Figure 2.7, right).

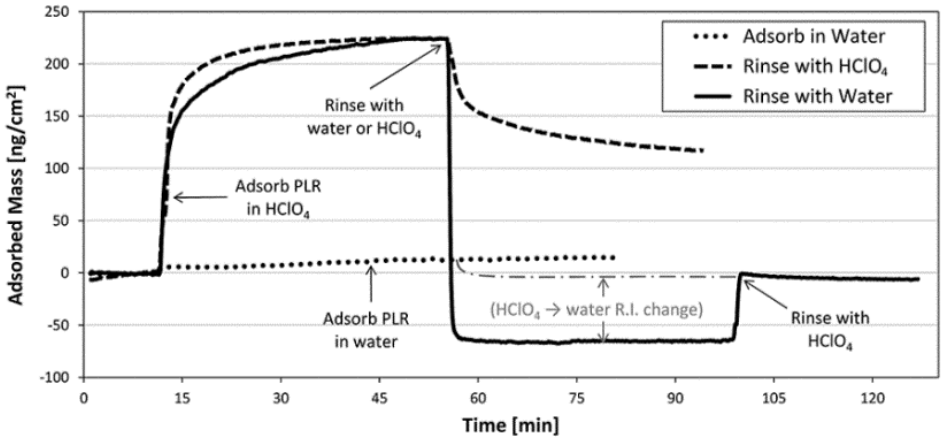

Figure 2.6. Adsorption and elution profiles of PLR on an OWLS waveguide coated with immobilized F108. Baseline was achieved using HPLC H_2O or 0.5 M perchloric acid, followed by adsorption of 0.1 mg/mL PLR in H_2O or $HClO_4$, and then elution with H_2O or $HClO_4$. Little PLR adsorption was observed in water (···), suggesting that aqueous (disordered) PLR does not integrate into the F108 brush layer. α-Helical PLR adsorbed substantially from $HClO_4$, but was nearly completely removed from the brush by rinsing with water (-). In contrast, PLR adsorbed from and rinsed with $HClO_4$ (--) was only partially eluted, suggesting stable integration of the peptide in the brush.

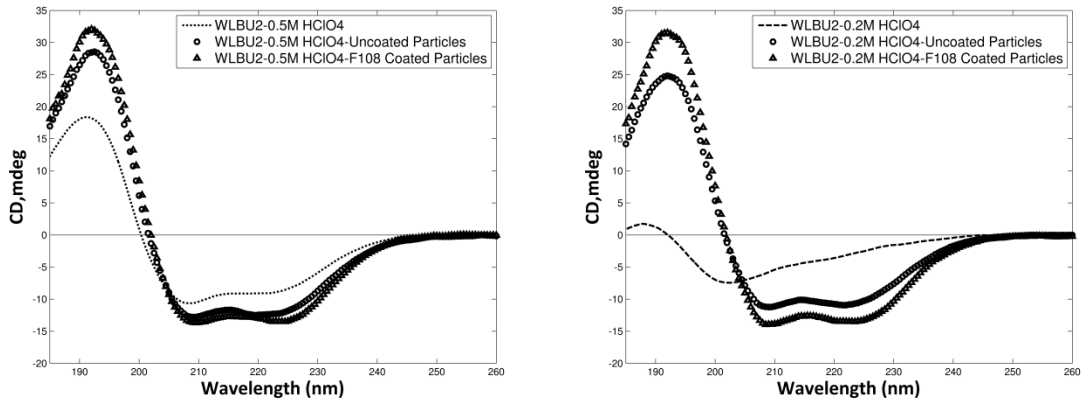

Figure 2.7. CD spectra of: (left) WLBU2 in 0.5 M $HClO_4$, and in suspension with uncoated and F108-coated nanoparticles, (right) WLBU2 in 0.2 M $HClO_4$, and in suspension with uncoated and F108-coated nanoparticles.

As previously described with PLR, uncoated and F108-coated nanoparticles were incubated with α-helical WLBU2 in $HClO_4$ solution, and then washed with $HClO_4$ or water. In all cases, a small fraction of peptide was removed by washing (Figure 2.8). However, while changing the solvent from the helix-promoting $HClO_4$ to water (which favors a "disordered" conformation) resulted in nearly complete loss of PLR (see Figure 2.5 and Figure 2.6), solution changes had little effect on the intensity or shape of CD spectra of adsorbed WLBU2 (Figure 2.8). It is reasonable to expect that amphiphilicy is the cause of this retention of WLBU2 (but not PLR) at F108-coated surfaces following a solvent change. While WLBU2 present in the hydrophilic outer region of PEO layer might be removed by rinsing with peptide-free buffer, an amphiphilic peptide WLBU2 which is entrapped in the hydrophobic inner region should show greater resistance to elution than would a non-amphiphilic peptide PLR. Moreover, the WLBU2 entrapped in the brush maintains its α-helical structure, even when the surrounding solvent has been

changed from $HClO_4$ to water (Figure 2.8), while entrapped PLR undergoes a helix-coil transition in response to changes in solution conditions (Figure 2.5). Unlike the disordered peptides (Figures 2.2 and 2.3), which do not interact with the interior of the brush, the spectra of PLR and WLBU2 on F108-coated and uncoated hydrophobic nanoparticles (Figures 2.5 and 2.7) are quite similar. This is consistent with partial helix formation in the peptides, which is presumably induced by either the hydrophobic environment at the particle surface or in the inner region of the brush.

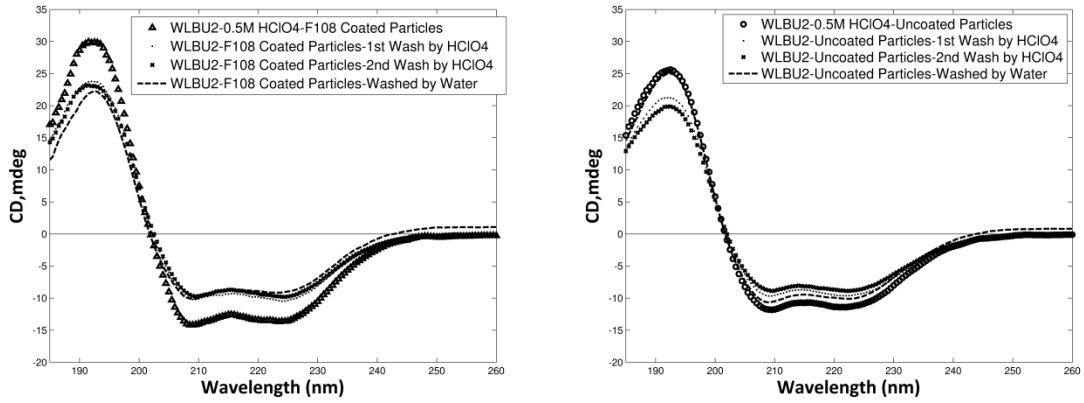

Figure 2.8. CD spectra of: WLBU2 in $HClO_4$, and in suspension with F108-coated (left) and uncoated (right) nanoparticles before and after washing with $HClO_4$ or water.

In summary, an initially more ordered (α-helical) structure promotes the adsorption of a peptide into the PEO layer. A partially helical peptide undergoes an increase in helicity, probably due to the loss of peptide-solvent H-bonding in the apolar region within the brush [16, 32]. An amphiphilic peptide (e.g. WLBU2) is expected to have a much stronger interaction with the hydrophobic inner region of the PEO layer than a non-amphiphilic one (e.g. PLR). This interaction results in entrapment and conformational

change of the amphiphilic peptide that is irreversible with respect to elution. In contrast, the adsorption and conformational change of non-amphiphilic peptides are reversible, making such peptides highly elutable because of their weak interaction with the brush.

2.4. Conclusions

The results reported here direct us to expect that some minimal degree of structural order (α-helix) is necessary for peptide entry into the PEO layer, and that peptide location within the hydrophobic inner region of the PEO brush may result in an increase in α-helix content. Once the non-amphiphilic peptide polyarginine (PLR) was entrapped among the PEO chains of the F108 brush, we found it to be partially elutable as long as the same helix-stabilizing solvent used during the adsorption step was used for elution. However, in contact with water (which favors its disordered, non-adsorbable conformation), the adsorbed PLR was entirely elutable.

In contrast, the amphiphilic peptide WLBU2 was highly resistant to elution in all cases, even upon contact with a solvent which promotes its disordered form. Previously, we suggested that the well-known helix-coil transition of homopolyamino acids (e.g. PLL or PLR) might be used to reversibly anchor peptides or their conjugates within a PEO brush as a novel drug-delivery strategy. It appears, however, that the property of amphiphilicity (such as exhibited by WLBU2) is required to control peptide desorption from a PEO brush when the bulk solution conditions are changed.

This work provides direction for development of responsive drug delivery systems based on modulation of solvent conditions and bioactive peptide structure within PEO brush layers. Previous studies indicate that cationic peptides entrapped in PEO brushes are protected from competitive elution by large blood proteins (e.g. fibrinogen) [34, 35]. In addition, our recent work indicates that peptide-loaded brushes retain their ability to repel fibrinogen (unpublished data). Therefore, the presence of a PEO layer at the surface of medical devices could stabilize entrapped therapeutic peptides against competitive desorption by blood proteins, as well as provide desirable non-fouling characteristics to the device. Entrapment of therapeutic peptides may also support novel drug delivery strategies (e.g., PEO-coated nanoparticle carriers) that can potentially overcome barriers to oral delivery of peptide drugs [36]. Work currently underway in our laboratory toward these ends features the sequential and competitive adsorption behavior of peptide and peptide-protein mixtures at pendant PEO brush layers, and will contribute to the subject of future reports.

Acknowledgements

The authors thank Dr. Kerry McPhail of the OSU College of Pharmacy for use of her CD instrument, and Dr. Victor Hsu and Dr. Elisar Babar for valuable discussion on interpretation of the CD spectra. This work was supported in part by the National Institute of Biomedical Imaging and Bioengineering (NIBIB, grant no. R01EB011567). The content is solely the responsibility of the authors and does not necessarily represent the official views of NIBIB or the National Institutes of Health.

2.5. References

[1] M.C. Lampi, X. Wu, K.F. Schilke, J. McGuire, Structural attributes affecting peptide entrapment in PEO brush layers, Colloids Surf. B. Biointerfaces 106 (2013) 79-85.

[2] W.T.E. Bosker, P.A. Iakovlev, W. Norde, M.A. Cohen Stuart, BSA adsorption on bimodal PEO brushes, J. Colloid Interface Sci. 286 (2005) 496-503.

[3] F. Fang, J. Satulovsky, I. Szleifer, Kinetics of protein adsorption and desorption on surfaces with grafted polymers, Biophys. J. 89 (2005) 1516-1533.

[4] S.R. Sheth, D. Leckband, Measurements of attractive forces between proteins and end-grafted poly(ethylene glycol) chains, Proc. Natl. Acad. Sci. U.S.A. 94 (1997) 8399-8404.

[5] H. Lee, D.H. Kim, K.N. Witte, K. Ohn, J. Choi, B. Akgun, S. Satija Y.-Y. Won, Water is a poor solvent for densely grafted poly (ethylene oxide) chains: A conclusion drawn from a self-consistent field theory-based analysis of neutron reflectivity and surface pressure–area isotherm data, J. Phys. Chem. B 116 (2012) 7367-7378.

[6] F. Costa, I.F. Carvalho, R.C. Montelaro, P. Gomes, M.C.L. Martins, Covalent immobilization of antimicrobial peptides (AMPs) onto biomaterial surfaces, Acta Biomater. 7 (2011) 1431-1440.

[7] B. Deslouches, I.A. Gonzalez, D. DeAlmeida, K. Islam, C. Steele, R.C. Montelaro T.A. Mietzner, De novo-derived cationic antimicrobial peptide activity in a murine model of Pseudomonas aeruginosa bacteraemia, J. Antimicrob. Chemother. 60 (2007) 669-672.

[8] B. Deslouches, K. Islam, J.K. Craigo, S.M. Paranjape, R.C. Montelaro T.A. Mietzner, Activity of the de novo engineered antimicrobial peptide WLBU2 against Pseudomonas aeruginosa in human serum and whole blood: Implications for systemic applications, Antimicrob. Agents Chemother. 49 (2005) 3208-3216.

[9] B. Deslouches, S.M. Phadke, V. Lazarevic, M. Cascio, K. Islam, R.C. Montelaro, T.A. Mietzner, De novo generation of cationic antimicrobial peptides: Influence of length and tryptophan substitution on antimicrobial activity, Antimicrob. Agents Chemother. 49 (2005) 316-322.

[10] I.A. Gonzalez, X.X. Wong, D. De Almeida, R. Yurko, S. Watkins, K. Islam, R.C. Montelaro, A. El-Ghannam T.A. Mietzner, Peptides as potent antimicrobials tethered to a solid surface: Implications for medical devices, Nat. Precedings (2008).

[11] S.A. Onaizi, S.S.J. Leong, Tethering antimicrobial peptides: Current status and potential challenges, Biotechnol. Adv. 29 (2011) 67-74.

[12] M.C. Skinner, A.O. Kiselev, C.E. Isaacs, T.A. Mietzner, R.C. Montelaro M.F. Lampe, Evaluation of WLBU2 peptide and 3-O-octyl-sn-glycerol lipid as active ingredients for a topical microbicide formulation targeting Chlamydia trachomatis, Antimicrob. Agents Chemother. 54 (2010) 627-636.

[13] A.A. Adzhubei, M.J.E. Sternberg, A.A. Makarov, Polyproline-II helix in proteins: Structure and function, J. Mol. Biol. 425 (2013) 2100-2132.

[14] B. Bochicchio, A.M. Tamburro, Polyproline II structure in proteins: Identification by chiroptical spectroscopies, stability, and functions, Chirality 14 (2002) 782-792.

[15] A.V. Mikhonin, N.S. Myshakina, S.V. Bykov S.A. Asher, UV resonance raman determination of polyproline II, extended 2.51-helix, and β-sheet ψ angle energy landscape in poly-*L*-lysine and poly-*L*-glutamic acid, J. Am. Chem. Soc. 127 (2005) 7712-7720.

[16] J.M. Rifkind, Helix–coil transition of poly-*L*-arginine: A comparison with other basic polypeptides, Biopolymers 8 (1969) 685-688.

[17] M.L. Tiffany, S. Krimm, Circular dichroism of the "random" polypeptide chain, Biopolymers 8 (1969) 347-359.

[18] Y.-C. Tai, J. McGuire, J.A. Neff, Nisin antimicrobial activity and structural characteristics at hydrophobic surfaces coated with the PEO–PPO–PEO triblock surfactant Pluronic® F108, J. Colloid Interface Sci. 322 (2008) 104-111.

[19] T.B. McPherson, H.S. Shim, K. Park, Grafting of PEO to glass, nitinol, and pyrolytic carbon surfaces by γ irradiation, J. Biomed. Mater. Res. 38 (1997) 289-302.

[20] Y.-C. Tseng, T. McPherson, C.S. Yuan, K. Park, Grafting of ethylene glycol-butadiene block copolymers onto dimethyl-dichlorosilane-coated glass by γ-irradiation, Biomaterials 16 (1995) 963-972.

[21] F. Höök, J. Vörös, M. Rodahl, R. Kurrat, P. Böni, J.J. Ramsden, M. Textor, N.D. Spencer, P. Tengvall, J. Gold B. Kasemo, A Comparative Study of Quantitative Protein Adsorption on Titanium Oxide Surfaces Using in situ Ellipsometry, Optical Waveguide Lightmode Spectroscopy, and Quartz Crystal Microbalance Techniques, Colloids Surf. B. Biointerfaces 24 (2002) 155-170.

[22] C. Calonder, Y. Tie, P.R. Van Tassel, History dependence of protein adsorption kineticsProc, Natl. Acad. Sci. U. S. A. 98 (2001) 10664-10669.

[23] H. Salmio, D. Brühwiler, Distribution of amino groups on a mesoporous silica surface after submonolayer deposition of aminopropylsilanes from an anhydrous liquid phase, The Journal of Physical Chemistry C 111 (2006) 923-929.

[24] N.J. Greenfield, Methods to estimate the conformation of proteins and polypeptides from circular dichroism data, Anal. Biochem. 235 (1996) 1-10.

[25] N.J. Greenfield, G.D. Fasman, Computed circular dichroism spectra for the evaluation of protein conformation, Biochemistry (Mosc). 8 (1969) 4108-4116.

[26] R.W. Woody, Theory of circular dichroism of proteins, in: G.D. Fasman (Ed.) Circular dichroism and the conformational analysis of biomolecules, Plenum Press, New York, 1996, pp. 25-30.

[27] L. Whitmore, B.A. Wallace, Dichroweb, an online server for protein secondary structure analyses from circular dichroism spectroscopic data, Nucleic Acids Res. 32 (2004) W668-W673.

[28] L. Whitmore, B.A. Wallace, Protein secondary structure analyses from circular dichroism spectroscopy: Methods and reference databases, Biopolymers 89 (2008) 392-400.

[29] V. Puddu, C.C. Perry, Peptide adsorption on silica nanoparticles: Evidence of hydrophobic interactions, ACS Nano 6 (2012) 6356-6363.

[30] E.K. Asciutto, I.J. General, K. Xiong, S.A. Asher, J.D. Madura, Sodium perchlorate effects on the helical stability of a mainly alanine peptide, Biophys. J. 98 (2010) 186-196.

[31] A. Halperin, Polymer brushes that resist adsorption of model proteins: design parameters, Langmuir 15 (1999) 2525-2533.

[32] Y. Takechi, C. Mizuguchi, M. Tanaka, T. Kawakami, S. Aimoto, E. Okamura, H. Saito, Physicochemical mechanism for the lipid membrane binding of polyarginine: The favorable enthalpy change with structural transition from random coil to a-helix, Chem. Lett. 41 (2012) 1374-1376.

[33] Y.-C. Tai, P. Joshi, J. McGuire J.A. Neff, Nisin adsorption to hydrophobic surfaces coated with the PEO–PPO–PEO triblock surfactant Pluronic® F108, J. Colloid Interface Sci. 322 (2008) 112-118.

[34] M.P. Ryder, K.F. Schilke, J.A. Auxier, J. McGuire, J.A. Neff, Nisin adsorption to polyethylene oxide layers and its resistance to elution in the presence of fibrinogen, J. Colloid Interface Sci. 350 (2010) 194-199.

[35] K.F. Schilke, J. McGuire, Detection of nisin and fibrinogen adsorption on poly (ethylene oxide) coated polyurethane surfaces by time-of-flight secondary ion mass spectrometry (TOF-SIMS), J. Colloid Interface Sci. 358 (2011) 14-24.

[36] W.H. De Jong, P.J. Borm, Drug delivery and nanoparticles: Applications and hazards, Int. J. Nanomed. 3 (2008) 133.

CONCENTRATION EFFECTS ON PEPTIDE ELUTION FROM PENDANT PEO LAYERS

Xiangming Wu, Matthew P. Ryder, Joseph McGuire, Karl F. Schilke

School of Chemical, Biological and Environmental Engineering, Oregon State University, Corvallis, OR 97331

Submitted to Colloids and Surfaces B: Biointerfaces
www.elsevier.com/locate/colsurfb

CHAPTER 3

CONCENTRATION EFFECTS ON PEPTIDE ELUTION FROM PENDANT PEO LAYERS

Abstract

In earlier work, we have provided direction for development of responsive drug delivery systems based on modulation of structure and amphiphilicity of bioactive peptides entrapped within pendant polyethylene oxide (PEO) brush layers. Amphiphilicity promotes retention of the peptides within the hydrophobic inner region of the PEO brush layer. In this work, we describe the effects of peptide surface density on the conformational changes caused by peptide-peptide interactions, and show that this phenomenon substantially affects the rate and extent of peptide elution from PEO brush layers. Three cationic peptides were used in this study: the arginine-rich amphiphilic peptide WLBU2, the chemically identical but scrambled peptide S-WLBU2, and the non-amphiphilic homopolymer poly-*L*-arginine (PLR). Circular dichroism (CD) was used to evaluate surface density effects on the structure of these peptides at uncoated (hydrophobic) and PEO-coated silica nanoparticles. UV spectroscopy and a quartz crystal microbalance with dissipation monitoring (QCM-D) were used to quantify changes in the extent of peptide elution caused by those conformational changes. For amphiphilic peptides at sufficiently high surface density, peptide-peptide interactions result in conformational changes which compromise their resistance to elution. In contrast, elution of a non-amphiphilic peptide is substantially independent of its surface density, presumably due to the absence of peptide-peptide interactions. The results presented here

provide a strategy to control the rate and extent of release of bioactive peptides from PEO layers, based on modulation of their amphiphilicity and surface density.

Keywords: peptide elution; PEO brush; WLBU2; cationic amphiphilic peptides; polyarginine; circular dichroism (CD); α-helix; coiled-coils

3.1. Introduction

In an earlier paper [1], we used circular dichroism (CD) to evaluate the structures of poly-*L*-arginine (PLR) and the cationic, amphiphilic peptide (CAP) WLBU2 in pendant PEO layers, as well as the reversibility of peptide location in such layers with changing solvent conditions. Those results indicated that some minimal degree of structural order (α-helix) is necessary for peptide entry into the PEO layer, and that peptide location within the hydrophobic inner region of the PEO brush may result in a cooperative increase in α-helix content. In addition, while peptide interaction with the PEO chains resulted in entrapment and conformational change that was irreversible to elution with changing solution conditions in the case of WLBU2, the adsorption and conformational change of the non-amphiphilic PLR was reversible.

Current work underway in our laboratory features the sequential and competitive adsorption behavior of peptides, including WLBU2 and PLR, at pendant PEO brush layers. In sequential adsorption experiments it is necessary to vary surface density of the first peptide introduced to the layer in order to properly interpret its replacement by the second peptide introduced. We determined during the course of these experiments that our previous conclusion of entrapment and conformational change being irreversible to elution for the amphiphilic WLBU2 was contextual, being valid only when its surface density is sufficiently low. Our objectives with this paper are to establish an improved understanding of surface density effects on peptide elution from PEO layers, and to provide evidence of concentration-dependent, peptide-peptide interactions likely contributing to those effects. The adsorption behavior of three peptides was evaluated for

this purpose, including, in addition to WLBU2 and PLR, a peptide chemically identical to WLBU2 but of scrambled sequence (S-WLBU2).

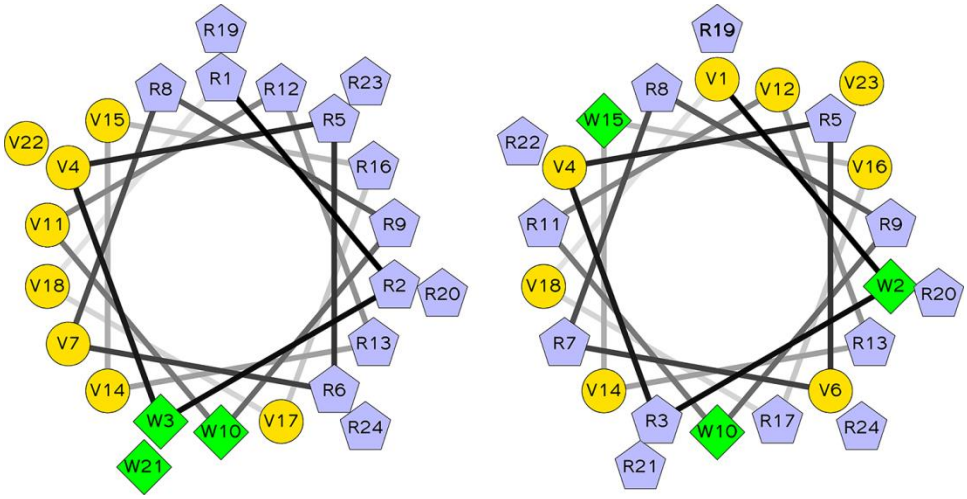

Figure 3.1. Helix wheel representations of WLBU2 (left), with face-segregation of positively-charged Arg residues on the α-helix, and S-WLBU2 (right) which has uniformly distributed charge.

WLBU2 is a synthetic, 24-residue CAP with 13 positively charged arginine residues, and 11 non-polar valine or tryptophan residues. It shows substantial promise for clinical applications, due to its wide spectrum antimicrobial activity against both Gram-negative and Gram-positive bacteria under physiological conditions [2-8]. The structure of WLBU2 in water is substantially disordered, but the peptide gains considerable secondary structure, involving segregation of its positively-charged and hydrophobic groups onto opposing faces of an α-helix, in the presence of counterions, membrane-mimetic solvents, or bacterial membranes. Moreover, WLBU2 retains its antimicrobial activity when immobilized at solid surfaces by a number of methods [2, 6-8]. While chemically identical to WLBU2, the scrambled sequence of S-WLBU2 eliminates the

ordered segregation of positively-charged and hydrophobic residues of WLBU2 during helix formation (Figure 3.1), and is associated with a very low hydrophobic moment in comparison to WLBU2 (0.1 vs. 10.7, respectively). PLR is chemically homogeneous and not amphiphilic. When dissolved in water under neutral pH, PLR adopts a combination of random coil and extended structures (e.g. polyprolone-II and 2.51 helix), while both WLBU2 and S-WLBU2 show a random coil structure [1, 3-5, 9-13]. An α-helical conformation can be achieved in all three peptides by addition of perchlorate ions (ClO_4^-) [12].

3.2. Materials and Methods

Peptides and materials. Synthetic poly-*L*-arginine hydrochloride (PLR, n ≈ 30, Mn = 4.7 kDa, PDI < 1.20) was purchased from Alamanda Polymers (Huntsville, AL). The 24-residue peptides WLBU2 (RRWVRRVRRWVRRVVRVVRRWVRR, 3.4 kDa) and the scrambled sequence S-WLBU2 (VWRVRVRRRWRVRVWVRVRRRRVR) were purchased from Genscript (Piscataway, NJ). All peptides were used without further purification. Stock solutions of each peptide at 5 mg/mL in HPLC water were frozen in 1 mL aliquots, which were thawed and then diluted immediately before use to 0.2 mg/mL in 0.2 M $HClO_4$ (to induce α-helical conformation). Diluted peptide solutions were degassed under vacuum immediately before use.

Self-assembled PEO brush layers were formed by suspension of hydrophobic silica nanoparticles (R816, Degussa, 190 m^2/g, 10-12 nm) in Pluronic® F108 (BASF) in HPLC

water for 10 h on a rotator. The expected surface coverage of F108 is about 3.3 mg/m^2 [14, 15]; a 5× excess of F108 over this amount was used to ensure good coverage of the nanoparticles (NPs). Uncoated and F108-coated NPs were then incubated with PLR, WLBU2 or S-WLBU2 (0.2 mg/mL in 0.2 M $HClO_4$) for 2 h at 20 ℃. The concentration of NPs was varied from 1 to 10 mg/mL to provide different available surface areas for peptide adsorption.

Evaluation of peptide structure and elutability. Peptide secondary structure, in the presence or absence of nanoparticles, was evaluated by circular dichroism (CD) using a Jasco J-815 spectropolarimeter (Easton, MD) at 25 ℃. The spectra from each of three replicates for each sample exhibited only slight (~5%) differences in signal intensity; representative spectra are thus shown throughout. The instrument was calibrated with 0.6 mg/mL *D*(+)-camphorsulfonic acid. Spectra were recorded from 185 to 260 nm in 0.5 nm increments (0.1 cm path length), with 5 scans recorded and averaged in order to increase the signal-to-noise ratio. All peptide solutions were filtered (0.20 μm) prior to contact with NPs and recording of CD spectra. All spectra were blanked against peptide-free solutions.

After the CD measurements, the peptide-NP suspensions were rinsed by centrifugation (10,000 rpm, 20 min) and resuspension in water; this process was repeated twice to remove excess peptide. The amount of peptide removed in each of the supernatants from the NPs was then quantified by UV spectrophotometry against the original peptide solutions at 230 nm (for PLR) or 280 nm (for WLBU2 and S-WLBU2), and the total eluted peptide calculated from this data.

Preparation of QCM-D sensors. QSX303 silicon dioxide QCM-D sensors (Q-Sense, Linthicum, MD) were cleaned according to manufacturer's protocol: 10 min UV/ozone treatment followed by immersion in 2% sodium dodecyl sulfate (SDS) for 30 min, and a 10 min rinse with HPLC water. After cleaning, sensors were dried under a stream of nitrogen and placed in the UV/ozone chamber again for 10 min.

The sensor surfaces were then modified by vapor deposition of trichlorovinylsilane (TCVS, TCI America, Portland, OR). 200 μL of TCVS was evaporated at 20 ℃ into a stream of dry nitrogen carrier gas, which was directed over the sensor surfaces for 4 h. The silanized, hydrophobic sensors were then incubated overnight with 5% Pluronic® F108 in water, and then γ-irradiated to 0.3 Mrad to covalently attach the F108 to the surface [14, 16]. The irradiated sensors were rinsed with water, dried with nitrogen, and stored in the dark to avoid oxidation of the vinyl moieties.

Measurement of the rate and extent of peptide adsorption and elution. The adsorption and elution of peptides were measured with a Q-Sense E4 QCM-D (Q-sense, Linthicum, MD). QCM-D allows simultaneously measuring changes in resonance frequency (ΔF) and energy dissipation (ΔD) of QCM-D sensors. Sample solutions were pumped across F108-coated silica sensors at 100 μL/min, and the sample stage was held at 25 ℃. QCM-D experiments began with a baseline of peptide-free 0.2M $HClO_4$, followed by introduction of 0.1 mg/mL or 0.005 mg/mL peptide in 0.2M $HClO_4$, and a subsequent rinse with water. Adsorption and elution steps were each allowed to proceed for 40 min.

3.3. Results and Discussion

Relationship between peptide surface density and peptide elution from PEO layers. Peptide concentration at PEO-coated nanoparticle surfaces was varied by altering nanoparticle concentration (from 1 to 10 mg/mL) in peptide-nanoparticle suspensions with constant peptide concentration (0.2 mg/mL). More than 95% of the dissolved peptide was entrapped in every suspension tested, corresponding to peptide surface densities ranging from about 0.02 to 0.2 molecules/nm^2. The elutability of each peptide recorded after contact with peptide-free water is plotted against peptide surface density in Figure 3.2.

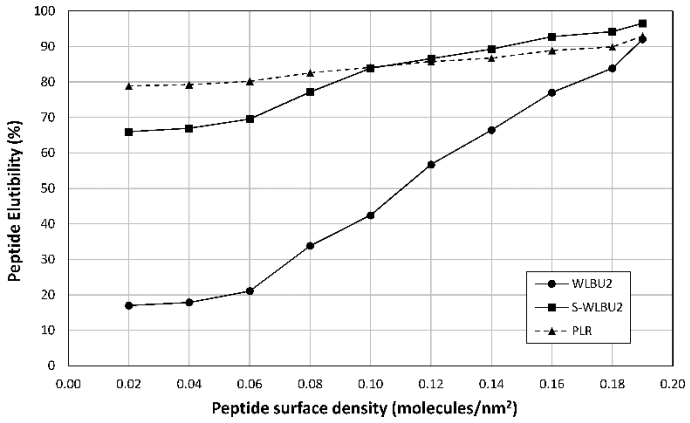

Figure 3.2. Effect of surface peptide density on elutability of WLBU2, S-WLBU2 and PLR from F108-coated nanoparticles.

As shown in Figure 3.2, entrapped WLBU2 showed a substantially greater concentration dependence on elution than shown by entrapped S-WLBU2 or PLR. The high resistance to elution at low peptide surface density is consistent with our earlier report and attributed to association of the amphiphilic WLBU2 with PEO chain segments in the hydrophobic

inner region of the brush [1, 14, 17]. The elutability of S-WLBU2 and PLR was less strongly affected by the peptide surface density, and both were more elutable than WLBU2 at all but the highest surface density tested.

S-WLBU2, while comprised of the same amino acids and carrying the same +13 charge as WLBU2, features arginine residues alternating with valine or tryptophan to distribute the positive charge uniformly around the α-helix (Figure 3.1). The tryptophan residues are also distributed along the full length of the peptide. S-WLBU2 was designed to have a very low hydrophobic moment, and these attributes are consistent with its elution from the PEO layer being greater than that recorded for WLBU2 at low peptide surface densities. The non-amphiphilic PLR is highly elutable from PEO layers (Figure 3.2), which is consistent with our earlier work using CD and optical waveguide lightmode spectroscopy [1]. The total absence of hydrophobic residues and the abundant positive charges on all sides of PLR lead to electrostatic repulsion among peptides within the brush, as well as making PLR highly soluble in water. In fact, the elutability of PLR is only slightly dependent on its surface density (Figure 3.2).

WLBU2 and S-WLBU2 both exhibit substantially increased elutability at high peptide surface densities (i.e. low nanoparticle concentrations). It is fair to expect that this high elutability is due to intermolecular interactions, which interfere with the stable hydrophobic association of the individual peptides within the brush, or otherwise promote their enhanced solubility in water.

WLBU2 is highly α-helical in $HClO_4$, and its entrapment in PEO is accompanied by a further increase in its helicity [1]. Upon sufficiently close approach, peptides like

WLBU2 which possess an amphiphilic-segregated α-helical conformation are able to form α-helical, "coiled-coil" conformations. These structures, which are comprised of two or more intertwined α-helical chains, are stabilized through multiple interchain hydrophobic interactions [18]. For example, Zhou et al. produced a two-stranded α-helical coiled-coil consisting of two identical 35-residue polypeptides. The peptides were designed with polar (lysine and glutamic acid) and non-polar (leucine and alanine) residues distributed on average 3.5 residues apart, in order to form face-segregated amphiphilic α-helices. These synthetic peptides spontaneously self-assembled into coiled-coil structures in physiological conditions [19, 20]. WLBU2 has a very similar distribution of polar and nonpolar residues, and is thus also expected to form α-helical coiled-coil structures at sufficiently high concentration. Such coiled-coils may consist of two or more peptides [18, 21], and in the case of WLBU2 would likely feature a hydrophobic interior, with an exterior dominated by positively-charged arginine groups. Such a coiled-coil structure would be expected to behave very similarly to the highly cationic but non-amphiphilic PLR, in terms of its interaction with the PEO brush (Figure 3.3). With respect to S-WLBU2, it has been shown [22, 23] that peptides with alternating hydrophobic and polar residues are able to self-assemble into stable β-sheet conformations. It is reasonable to expect that, as favorable peptide-PEO interactions which hold entrapped peptides in place give way at high surface densities to peptide-peptide associations, the peptides become more elutable as the population of coiled-coils increases.

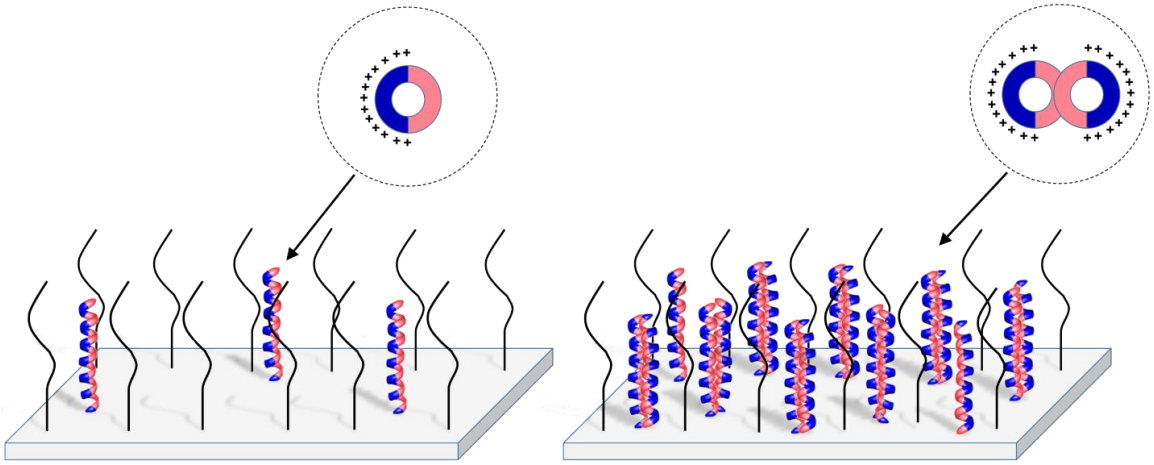

Figure 3.3. Schematic representation of WLBU2 as single-stranded amphiphilic α-helices at low peptide surface density (left), and formation of less-amphiphilic α-helical coiled-coil structures at high peptide surface density (right). Figure not to scale.

Surface density effects on peptide structure in PEO layers. Formation of coiled-coil or other structures associated with increasing peptide surface density and elutability should be detectable by specific changes in the CD signal. The surface density of peptides at uncoated (hydrophobic) and PEO-coated nanoparticle surfaces was varied as above, by altering the nanoparticle concentration (from 1 to 10 mg/mL) in peptide-nanoparticle suspensions with constant peptide concentration (0.2 mg/mL). CD spectra were acquired for WLBU2 in contact with uncoated or PEO-coated nanoparticles at different peptide surface densities (Figure 3.4).

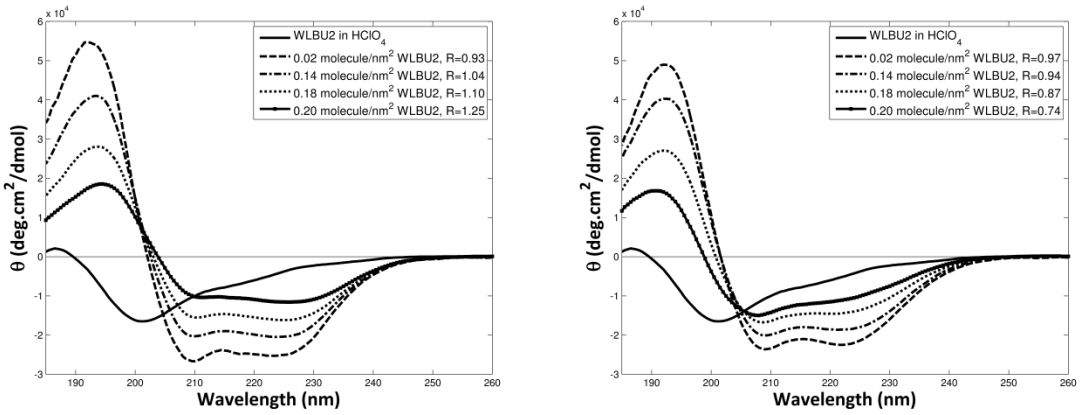

Figure 3.4. CD spectra of WLBU2 in 0.2M $HClO_4$ at different peptide surface densities on F108-coated (left) and uncoated (right) NPs.

The CD spectrum of an α-helix typically exhibits a maximum at 193 nm, and two minima at 208 and 222 nm. An increase in the magnitude of ellipticity at 222 nm for a given sample is associated with an increase in α-helix content [24, 25]. Deconvolution of these CD spectra with DichroWeb [26, 27] indicate that WLBU2 in 0.2 M $HClO_4$ exhibits 17% α-helicity. In the presence of F108-coated nanoparticles at 1, 2, 4 and 10 mg/mL (corresponding to decreasing peptide surface densities of 0.20, 0.18, 0.14 and 0.02 molecules/nm^2), the helicity of WLBU2 was increased to 50, 65, 84 and 95%, respectively. The increase in helicity is due to promotion of hydrogen-bonding along the peptide backbone, which accompanies the change in microenvironment caused by location within the hydrophobic interior of the PEO layer [1, 5, 17]. Interference with this intra-chain hydrogen-bonding by neighboring peptides is presumably responsible for the reduction in α-helix content observed at increased peptide surface densities (Figure 3.4, left panel).

While the ellipticity at 222 nm is primarily responsive to the α-helix content, the minimum at 208 nm is itself sensitive to helix-helix interactions [20, 28]. In fact, CD has been applied extensively to the study of the formation of α-helical, coiled-coil structures [28-32]. In particular, the ratio, R, of the ellipticities at 222 nm and 208 nm can be used to distinguish coiled-coils from single-stranded α-helices. Typically, a value of $R > 1$ (i.e. $\theta_{222\ nm} > \theta_{208\ nm}$) is associated with coiled-coil structures, while a value of $R \leqslant 1$ is indicative of single-stranded α-helices [28-32]. WLBU2 exhibits a large amount of predominantly single-stranded α-helix structure ($R = 0.93$) on F108-coated nanoparticles at a surface density of 0.02 peptides/nm^2 (dashed line in Figure 3.4, left panel). This suggests that at sufficiently low peptide surface density, peptides exist mainly as single α-helical molecules (Figure 3.3, left). As the surface density of peptides increases, the ratio R increases to values greater than unity, indicating the formation of a substantial number of α-helical coiled-coil structures (Figure 3.3, right) [29-32].

While the CD spectra of WLBU2 adsorbed at uncoated, hydrophobic nanoparticles (Figure 3.4, right panel) indicate an increase in α-helicity, especially at low peptide surface density, there is no evidence of α-helical coiled-coils, as $R < 1$ at all of the surface densities tested. The increase in peptide helicity is likely due to the preferential association of the non-polar Val/Trp residues with the hydrophobic surface, which promotes the segregation of polar and non-polar residues onto opposing sides of the peptide and stabilizes the α-helix [14]. Electrostatic repulsion by the positively-charged Arg residues on the solvent-exposed helix face would make formation of coiled-coil structures unfavorable, even if the peptide surface density were high. However, peptides

which are entrapped within a PEO brush apparently do not directly interact with the underlying surface [16]. Thus, WLBU2 peptides entrapped in a PEO brush still form highly-charged coiled-coil structures, with low resistance to elution, at sufficiently high surface density.

Similarly to WLBU2, the CD spectra of S-WLBU2 in suspension with PEO-coated nanoparticles (Figure 3.5, left panel) indicate a substantial gain (from 17 to 89%) in α-helix content after entering the brush, when the surface density is low (0.02 peptides/nm^2). However, with increasing peptide surface density, the structure adopted by the peptide becomes β-sheet rather than α-helical coiled-coils. The CD spectra of peptides with β-sheet conformation usually have a single minimum between 210 and 220 nm, and a single maximum between 195 and 200 nm, and overall intensities much lower than the minima consistent with α-helices [24, 25]. Deconvolution of the spectra with DichroWeb indicate that S-WLBU2 exhibits 31% β-sheet and 53% α-helix structure at a surface density of 0.14 peptides/nm^2, has 54% β-sheet and 16% α-helix at 0.18 peptides/nm^2, and reaches 67% β-sheet with only negligible α-helix (3%) at 0.20 peptides/nm^2. The amino acid sequence of S-WLBU2 is not conducive to formation of face-segregated amphiphilic α-helices (Figure 3.1); instead, the peptide likely extends into β-strands, isolating the alternating non-polar residues onto one side of the sheet [23]. At sufficiently high peptide surface densities, these β-strands may self-assemble into stable β-sheet structures stabilized by inter-chain hydrogen-bonding and hydrophobic interactions [33].

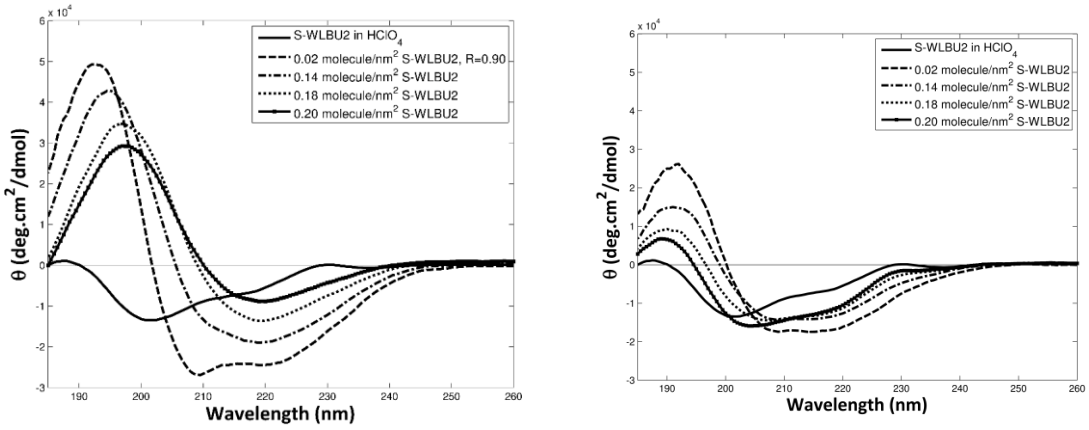

Figure 3.5. CD spectra of S-WLBU2 in 0.2 M $HClO_4$ at different peptide surface densities on F108-coated (left) and uncoated (right) NPs.

The effects of peptide concentration on the conformation of adsorbed S-WLBU2 are less obvious at uncoated, hydrophobic surfaces than at PEO-coated surfaces (Figure 3.5, right panel). While S-WLBU2 in a PEO brush was almost completely α-helical (89%) at the lowest peptide surface density (0.02 peptides/nm^2), the same peptide adopts a substantial β-sheet structure (30%) on the uncoated, hydrophobic surface. Interactions between the hydrophobic surface and the alternating, non-polar residues of S-WLBU2 likely result in extension of the peptide chain, thus favoring β-sheet formation on the surface. Increasing the surface density of S-WLBU2 appears only to increase the number of layers of β-sheet, as no major conformational change is associated with increasing peptide density (Figure 3.5, right panel).

Unlike WLBU2 and S-WLBU2, PLR is a non-amphiphilic homopolymer with positive charges which uniformly surround the α-helix. Accordingly, electrostatic repulsions are expected to prevent peptide-peptide interactions, even at high surface density. CD spectra

show that the helicity of PLR in 0.2 M $HClO_4$ solution is 55%, and is increased to 65% after contact with a PEO layer (Figure 3.6, left). Changes in surface density have little or no further effect on the conformation of PLR, whether on PEO-coated or uncoated hydrophobic surfaces (Figure 3.6).

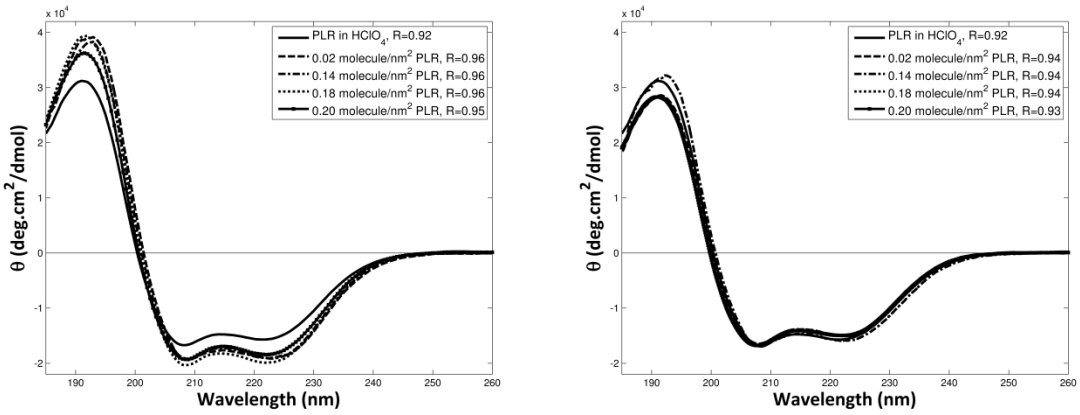

Figure 3.6. CD spectra of PLR in 0.2M $HClO_4$ at different peptide surface densities on F108-coated (left) and uncoated (right) NPs.

In summary, interactions between peptide molecules within the PEO brush layer are highly dependent on the properties of the peptide, specifically amphiphilicity, distribution of polar and non-polar residues, and charge. Elution of an amphiphilic peptide from the PEO brush layer is significantly affected by its surface density, while elution of a non-amphiphilic peptide is substantially independent of surface density. This difference in elution behavior is attributed to peptide-peptide interactions in the former case and the absence of such interactions in the latter.

Direct detection of peptide adsorption and elution at covalently immobilized PEO layers. We used QCM-D to measure the effect of surface concentration on the rate and extent of peptide elution. Figure 3.7 shows the representative changes in resonant frequency (ΔF) and viscous dissipation (ΔD) upon adsorption and elution of peptides from F108-coated silica sensors [34, 35]. The decrease in frequency (indicative of an increase in adsorbed mass) upon introduction of WLBU2 to F108-coated sensors at a peptide concentration of 0.1 mg/mL was about three times greater than that recorded for WLBU2 at 0.005 mg/mL (Figure 3.7, top panels). Upon elution, the frequency change indicated rapid and substantially complete removal of WLBU2 from the PEO brush that had been introduced at 0.1 mg/mL. However, a much slower, and only partial, removal of WLBU2 was observed when the peptide had been introduced at 0.005 mg/mL. These results are consistent with the greater resistance to elution by peptides at low surface density within the brush observed on nanoparticles (Figure 3.2).

Modeling of the frequency and dissipation data of Figure 3.7, in order to determine the adsorbed mass and effective layer viscosity, could not be performed with good certainty, as neither the Sauerbrey equation nor the Voigt model are appropriately applied in this context. The Sauerbrey equation should only be used with relatively uniform, rigid, thin films that show negligible dissipation change, while the Voigt model did not successfully calculate adsorbed mass from a simultaneous decrease in frequency and dissipation [36, 37]. Qualitatively, however, the frequency and dissipation patterns in Figure 3.7 (top panel) likely represent the incorporation of WLBU2 into an initially “soft” dissipative surface (i.e. a pendant PEO layer, as opposed to a solid surface), and a concomitant

increase in the layer stiffness. In comparison, a decrease in layer stiffness (i.e. increased viscoelasticity) is associated with protein adsorption on a rigid surface, suggesting that the observed frequency change was not due to adsorption of WLBU2 at "bare spots" in the brush. In contrast, the changes in resonant frequency (ΔF) for S-WLBU2 indicate a rapid and nearly complete removal of the peptide, whether originally introduced at high or low concentrations (Figure 3.7, bottom panels). This suggests that elution of the scrambled peptide is much less affected by its concentration at the surface than the face-segregated α-helix formed by WLBU2. Using optical waveguide lightmode spectroscopy (OWLS), we have observed that, like S-WLBU2, the non-amphiphilic PLR remains completely elutable from a PEO brush, even at very low surface peptide density [1].

Interestingly, the dissipation recorded during the adsorption of S-WLBU2 at high concentration decreased rapidly at first, then slowly increased (Figure 3.7, bottom left). An increase in the dissipation is associated with decreases in the stiffness of the adsorbed layer. Such a change would be consistent with a slow conformational change undergone by S-WLBU2 at the interface. Presumably, S-WLBU2 retains the α-helix structure induced by perchlorate ion during the initial adsorption, but rearranges to a β-sheet conformation as the peptide concentration in the PEO layer becomes sufficiently high. This is also consistent with recent reports that α-helical peptide layers adsorbed on gold QCM-D sensors are more rigid than peptide layers adsorbed as β-sheets [36]. No such increase in dissipation was recorded during adsorption of S-WLBU2 at low concentration (Figure 3.7, bottom right), suggesting that there is no significant α-helix → β-sheet transition of S-WLBU2 within the PEO layer. The QCM-D results of Figure 3.7 are

entirely consistent with the other results discussed above, and are also in agreement with the hypothesis that highly-elutable coiled-coil structures are formed at high peptide densities in the PEO brush.

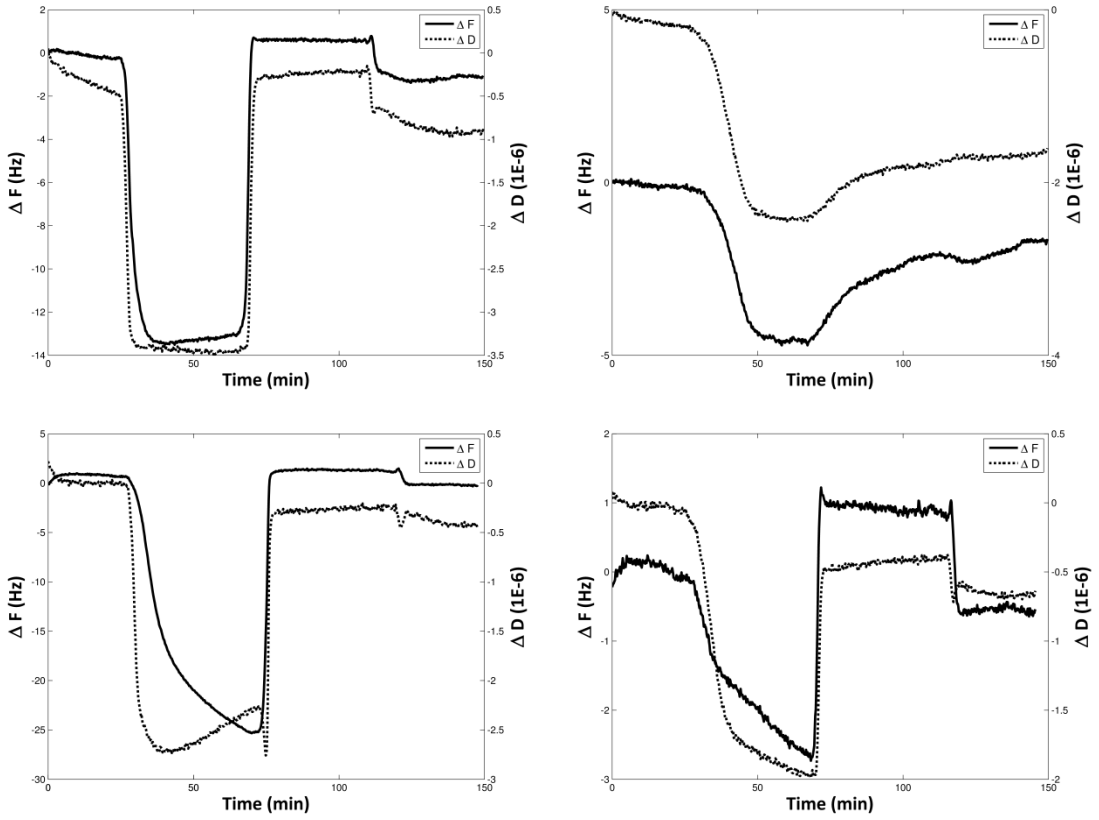

Figure 3.7. Representative ΔF and ΔD vs. time for WLBU2 (top panels) and S-WLBU2 (bottom panels) adsorption and elution on F108-coated SiO_2 QCM-D sensors. Baselines were achieved using 0.2 M $HClO_4$, followed by introduction of peptide in $HClO_4$, then elution with H2O, and finally switch back to $HClO_4$. Peptide concentrations used for QCM-D experiments were 0.1 mg/mL (left panels) and 0.005 mg/mL (right panels). Note change of scale between peptide concentrations (left and right panels).

3.4. Conclusions

Elution of peptides from PEO brush layers is governed by their amphiphilicity and surface density. Peptides of high amphiphilicity can be expected to interact strongly with PEO chains after location within the layer, thus promoting their resistance to elution. However, at sufficiently high surface density, peptide-peptide interactions may result in conformational changes (e.g. formation of coiled-coils) which can compromise this resistance to elution. In this work, WLBU2, a peptide with a face-segregated amphiphilic α-helical structure, was observed to form α-helices and coiled-coils, while the amphiphilic peptide (S-WLBU2) with a more uniform charge distribution formed β-sheets. These conformational changes (from α-helix to coiled-coil and β-sheet) increased the elutability of WLBU2 and S-WLBU2, presumably by reducing the amphiphilic character of the resulting complex. In contrast, the non-amphiphilic peptide (PLR) showed no substantial change in structure or elutability with increasing peptide surface density.

Entrapment of bioactive peptides within otherwise non-fouling PEO brush layers holds promise for contributing to development of responsive drug delivery systems. These results will inform research efforts focused on the sequential and competitive adsorption and release of such peptides at PEO layers. They will also be valuable for development of systems to control the rate and extent of therapeutic peptide release from PEO layers, based on modulation of their amphiphilicity and surface density.

Acknowledgments

The authors thank Dr. Kerry McPhail of the OSU College of Pharmacy for use of her CD instrument. This work was supported in part by the National Institute of Biomedical Imaging and Bioengineering (NIBIB, Grant No. R01EB011567). The content is solely the responsibility of the authors and does not necessarily represent the official views of NIBIB or the National Institute of Health.

3.5. References

[1] X. Wu, M.P. Ryder, J. McGuire, K.F. Schilke, Adsorption, structural alteration and elution of peptide from pendant PEO layers, Colloids Surf. B. Biointerfaces 112 (2013) 23-29.

[2] F. Costa, I.F. Carvalho, R.C. Montelaro, P. Gomes, M.C.L. Martins, Covalent immobilization of antimicrobial peptides (AMPs) onto biomaterial surfaces, Acta Biomater. 7 (2011) 1431-1440.

[3] B. Deslouches, I.A. Gonzalez, D. DeAlmeida, K. Islam, C. Steele, R.C. Montelaro T.A. Mietzner, De novo-derived cationic antimicrobial peptide activity in a murine model of Pseudomonas aeruginosa bacteraemia, J. Antimicrob. Chemother. 60 (2007) 669-672.

[4] B. Deslouches, K. Islam, J.K. Craigo, S.M. Paranjape, R.C. Montelaro T.A. Mietzner, Activity of the de novo engineered antimicrobial peptide WLBU2 against Pseudomonas aeruginosa in human serum and whole blood: Implications for systemic applications, Antimicrob. Agents Chemother. 49 (2005) 3208-3216.

[5] B. Deslouches, S.M. Phadke, V. Lazarevic, M. Cascio, K. Islam, R.C. Montelaro, T.A. Mietzner, De novo generation of cationic antimicrobial peptides: Influence of length and tryptophan substitution on antimicrobial activity, Antimicrob. Agents Chemother. 49 (2005) 316-322.

[6] I.A. Gonzalez, X.X. Wong, D. De Almeida, R. Yurko, S. Watkins, K. Islam, R.C. Montelaro, A. El-Ghannam T.A. Mietzner, Peptides as potent antimicrobials tethered to a solid surface: Implications for medical devices, Nat. Precedings (2008).

[7] S.A. Onaizi, S.S.J. Leong, Tethering antimicrobial peptides: Current status and potential challenges, Biotechnol. Adv. 29 (2011) 67-74.

[8] M.C. Skinner, A.O. Kiselev, C.E. Isaacs, T.A. Mietzner, R.C. Montelaro, M.F. Lampe, Evaluation of WLBU2 peptide and 3-O-octyl-sn-glycerol lipid as active ingredients for a topical microbicide formulation targeting Chlamydia trachomatis, Antimicrob. Agents Chemother. 54 (2010) 627-636.

[9] A.A. Adzhubei, M.J.E. Sternberg, A.A. Makarov, Polyproline-II helix in proteins: Structure and function, J. Mol. Biol. 425 (2013) 2100-2132.

[10] B. Bochicchio, A.M. Tamburro, Polyproline II structure in proteins: Identification by chiroptical spectroscopies, stability, and functions, Chirality 14 (2002) 782-792.

[11] A.V. Mikhonin, N.S. Myshakina, S.V. Bykov, S.A. Asher, UV resonance raman determination of polyproline II, extended 2.51-helix, and β-sheet ψ angle energy landscape in poly-*L*-lysine and poly-*L*-glutamic acid, J. Am. Chem. Soc. 127 (2005) 7712-7720.

[12] J.M. Rifkind, Helix–coil transition of poly-*L*-arginine: A comparison with other basic polypeptides, Biopolymers 8 (1969) 685-688.

[13] M.L. Tiffany, S. Krimm, Circular dichroism of the "random" polypeptide chain, Biopolymers 8 (1969) 347-359.

[14] M.C. Lampi, X. Wu, K.F. Schilke, J. McGuire, Structural attributes affecting peptide entrapment in PEO brush layers, Colloids Surf. B. Biointerfaces 106 (2013) 79-85.

[15] Y.-C. Tai, J. McGuire, J.A. Neff, Nisin antimicrobial activity and structural characteristics at hydrophobic surfaces coated with the PEO–PPO–PEO triblock surfactant Pluronic® F108, J. Colloid Interface Sci. 322 (2008) 104-111.

[16] J.K. Dill, J.A. Auxier, K.F. Schilke, J. McGuire, Quantifying nisin adsorption behavior at pendant PEO layers, J. Colloid Interface Sci., 395 (2013) 300-305.

[17] H. Lee, D.H. Kim, K.N. Witte, K. Ohn, J. Choi, B. Akgun, S. Satija Y.-Y. Won, Water is a poor solvent for densely grafted poly (ethylene oxide) chains: A conclusion drawn from a self-consistent field theory-based analysis of neutron reflectivity and surface pressure–area isotherm data, J. Phys. Chem. B 116 (2012) 7367-7378.

[18] D.A.D. Parry, R.D.B. Fraser, J.M. Squire, Fifty years of coiled-coil and α-helical bundles: A close relationship between sequence and structure, J. Struct. Biol. 163 (2008) 258-269.

[19] N.E. Zhou, C.M. Kay, R.S. Hodges, Synthetic model proteins: position effects of interchain hydrophobic interactions on stability of two-stranded α-helical coiled-coils, J. Biol. Chem. 267 (1992) 2664-2670.

[20] N.E. Zhou, C.M. Kay, R.S. Hodges, Synthetic model proteins: The relative contribution of leucine residues at the nonequivalent positions of the 3-4 hydrophobic repeat to the stability of the two-stranded α-helical coiled-coil, Biochemistry 31 (1992) 5739-5746.

[21] G. Grigoryan, A.E. Keating, Structural specificity in coiled-coil interactions, Curr. Opin. Struc. Biol. 18 (2008) 477-483.

[22] B. Rubinov, N. Wagner, H. Rapaport, G. Ashkenasy, Self-replicating amphiphilic beta-sheet peptides. Angew. Chem. Int. Ed. Engl. 48 (2009) 6683-6686.

[23] K. Wang, J.D. Keasling, S.J. Muller, Effects of the sequence and size of non-polar residues on self-assembly of amphiphilic peptides, Int. J. Biol. Macromol. 36 (2005) 232-240.

[24] N.J. Greenfield, Methods to estimate the conformation of proteins and polypeptides from circular dichroism data, Anal. Biochem. 235 (1996) 1-10.

[25] N.J. Greenfield, G.D. Fasman, Computed circular dichroism spectra for the evaluation of protein conformation, Biochemistry (Mosc). 8 (1969) 4108-4116.

[26] L. Whitmore, B.A. Wallace, Dichroweb, an online server for protein secondary structure analyses from circular dichroism spectroscopic data, Nucleic Acids Res. 32 (2004) W668-W673.

[27] L. Whitmore, B.A. Wallace, Protein secondary structure analyses from circular dichroism spectroscopy: Methods and reference databases, Biopolymers 89 (2008) 392-400.

[28] T.M. Cooper, R.W. Woody, The effect of conformation on the CD of interacting helices: a theoretical study of tropomyosin, Biopolymers 30 (1990) 657-676.

[29] R. Cukalevski, M. Lundqvist, C. Oslakovic, B. Dahlback, S. Linse, T. Cedervall, Structural changes in apolipoproteins bound to nanoparticles, Langmuir, 27 (2011) 14360-14369.

[30] F. Fiumara, L. Fioriti, E.R. Kandel, W.A. Hendrickson, Essential role of coiled coils for aggregation and activity of Q/N-rich prions and polyQ proteins, Cell 143 (2010) 1121-1135.

[31] N.D. Lazo, D.T. Downing, Circular dichroism of model peptides emulating the amphipathic α-helical regions of intermediate filaments, Biochemistry 36 (1997) 2559-2565.

[32] S.A. Potekhin, T.N. Melnik, V. Popov, N.F. Lanina, A.A. Vazina, P. Rigler, A.S.Verdini, G. Corradin, A.V. Kajava, De novo design of fibrils made of short α-helical coiled coil peptides, Chem. Biol. 8 (2001) 1025-1032.

[33] J.P. Schneider, J.W. Kelly, Templates that induce α-helical, β-sheet, and loop conformations, Chem. Rev. 95 (1995) 2169-2187.

[34] F. Höök, B. Kasemo, T. Nylander, C. Fant, K. Sott, H. Elwing, Variations in Coupled Water, Viscoelastic Properties, and Film Thickness of a Mefp-1 Protein Film during Adsorption and Cross-Linking: A Quartz Crystal Microbalance with Dissipation Monitoring, Ellipsometry, and Surface Plasmon Resonance Study, Anal. Chem. 73 (2001) 5796-5804.

[35] F. Höök, J. Vörös, M. Rodahl, R. Kurrat, P. Böni, J.J. Ramsden, M. Textor, N.D. Spencer ND, P. Tengvall, J. Gold, B. Kasemo, A comparative study of protein adsorption on titanium oxide surfaces using in situ ellipsometry, optical waveguide lightmode spectroscopy, and quartz crystal microbalance/dissipation. Colloids Surf. B. Biointerfaces 24 (2002) 155-170.

[36] M.V. Voinova, M. Jonson, B. Kasemo, 'Missing mass' effect in biosensor's QCM applications. Biosens. Bioelectron. 17(2002): 835-841.

[37] M. Binazadeh, H. Zeng, L.D. Unsworth, Effect of peptide secondary structure on adsorption and adsorbed film properties, Acta Biomater. 9 (2013) 6403-6413.

SEQUENTIAL AND COMPETITIVE ADSORPTION OF PEPTIDES AT PENDANT PEO LAYERS

Xiangming Wu, Matthew P. Ryder, Joseph McGuire, Karl F. Schilke

School of Chemical, Biological and Environmental Engineering, Oregon State University, Corvallis, OR 97331

For submission to Biomaterials Literature

CHAPTER 4

SEQUENTIAL AND COMPETITIVE ADSORPTION OF PEPTIDES AT PENDANT PEO LAYERS

Abstract

Our earlier work provided direction for development of responsive drug delivery systems based on modulation of structure, amphiphilicity and surface density of bioactive peptides entrapped within pendant polyethylene oxide (PEO) brush layers. At low peptide surface density, amphiphilicity promotes retention of the peptides within the hydrophobic inner region of the PEO layer, thereby increases their adsorption affinity. Peptide-peptide interactions which take place when peptide surface density is sufficiently high can substantially affect the rate and extent of peptide elution from the PEO brush layer. In this work, we describe the sequential and competitive adsorption behavior of peptides at pendant PEO brush layers, and show that adsorption and desorption of each peptide is governed by peptide amphiphilicity. Three cationic peptides were used in this study: the arginine-rich amphiphilic peptide WLBU2, the chemically identical but scrambled peptide S-WLBU2, and the non-amphiphilic peptide poly-*L*-arginine (PLR). Optical waveguide lightmode spectroscopy (OWLS) was used to quantify the rate and extent of peptide adsorption and elution at surfaces coated with PEO. UV spectroscopy and time-of-flight secondary ion mass spectrometry (TOF-SIMS) were used to quantify the extent of peptide exchange during the course of sequential and competitive adsorption. Circular dichroism (CD) was used to evaluate conformational changes of peptide mixture at PEO-coated silica nanoparticles. Results show that amphiphilic peptides are able to displace

adsorbed non-amphiphilic peptides in PEO layers, while non-amphiphilic peptides cannot displace amphiphilic ones. Peptides of high amphiphilicity are expected to dominate the competitive adsorption with less amphiphilic or non-amphiphilic peptides in PEO layers.

Keywords: sequential adsorption; competitive adsorption; PEO brush; WLBU2; cationic amphiphilic peptides; polyarginine; circular dichroism (CD)

4.1. Introduction

In earlier work [1, 2] we used circular dichroism (CD), optical waveguide lightmode spectroscopy (OWLS), and quartz crystal microbalance with dissipation monitoring (QCM-D) to study the adsorption and desorption behavior of poly-*L*-arginine (PLR) and the cationic amphiphilic peptide (CAP) WLBU2 in pendant PEO layers. Those results indicated that the adsorption of small peptides of similar size is governed by their secondary structure, with entrapment and elution at the PEO layer being determined by peptide amphiphilicity and surface density. Specifically, some degree of structural order (α-helix content) is necessary for peptide entry into PEO layers [1]. At low peptide surface density, interactions between non-polar groups of WLBU2 and the hydrophobic inner region of the PEO brush result in irreversible entrapment and resistance to elution. However, at high peptide surface density, intermolecular interactions between WLBU2 peptides resulted in conformational changes which compromised this resistance to elution. The non-amphiphilic peptide PLR did not show strong peptide-PEO chain interactions and its entrapment was always reversible [2].

WLBU2 is a synthetic, 24-residue CAP with 13 positively charged arginine residues, and 11 non-polar valine or tryptophan residues. It shows substantial promise for clinical applications, due to its wide spectrum antimicrobial activity against both Gram-negative and Gram-positive bacteria under physiological conditions [3-9]. The structure of WLBU2 in water is substantially disordered, but the peptide gains considerable secondary structure, involving segregation of its positively-charged and hydrophobic groups onto opposing faces of an α-helix, in the presence of counterions, membrane-

mimetic solvents, or bacterial membranes. Moreover, WLBU2 retains its antimicrobial activity when immobilized at solid surfaces by a number of methods [3, 7-9]. While chemically identical to WLBU2, the scrambled sequence of S-WLBU2 eliminates the ordered segregation of positively-charged and hydrophobic residues of WLBU2 during helix formation [2], and is associated with a very low hydrophobic moment in comparison to WLBU2 (0.1 vs. 10.7, respectively) [10]. PLR is chemically homogeneous and not amphiphilic. When dissolved in water under neutral pH, PLR adopts a combination of random coil and extended structures (e.g. polyproline-II and 2.5_1 helix), while both WLBU2 and S-WLBU2 show a random coil structure [1, 4-6, 11-14]. An α-helical conformation can be achieved in all three peptides by addition of perchlorate ions (ClO_4^-) [1, 13].

In this paper, we describe the sequential and competitive adsorption behavior of peptides, including PLR, WLBU2 and S-WLBU2, at pendant PEO brush layers. Solution depletion method and CD were used to evaluate competitive peptide exchange and peptide conformational change at PEO-coated silica nanoparticles. OWLS and time-of-flight secondary ion mass spectrometry (TOF-SIMS) were used to directly detect peptide sequential and competitive adsorption on covalently-immobilized PEO brush layers.

4.2. Materials and Methods

Peptides and materials. Synthetic poly-*L*-arginine hydrochloride (PLR, n ≈ 30, M_n = 4.7 kDa, PDI < 1.20) was purchased from Alamanda Polymers (Huntsville, AL). The 24-

residue peptides WLBU2 (RRWVRRVRRWVRRVVRVVRRWVRR, 3.4 kDa) and the scrambled sequence S-WLBU2 (VWRVRVRRRWRVRVWVRVRRRRVR) were purchased from Genscript (Piscataway, NJ). All peptides were used without further purification. Stock solutions of each peptide at 5 mg/mL in HPLC water were frozen in 1 mL aliquots, which were thawed and then diluted immediately before use to 0.2 mg/mL in 0.2 M $HClO_4$ (to induce α-helical conformation). Diluted peptide solutions were degassed under vacuum immediately before use.

Self-assembled PEO brush layers were formed by suspension of hydrophobic silica nanoparticles (R816, Degussa, 190 m^2/g, 10-12 nm) in Pluronic® F108 (BASF) in HPLC water for 10 h on a rotator [1, 16]. The complete surface coverage of F108 is about 3.3 mg/m^2 [16, 17]. A 5× excess of F108 over this amount was used to ensure good coverage of the nanoparticles. In the sequential adsorption experiments, F108-coated nanoparticles were incubated with the first peptide (PLR, WLBU2 or S-WLBU2) under 0.2 M $HClO_4$ for 40 min at 20 ℃. In the peptide competitive adsorption experiments, an equimolar mixture of PLR and WLBU2, or PLR and S-WLBU2 were incubated with F108-coated nanoparticles under the same conditions. The concentration of nanoparticles was varied between 1 mg/mL to 4 mg/mL, in order to provide different available surface area (0.2 – 0.05 peptides/nm^2) for peptide adsorption and exchange.

Quantify peptide exchange on PEO-coated nanoparticles. In the sequential adsorption experiments, the peptide-nanoparticle suspensions were rinsed by centrifugation (10,000 rpm, 20 min) and resuspension in 0.2 M $HClO_4$; this process was repeated twice to remove excess peptide. The amount of peptide removed in each of the supernatants from

the nanoparticles was then quantified by UV spectrophotometry at 230 nm (for PLR) or 280 nm (for WLBU2 and S-WLBU2), in order to calculate the initial amount of first peptide in the PEO layer. The second peptide was then introduced to the resuspended nanoparticles, followed by 40 min incubation and rinsing with $HClO_4$. The amount of each peptide in the supernatants was again quantified by UV spectrophotometry at 230 nm and 280 nm. In the competitive adsorption experiment, F108-coated nanoparticles were incubated with peptide mixture for 40 min. The peptide-nanoparticle suspensions were centrifuged, and the change in supernatant absorbance at 230 and 280 nm was used to calculate the amount of each peptide entrapped the PEO layer. Experiments were conducted in triplicate and only slight (< 5%) differences in absorbance were observed.

Evaluation of time-dependent peptide secondary structure. The secondary structure change of WLBU2 and S-WLBU2 with respect to time after introduction to F108-coated nanoparticles was evaluated by circular dichroism (CD) using a Jasco J-815 spectropolarimeter (Eaton, MD) at 25 ℃. The instrument was calibrated using 0.6 mg/mL *D*(+)–camphorsulfonic acid. Spectra were recorded in a cylindrical cuvette (0.1 cm pathlength) from 185 to 260 nm in 0.5 nm increments, and five scans were averaged to increase the signal-to-noise ratio. All peptide solutions were filtered (0.2 μm) prior to contact with nanoparticles and recording of CD spectra. All spectra were blanked against peptide-free nanoparticles suspensions. The spectra from each of three replicates for each sample exhibited only slight (~5%) differences in signal intensity; representative spectra are thus shown throughout.

Stabilization of F108 coatings on OWLS waveguides and silicon wafers. SiO_2-coated OW2400c OWLS sensors (MicroVacuum, Budapest, Hungary) and silicon wafers with 300 nm thermal SiO_2 were cleaned by submersion in 5% w/v sodium dodecyl sulfate (SDS) for 30 min, followed by 10 min wash at 80 ℃ in 5:1:1 mixture of H_2O:HCl:H_2O_2, then rinsed with HPLC H_2O and dried under a stream of nitrogen [18]. The surfaces of OWLS sensors and silicon wafers were then modified by vapor deposition of trichlorovinylsilane (TCVS, TCI America, Portland, OR). 200 μL of TCVS was evaporated at 20 ℃ into a stream of dry nitrogen carrier gas, which was directed over the waveguide and silicon wafers surfaces for 4 h. The silanized waveguides and silicon wafers were then immersed in a solution of 5% w/v Pluronic® F108 in water, and were rotated in solution overnight. After incubation, samples were γ-irradiated to 0.3 Mrad to covalently attach the F108 to the surface [16, 19]. The irradiated sensors were rinsed with HPLC water, dried with nitrogen, and stored in the dark used.

Measurement of the rate and extent of peptide adsorption. Sequential and competitive adsorption of peptides were measured with an OWLS 210 instrument (MicroVacuum, Budapest, Hungary). A Rheodyne manual sample injector was used to inject sample solutions through a flow loop (~4.0 mL) into the OWLS flow cell. Flow rates were maintained at 50 μL/min and solution temperature was kept at 20 ℃ by the internal TC heater/cooler unit. Incident angle scans were performed from -5 ° to 5 ° at a step size of 0.01 °. Both peaks of each of the transverse electric and magnetic modes were measured to determine the relative refractive index of the surface adlayer. OWLS experiments began with a baseline of peptide-free perchloric acid ($HClO_4$), followed by injection of

0.2 mg/mL peptide $HClO_4$, and a subsequent rinse with $HClO_4$. Adsorption and elution steps were each allowed to proceed for 40 min.

Peptide adsorption on F108-coated silicon wafers. For sequential adsorption of peptides to the PEO brush layer, F108-coated silicon wafers were incubated with freshly made peptide solutions (PLR, WLBU2 or S-WLBU2) at 20 ℃ for 40 min, then rinsed with peptide-free $HClO_4$ to remove loosely-bound peptides. The rinsed wafers were then incubated with the second peptide for 40 min, and the rinse step was repeated. In competitive adsorption experiments, F108-coated silicon wafers were incubated with either a binary mixture of PLR and WLBU2, or PLR and S-WLBU2, followed by a rinse step with peptide-free $HClO_4$. After rinse, all peptide-loaded wafers, and peptide-free F108-coated and uncoated TCVS silicon wafers were dried under vacuum at ambient temperature overnight prior to analysis with TOF-SIMS.

Time-of-flight secondary ion mass spectrometry (TOF-SIMS). Positive secondary ion spectra were acquired for each sample on a TOF-SIMS IV instrument (Ion-TOF GmbH, Germany) using a pulsed 25 keV bismuth primary ion beam. The dose density of the primary beam was kept below 10^{12} ions/cm^2 to ensure that the static limit was not exceeded. Spectra were collected from three randomly chosen 100 × 100 μm areas on each sample. Secondary ions were collected over a range of 0 – 400 *m/z*. The mass resolution of each spectrum was between 4000 and 8000, and the spectra were calibrated to less than 20 ppm using three or more C_nH_{2n-1} peaks (*n* from 2 to 5). Peak intensities were normalized against the total ion intensity of each spectrum.

4.3. Results and Discussion

Peptide sequential and competitive adsorption on PEO-coated nanoparticles. Our earlier report [1] demonstrated that peptides of high amphiphilicity such as WLBU2 (hydrophobic moment 10.7) are able to interact strongly with the hydrophobic inner region of the PEO brush layer, resulting in peptide entrapment and conformational change that is irreversible to elution [1, 16, 20]. In contrast, the adsorption and conformational change is reversible with changing solution conditions for a chemically identical but less amphiphilic peptide (S-WLBU2, hydrophobic moment 0.1) or a non-amphiphilic peptide (PLR). When the surface density of WLBU2 is sufficiently high, the peptide-PEO interaction would be compromised and result in an increase in the elutability [2]. It is still fair to expect that the adsorption affinity of a peptide at a PEO layer is increased with its amphiphilicity.

In all peptide sequential and competitive adsorption experiments, the concentration of each peptide was held at a concentration (0.2 mg/mL), which theoretically fully covers the surface of 1 mg/mL F108-coated nanoparticles in monolayers [16, 17]. Figure 4.1 shows the percentage of first peptide displaced by the second (e.g., %PLR displaced by WLBU2 in the case of PLR → WLBU2) during the whole course of sequential adsorption of two peptides. Generally, an amphiphilic peptide (WLBU2 or S-WLBU2) is able to displace most of the non-amphiphilic peptide PLR (98% and 76%, respectively) in a PEO layer when there is limited space for peptide adsorption (i.e. 1 mg/mL F108-coated NPs, peptide surface density 0.2 molecules/nm^2). In contrast, only a small amount of adsorbed WLBU2 or S-WLBU2 (8% and 6%, respectively) in the PEO brush layer can

be displaced by the sequentially introduced PLR. This is consistent with the well-known displacement of adsorbed fibrinogen or other biopolymers by introduction of proteins of higher adsorption affinity for the surface [21-23]. As the peptide surface density decreased, the amount of PLR displaced by WLBU2 or S-WLBU2 substantially decreased (Figure 4.1). This is due to the increase in the amount of nanoparticles provides more available surface area for peptide adsorption, therefore more WLBU2 or S-WLBU2 can be incorporate into the PEO layer without significantly displacing pre-adsorbed PLR.

It is important to note that the amount of PLR displaced by S-WLBU2 is always less than that by WLBU2 (Figure 4.1). We have previously shown that the interaction between S-WLBU2 and the hydrophobic inner region of the PEO layer is weaker than for WLBU2, due to the low amphiphilicity of S-WLBU2 [2]. Taken together, it is reasonable to expect that the ability of one peptide to displace the other at a PEO brush layer is directly related to their amphiphilicity and free surface area.

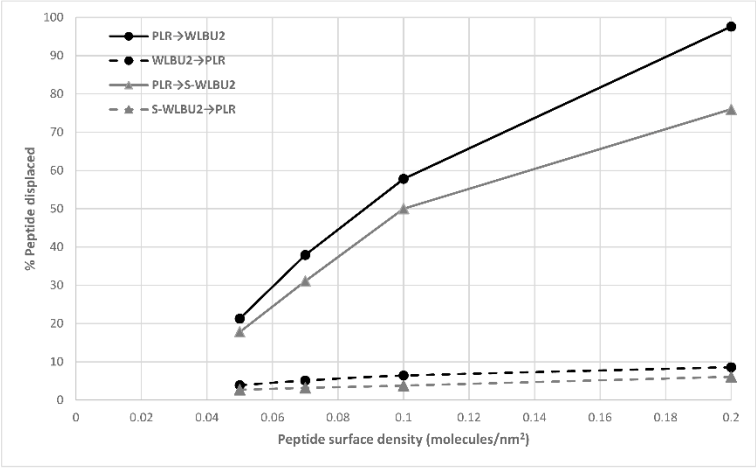

Figure 4.1. Percentage of first peptide being displaced by the second during the sequential adsorption of PLR, WLBU2 and S-WLBU2.

When peptides are introduced to F108-coated nanoparticles in a binary mixture, the amphiphilic peptide (WLBU2 or S-WLBU2) usually dominates the adsorption (Table 4.1). When the mixture of PLR and WLBU2 is introduced to 1 mg/mL F108-coated nanoparticles, 95% of WLBU2 peptides adsorb into the PEO brush layer from the solution, while only 8.5% PLR is able to enter the brush. The percentage of adsorbed PLR increases with the concentration of nanoparticles, due to the presence of space in the PEO layer that is not occupied by WLBU2. Similarly, when the mixture of PLR and S-WLBU2 was introduced to 1 mg/mL F108-coated nanoparticles, 94% S-WLBU2 and 9% PLR adsorbs. As the concentration of nanoparticles increases, surface area increases and PLR is able to adsorb to a greater extent. The change in the amount of adsorbed WLBU2 and S-WLBU2 with respect to nanoparticle concentration is negligible. These results strongly suggest that an amphiphilic peptide will dominate the PEO layer when competing with a non-amphiphilic peptide for the fixed surface capacity. This is entirely consistent with many previous findings on competitive protein adsorption: proteins of greater affinity for the solid surfaces normally dominate the adsorption from binary or ternary mixtures [23-25].

Table 4.1. Competitive adsorption of PLR and WLBU2, and PLR and S-WLBU2 binary mixture

	PLR+WLBU2 mixture		**PLR+S-WLBU2 mixture**	
	%PLR adsorbed	%WLBU2 adsorbed	%PLR adsorbed	%S-WLBU2 adsorbed
1 mg/mL NPs (0.2 peptide/nm^2)	8%	95%	9%	94%
2 mg/mL NPs (0.1 peptide/nm^2)	19%	97%	23%	96%
3 mg/mL NPs (0.07 peptide/nm^2)	25%	98%	32%	98%
4 mg/mL NPs (0.05 peptide/nm^2)	47%	99%	63%	98%

Sequential and competitive adsorption kinetics at covalently immobilized PEO layers.

Figure 4.2 shows the adsorption and elution kinetics of sequential and competitive adsorption of PLR, WLBU2 and S-WLBU2 on covalently attached PEO layers. Both PLR and WLBU2 have very similar and fast adsorption kinetics, while the adsorbed mass of WLBU2 is significantly higher than PLR (Figure 4.2a). PLR is resistant to elution with $HClO_4$, a helix-stabilizing solvent [1], while a large portion of the adsorbed WLBU2 is elutable. This is due to the high peptide surface density ~550 ng/cm^2 (i.e., 1.1 molecules/nm^2) which promotes hydrophobic interactions between WLBU2 molecules. At high surface density, WLBU2 forms intertwined α-helical coiled-coils, which compromise its resistance to elution [2]. Unlike WLBU2, PLR is non-amphiphilic and has positive charges which uniformly surround the α-helix. The electrostatic repulsions are expected to prevent interactions and increase the average distance between PLR molecules, therefore the adsorbed mass of PLR in the PEO layer is substantially less than WLBU2 [2].

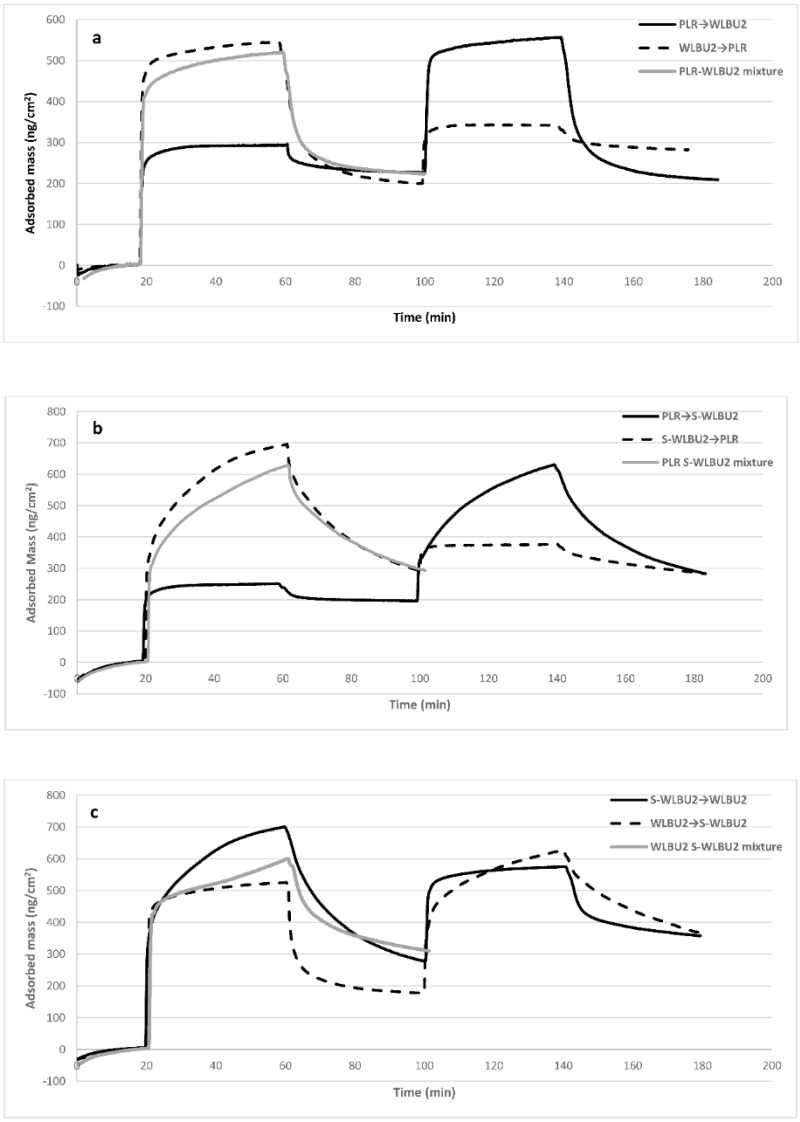

Figure 4.2. Sequential and competitive adsorption of (a) PLR and WLBU2, (b) PLR and S-WLBU2, (c) WLBU2 and S-WLBU2. Baseline was achieved using 0.2 M $HClO_4$, followed by adsorption of peptide 1 (sequential adsorption) or peptide 1 & 2 mixture (competitive adsorption), and then elution with 0.2 M $HClO_4$. Adsorption of peptide 2 started immediately after elution for sequential adsorption experiments, followed by elution with 0.2 M $HClO_4$.

The difference in adsorption patterns of PLR and WLBU2 are used to evaluate their adsorption when introduced to the PEO layer sequentially or simultaneously. As shown

in Figure 4.2a, the sequential adsorption and elution of WLBU2 is not affected by the presence of pre-adsorbed PLR in the PEO layer. The adsorbed mass of WLBU2 at the peptide-free PEO layer reaches 550 ng/cm^2, and decreases to 200 ng/cm^2 after elution with $HClO_4$. Similarly, at the PLR-occupied PEO layer, the adsorbed mass also reaches 550 ng/cm^2 upon introduction of WLBU2, and decreased to 200 ng/cm^2 after elution. At the WLBU2-adsorbed PEO layer, however, the adsorbed mass increased from 200 to 340 ng/cm^2 and decreased to 294 ng/cm^2 upon elution. Both of these values are higher than observed for PLR adsorption and elution in a peptide-free PEO layer (300 and 230 ng/cm^2, respectively). This indicates the co-existence of the two peptides after sequential introduction of WLBU2 and PLR to a PEO layer. Based on these results and those from F108-coated nanoparticles presented above (Figure 4.1), it is fair to expect that PLR does not displace pre-adsorbed WLBU2 to a large extent, while WLBU2 can displace most of the pre-adsorbed PLR. The competitive adsorption of the binary mixture of PLR and WLBU2 is much more similar to the adsorption of WLBU2 than of PLR. This suggests that WLBU2 dominates the competitive adsorption with PLR at a PEO layer. The slight difference between adsorption and elution kinetics is likely due to the presence of small amounts of PLR.

In contrast, when S-WLBU2 is introduced to the PEO-coated surface, it adsorbs to a higher extent than does WLBU2 (Figure 4.2b). Previously, we have shown that WLBU2 adopts an α-helical coiled-coil conformation, while S-WLBU2 adopts a β-sheet structure at high peptide surface density in the PEO layer [2]. It has been shown that polylysine in a β-sheet conformation adsorbs more slowly, but to a significantly higher extent than α-

helical polylysine on bare gold surfaces, presumably due to stronger intermolecular hydrogen bonding among β-sheet polylysine [26-28]. More specifically, the early-stage fast adsorption is likely due to strong interactions between S-WLBU2 and the surface. The large surface area of β-sheet S-WLBU2 promotes intermolecular hydrogen bonding and hydrophobic interactions to form dense aggregates, and consequently drive further peptide adsorption with a slower rate [28, 29].

As shown in Figure 4.2b, the adsorption of S-WLBU2 is somewhat affected by the existence of PLR in the PEO layer. The adsorbed mass of S-WLBU2 at a peptide-free PEO layer reaches 700 ng/cm^2 after 40 min, and was decreased to 620 mg/cm^2 in the presence of pre-adsorbed PLR. This can be either S-WLBU2 can only partially displace PLR, or the displacement by S-WLBU2 is slower than WLBU2 displacing PLR. Introduction of PLR after S-WLBU2 (Figure 4.2a) again indicates the co-existence of PLR and S-WLBU2 at the PEO layer. The adsorption of PLR and S-WLBU2 mixtures is very similar to S-WLBU2 → PLR, suggesting that adsorption is dominated by S-WLBU2 (Figure 4.2b).

In addition, we investigated the effect of structure on sequential and competitive adsorption using WLBU2 and S-WLBU2 (Figure 4.2c). WLBU2 adsorbed to a slightly higher extent (60 ng/cm^2 more) on a S-WLBU2-loaded PEO layer than on a peptide-free PEO layer, while the peptide remaining on the surface after 40 min elution is significantly higher (180 ng/cm^2 more). However, S-WLBU2 adsorbed to a lower extent (80 ng/cm^2 less) in the presence of WLBU2 in the PEO layer, and the elution shows slower kinetics than at a PEO layer which contains only S-WLBU2. This suggests the co-

existence of the two peptides after being sequentially introduced to the PEO layer, and presumably peptide-peptide interactions promote their resistance to elution. When WLBU2 and S-WLBU2 are introduced to the PEO-coated surface simultaneously (Figure 4.2c, gray curve), the adsorption appears to occur by a two-step process. The early step (first 10 min) appears identical to WLBU2-only adsorption, followed by a slow adsorption which is similar to S-WLBU2 adsorption kinetics. It is reasonable to expect that the highly amphiphilic peptide WLBU2 dominates the early adsorption, while the adsorption of S-WLBU2 is hindered by WLBU2 until WLBU2 approaching its maximum adsorbed mass (550 ng/cm^2). Further increase in the adsorbed mass is likely due to the slow adsorption of S-WLBU2 driven by intermolecular interactions of peptides [29]. The increase in the resistance to elution with $HClO_4$ again suggests the existence of interactions between WLBU2 and S-WLBU2 in the PEO layer.

Circular dichroism was applied to evaluate time-dependent conformational changes of WLBU2 and S-WLBU2 mixture after being introduced to F108-coated nanoparticles in $HClO_4$. We have shown that both WLBU2 and S-WLBU2 show a low α-helicity (15%) in 0.2 M $HClO_4$ solution [1], and once adsorbed into the PEO layer to a large extent, WLBU2 forms α-helical coiled-coils while S-WLBU2 forms β-sheets [2]. In the first two minutes of the experiment (Figure 4.3), CD shows an α-helical coiled-coil conformation, which exhibits two minima around 208 and 222 nm with ellipticity ratio $\theta_{222nm} > \theta_{208\ nm}$ (indicating coiled-coil conformation) [30-33]. Note that after 5 min, spectrum is substantially β-sheet. This confirms that WLBU2 dominates the early adsorption. After 60 min, the peptides have largely undergone a transition from α-helical coiled-coil to β-

sheet [34-35], and no further change in spectra was observed. Moreover, the supernatant had negligible absorbance at 280 nm, which indicates the complete adsorption of both WLBU2 and S-WLBU2. These results suggest that WLBU2 adsorbs at a much higher rate than S-WLBU2. As S-WLBU2 adsorbed to some large extent, interactions between WLBU2 and S-WLBU2 will result in the conformational change of WLBU2 (from α-helical coiled-coils to β-sheet), which possibly drives further S-WLBU2 adsorption.

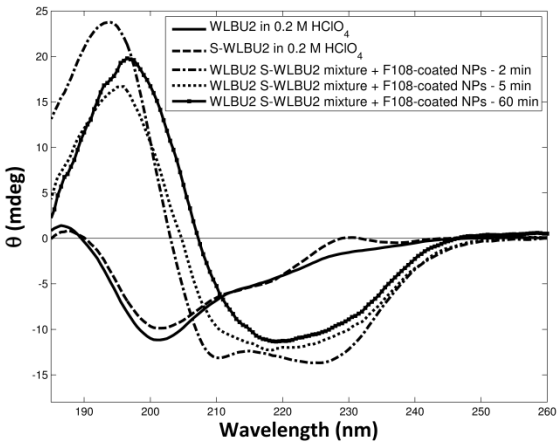

Figure 4.3. CD of the secondary structure of WLBU2 and S-WLBU2 mixture after incubation with F108-coated nanoparticles suspension for 2, 5 and 60 min.

In order to obtain more quantitative results of the peptide exchange in the PEO layer, TOF-SIMS was applied to analyze the PEO-coated surface after sequential and competitive adsorption of peptides at PEO layers.

TOF-SIMS analysis on covalently immobilized PEO layers. Sequential and competitive adsorption of PLR, WLBU2 and S-WLBU2 on OWLS waveguides was repeated on F108-coated silicon wafers.

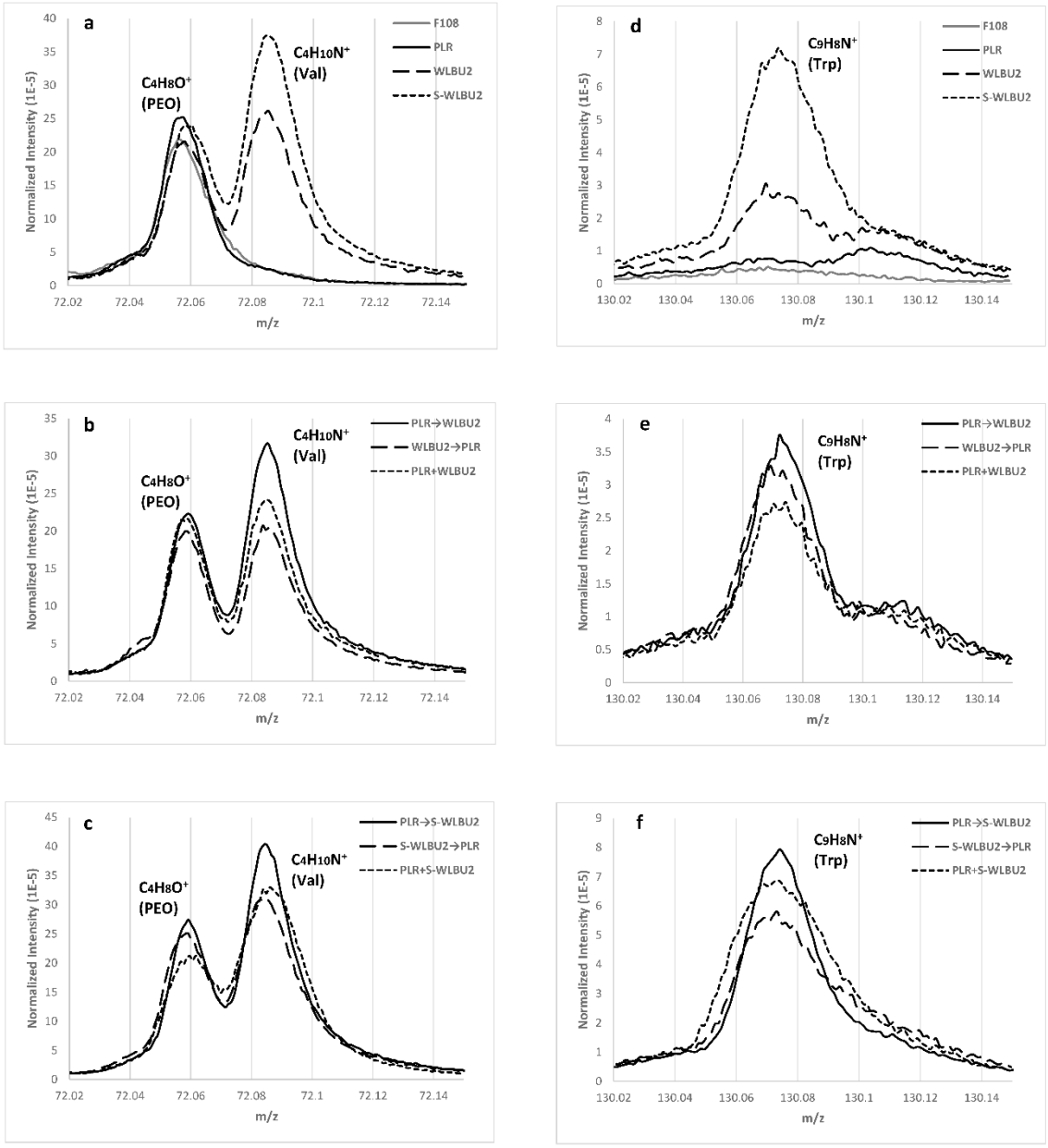

Figure 4.4. Representative secondary ion intensity of PEO, valine and tryptophan from peptide-adsorbed PEO layers on silicon wafers. All intensitites were normalized to total ion yield.

Peptide-free F108-immobilzed silicon wafer substrates show increased hydrocarbon and strong polyether signals (e.g., $C_2H_5O^+$, $C_4H_8O^+$) with respect to bare TCVS-silanized

silicon wafers (data not shown). This confirms the presence of the PEO layer on the surface. Individual peaks corresponding to valine and tryptophan in WLBU2 and S-WLBU2 can be used to distinguish them from PLR on the surface. Interferences on the amino acid peaks from the underlying substrate can be neglected in these tests since the spectra of bare TCVS and peptide-free F108-immobilized wafers both show negligible intensities at the characteristic peaks of arginine (*m/z* 59.05, 70.07, 100.08 and 127.1), valine (*m/z* 72.08 and 83.09) and tryptophan (*m/z* 130.07 and 159.09) [36-38]. Figure 4.4 shows the characteristic peaks of valine ($C_4H_{10}N^+$, *m/z* 72.08) and tryptophan ($C_9H_8N^+$, *m/z* 130.07) on surfaces before and after challenge with peptides. Surfaces contacted with WLBU2 or S-WLBU2 exhibit strong peaks at both 72.08 (Val) and 130.07 (Trp), while these peaks are absent on PLR-only and peptide-free PEO-coated surfaces (Figure 4.4, a and d). After sequential or simultaneous introduction of PLR and WLBU2, all the surfaces show strong peaks at both 72.08 and 130.07, and the normalized intensities of those peaks are similar to the surface contacted with WLBU2 only (Figure 4.4, b and e). This suggests that the presence of PLR in the PEO layer or solution does not interfere with the adsorption of WLBU2. Similarly, the presence of PLR does not have significant impact on S-WLBU2 (Figure 4.4, c and f). Both findings are consistent with OWLS results presented above.

The secondary ion intensity ratio (*R*) can provide more quantitative insight into the surface composition. *R* was calculated as the sum of intensities of valine (*m/z* 72.08 and 83.09) and tryptophan (*m/z* 130.07 and 159.09) divided by the sum of intensities of arginine (*m/z* 70.07, 100.08 and 127.1) [39, 40].

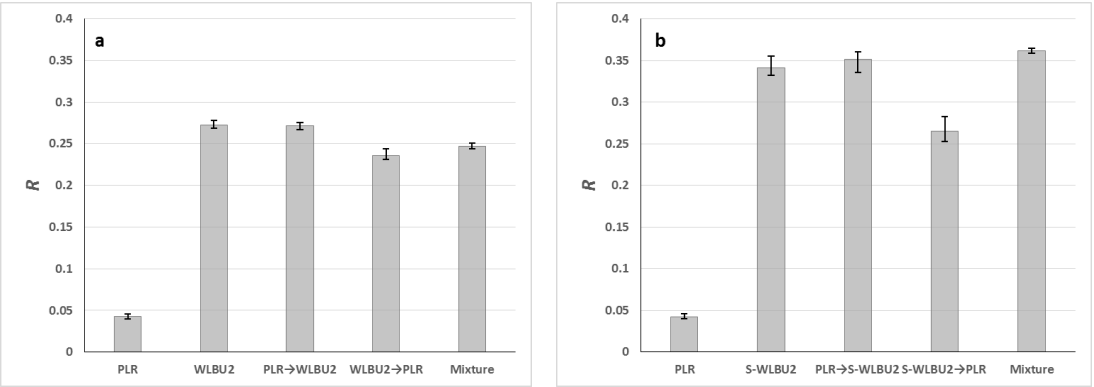

Figure 4.5. TOF-SIMS secondary ion peak intensity ratios (*R*) of: (a) PLR and WLBU2, and (b) PLR and S-WLBU2 sequential and competitive adsorption on PEO-coated silicon wafers. Peak ratios were calculated as the sum of intensities of valine and tryptophan peaks divided by the sum of intensities of arginine peaks. Error bars represent the standard deviation across three analysis areas.

Since PLR does not have valine and tryptophan residues, the *R* value of PLR-occupied surface is very low (0.0425). For WLBU2 and S-WLBU2 contacted surfaces, the ratios increased to 0.272 and 0.341, respectively (Figure 4.5). Thus, if a surface contains both PLR and WLBU2 or S-WLBU2, its *R* value should lie between 0.0425 and 0.272 or 0.341, depending on the relative amount of each peptide. As shown in Figure 4.5a, the *R* of WLBU2 adsorption on a PLR-adsorbed PEO layer (0.271) indicates the peptide on the surface is nearly 100% of WLBU2, which further suggests the complete displacement of PLR by WLBU2. The *R* values for sequential adsorption PLR on a WLBU2-adsorbed surface and the competitive adsorption of PLR and WLBU2 mixture are both slightly less than 0.271 (0.236 and 0.247, respectively). This confirms the co-existence of two peptides (Figure 4.2), and PLR only presences in a very small amount in the PEO layer. Similarly, S-WLBU2 displaces most adsorbed PLR in the PEO layer, and hinders PLR adsorption (Figure 4.5b).

In summary, the results from two distinct surface analytical techniques (OWLS and TOF-SIMS) are consistent with results from the solution depletion method using PEO-coated nanoparticles. They also further suggest that amphiphilic peptides (WLBU2 and S-WLBU2) can displace adsorbed non-amphiphilic peptides (e.g. PLR) at PEO brush layers, while PLR can displace neither WLBU2 nor S-WLBU2. When peptides are introduced simultaneously and compete for a limited surface capacity, the amphiphilic peptides are expected to dominate the adsorption.

4.4. Conclusions

The results reported here direct us to expect that the sequential and competitive adsorption behaviors of peptides at pendant PEO brush layers are governed primarily by peptide amphiphilicity. When the surface capacity is limited, amphiphilic peptides are able to displace adsorbed non-amphiphilic peptides in a PEO layer, while non-amphiphilic peptides cannot displace amphiphilic peptides. Peptides of high amphiphilicity are expected to dominate the competitive adsorption over less amphiphilic or non-amphiphilic peptides. Moreover, in this work, the interactions between adsorbed WLBU2 and S-WLBU2 in the PEO brush layer resulted in peptide conformational changes which promote their resistance to elution. Entrapment of bioactive peptides within otherwise non-fouling PEO brush layers holds promise for development of responsive drug delivery systems. These results provide information for further research on issues surrounding peptide loading and release at PEO layers.

Acknowledgements

The authors thank Dr. Kerry McPhail of the OSU College of Pharmacy for use of her CD instrument, and Dr. Joe Baio for valuable discussion on interpretation of the TOF-SIMS data. This work was supported in part by the National Institute of Biomedical Imaging and Bioengineering (NIBIB, Grant No. R01EB011567). The content is solely the responsibility of the authors and does not necessary represent the official views of NIBIB or the National Institute of Health.

4.5. References

[1] X. Wu, M.P. Ryder, J. McGuire, K.F. Schilke, Adsorption, structural alteration and elution of peptides from pendant PEO layers, Colloids Surf. B. Biointerfaces 112 (2013) 23-29.

[2] X. Wu, M.P. Ryder, J. McGuire, K.F. Schilke, Concentration effects on peptide elution from pendant PEO layers, submitted to Colloids Surf. B. Biointerfaces.

[3] F. Costa, I.F. Carvalho, R.C. Montelaro, P. Gomes, M.C.L. Martins, Covalent immobilization of antimicrobial peptides (AMPs) onto biomaterial surfaces, Acta Biomater. 7 (2011) 1431-1440.

[4] B. Deslouches, I.A. Gonzalez, D. DeAlmeida, K. Islam, C. Steele, R.C. Montelaro T.A. Mietzner, De novo-derived cationic antimicrobial peptide activity in a murine model of Pseudomonas aeruginosa bacteraemia, J. Antimicrob. Chemother. 60 (2007) 669-672.

[5] B. Deslouches, K. Islam, J.K. Craigo, S.M. Paranjape, R.C. Montelaro T.A. Mietzner, Activity of the de novo engineered antimicrobial peptide WLBU2 against Pseudomonas aeruginosa in human serum and whole blood: Implications for systemic applications, Antimicrob. Agents Chemother. 49 (2005) 3208-3216.

[6] B. Deslouches, S.M. Phadke, V. Lazarevic, M. Cascio, K. Islam, R.C. Montelaro, T.A. Mietzner, De novo generation of cationic antimicrobial peptides: Influence of length and

tryptophan substitution on antimicrobial activity, Antimicrob. Agents Chemother. 49 (2005) 316-322.

[7] I.A. Gonzalez, X.X. Wong, D. De Almeida, R. Yurko, S. Watkins, K. Islam, R.C. Montelaro, A. El-Ghannam T.A. Mietzner, Peptides as potent antimicrobials tethered to a solid surface: Implications for medical devices, Nat. Precedings (2008).

[8] S.A. Onaizi, S.S.J. Leong, Tethering antimicrobial peptides: Current status and potential challenges, Biotechnol. Adv. 29 (2011) 67-74.

[9] M.C. Skinner, A.O. Kiselev, C.E. Isaacs, T.A. Mietzner, R.C. Montelaro, M.F. Lampe, Evaluation of WLBU2 peptide and 3-O-octyl-sn-glycerol lipid as active ingredients for a topical microbicide formulation targeting Chlamydia trachomatis, Antimicrob. Agents Chemother. 54 (2010) 627-636.

[10] T.C. Terwilliger, The helical hydrophobic moment: a measure of the amphiphilicity of a helix. Nature, 299 (1982), 371-374.

[11] A.A. Adzhubei, M.J.E. Sternberg, A.A. Makarov, Polyproline-II helix in proteins: Structure and function, J. Mol. Biol. 425 (2013) 2100-2132.

[12] A.V. Mikhonin, N.S. Myshakina, S.V. Bykov, S.A. Asher, UV resonance raman determination of polyproline II, extended 2.51-helix, and β-sheet ψ angle energy landscape in poly-*L*-lysine and poly-*L*-glutamic acid, J. Am. Chem. Soc. 127 (2005) 7712-7720.

[13] J.M. Rifkind, Helix–coil transition of poly-*L*-arginine: A comparison with other basic polypeptides, Biopolymers 8 (1969) 685-688.

[14] M.L. Tiffany, S. Krimm, Circular dichroism of the “random” polypeptide chain, Biopolymers 8 (1969) 347-359.

[16] M.C. Lampi, X. Wu, K.F. Schilke, J. McGuire, Structural attributes affecting peptide entrapment in PEO brush layers, Colloids Surf. B. Biointerfaces 106 (2013) 79-85.

[17] Y.-C. Tai, J. McGuire, J.A. Neff, Nisin antimicrobial activity and structural characteristics at hydrophobic surfaces coated with the PEO–PPO–PEO triblock surfactant Pluronic® F108, J. Colloid Interface Sci. 322 (2008) 104-111.

[18] M.P. Ryder, J. McGuire K.F. Schilke, Cleaning requirements for silica-coated sensors used in optical waveguide lightmode spectroscopy, Surf. Interface Anal. 45 (2013) 1805-1809.

[19] J.K. Dill, J.A. Auxier, K.F. Schilke, J. McGuire, Quantifying nisin adsorption behavior at pendant PEO layers, J. Colloid Interface Sci., 395 (2013) 300-305.

[20] H. Lee, D.H. Kim, K.N. Witte, K. Ohn, J. Choi, B. Akgun, S. Satija Y.-Y. Won, Water is a poor solvent for densely grafted poly (ethylene oxide) chains: A conclusion drawn from a self-consistent field theory-based analysis of neutron reflectivity and surface pressure–area isotherm data, J. Phys. Chem. B 116 (2012) 7367-7378.

[21] S.Y. Jung, S.M. Lim, F. Albertorio, G. Kim, M.C. Gurau, R.D. Yang, M.A. Holden, P.S Cremer, The Vroman effect: A molecular level description of fibrinogen displacement, J. Am. Chem. Soc. 125 (2003), 12782-12786.

[22] E. Dickinson, Mixed biopolymers at interfaces: Competitive adsorption and multilayer structures, Food Hydrocolloid. 25 (2011), 1966-1983.

[23] M. Rabe, D. Verdes, S. Seeger, Understanding protein adsorption phenomena at solid surfaces, Adv. Colloid. Interfac. 162 (2011), 87-106.

[24] S.L. Hirsh, D.R. McKenzie, N.J. Nosworthy, J.A. Denman, O.U. Sezerman, M.M.M. Bilek, The Vorman effect: Competitive protein exchange with dynamic multilayer protein aggregates, Colloids Surf. B. Biointerfaces 103 (2013) 395-404.

[25] H. Noh, E.A. Vogler, Volumetric interpretation of protein adsorption: competition from mixtures and the Vroman effect, Biomaterials 28 (2007) 405-422.

[26] K. Wang, J.D. Keasling, S.J. Muller, Effects of the sequence and size of non-polar residues on self-assembly of amphiphilic peptides, Int. J. Biol. Macromol. 36 (2005) 232-240.

[27] J.P. Schneider, J.W. Kelly, Templates that induce α-helical, β-sheet, and loop conformations, Chem. Rev. 95 (1995) 2169-2187.

[28] M. Binazadeh, H. Zeng, L.D. Unsworth, Effect of peptide secondary structure on adsorption and adsorbed film properties, Acta Biomater. 9 (2013) 6403-6413.

[29] J.J Grigsby, H.W. Blanch, J.M. Prausnitz, Effect of secondary structure on the potential of mean force for poly-lysine in the α-helix and β-sheet conformations, Biophys. Chem. 99 (2002) 107-116.

[30] T.M. Cooper, R.W. Woody, The effect of conformation on the CD of interacting helices: a theoretical study of tropomyosin, Biopolymers 30 (1990) 657-676.

[31] N.D. Lazo, D.T. Downing, Circular dichroism of model peptides emulating the amphipathic α-helical regions of intermediate filaments, Biochemistry 36 (1997) 2559-2565.

[32] F. Fiumara, L. Fioriti, E.R. Kandel, W.A. Hendrickson, Essential role of coiled coils for aggregation and activity of Q/N-rich prions and polyQ proteins, Cell 143 (2010) 1121-1135.

[33] R. Cukalevski, M. Lundqvist, C. Oslakovic, B. Dahlback, S. Linse, T. Cedervall, Structural changes in apolipoproteins bound to nanoparticles, Langmuir, 27 (2011) 14360-14369.

[34] N.J. Greenfield, Methods to estimate the conformation of proteins and polypeptides from circular dichroism data, Anal. Biochem. 235 (1996) 1-10.

[35] N.J. Greenfield, G.D. Fasman, Computed circular dichroism spectra for the evaluation of protein conformation, Biochemistry (Mosc). 8 (1969) 4108-4116.

[36] N.T. Samuel, M.S. Wagner, K.D. Dornfeld, D.G. Castner, Analysis of poly (amino acids) by static time-of-flight secondary ion mass spectrometry (TOF-SIMS), Surf. Sci. Spectra 8 (2001) 163-184.

[37] D.S. Mantus, B.D. Ratner, B.A. Carlson, J.F. Moulder, Static secondary ion mass spectrometry of adsorbed proteins. Anal. Chem. 65 (1993) 1431-1438.

[38] K.F. Schilke, J. McGuire, Detection of nisin and fibrinogen adsorption on poly (ethylene oxide) coated polyurethane surfaces by time-of-flight secondary ion mass spectrometry (TOF-SIMS), J. Colloid Interface Sci., 358 (2011) 14-24.

[39] J.E. Baio, T. Weidner, G. Interlandi, C. Mendoza-Barrera, H.E. Canavan, R. Michel, D.G. Castner, Probing albumin adsorption onto calcium phosphates by x-ray photoelectron spectroscopy and time-of-flight secondary ion mass spectrometry, J. Vac. Sci. Technol. B 29 (2011), 04D113 1-6.

[40] L. Baugh, T. Weidner, J.E. Baio, P.C.T. Nguyen, L.J. Gamble, P.S. Stayton, D.G. Castner, Probing the orientation of surface-immobilized protein G B1 using ToF-SIMS, sum frequency generation, and NEXAFS spectroscopy. Langmuir, 26 (2010), 16434-16441.

CHAPTER 5

GENERAL CONCLUSIONS

Chapter 2 shows that some minimal degree of structural order (α-helix) is necessary for peptide entry into the PEO layer, and that peptide location within the hydrophobic inner region of the PEO brush may result in an increase in α-helix content. Once the non-amphiphilic peptide polyarginine (PLR) was entrapped among the PEO chains of the F108 brush, we found it to be partially elutable as long as the same helix-stabilizing solvent used during the adsorption step was used for elution. However, in contact with water (which favors its disordered, non-adsorbable conformation), the adsorbed PLR was entirely elutable. In contrast, the amphiphilic peptide WLBU2 was highly resistant to elution in all cases, even upon contact with a solvent which promotes its disordered form. Therefore, it appears that the property of amphiphilicity (such as exhibited by WLBU2) is required to control peptide desorption from a PEO brush when the bulk solution conditions are changed.

Chapter 3 indicates that elution of peptides from PEO brush layers is also governed by their surface density. Peptides of high amphiphilicity can be expected to interact strongly with PEO chains after location within the layer, thus promoting their resistance to elution. However, at sufficiently high surface density, peptide-peptide interactions may result in conformational changes (e.g. formation of coiled-coils) which can compromise this resistance to elution. WLBU2, which adopts a face-segregated amphiphilic α-helical structure, was observed to form α-helices and coiled-coils, while the amphiphilic peptide (S-WLBU2) with a more uniform charge distribution formed β-sheets. These

conformational changes (from α-helix to coiled-coil and β-sheet) increased the elutability of WLBU2 and S-WLBU2, presumably by reducing the amphiphilic character of the resulting complex. In contrast, the non-amphiphilic peptide (PLR) showed no substantial change in structure or elutability with increasing peptide surface density.

Chapter 4 directs us to expect that the sequential and competitive adsorption behaviors of peptides at pendant PEO brush layers are governed primarily by peptide amphiphilicity. When the surface capacity is limited, amphiphilic peptides are able to displace adsorbed non-amphiphilic peptides in a PEO layer, while non-amphiphilic peptides cannot displace amphiphilic peptides. Peptides of high amphiphilicity are expected to dominate the competitive adsorption over less amphiphilic or non-amphiphilic peptides. Moreover, the interactions between adsorbed WLBU2 and S-WLBU2 in the PEO brush layer resulted in peptide conformational changes which promote their resistance to elution.

This work provides direction for development of responsive drug delivery systems based on modulation of solvent conditions, and the structure and amphiphilicity of bioactive peptides within PEO brush layers. Moreover, entrapment of therapeutic peptides may also support novel drug delivery strategies (e.g., PEO-coated nanoparticle carriers) that can potentially overcome barriers to oral delivery of peptide drugs.

BIBLIOGRAHY

A. Halperin, Polymer brushes that resist adsorption of model proteins: design parameters, Langmuir 15 (1999) 2525-2533.

A.A. Adzhubei, M.J.E. Sternberg, A.A. Makarov, Polyproline-II helix in proteins: Structure and function, J. Mol. Biol. 425 (2013) 2100-2132.

A.V. Mikhonin, N.S. Myshakina, S.V. Bykov S.A. Asher, UV resonance raman determination of polyproline II, extended 2.51-helix, and β-sheet ψ angle energy landscape in poly-*L*-lysine and poly-*L*-glutamic acid, J. Am. Chem. Soc. 127 (2005) 7712-7720.

B. Bochicchio, A.M. Tamburro, Polyproline II structure in proteins: Identification by chiroptical spectroscopies, stability, and functions, Chirality 14 (2002) 782-792.

B. Deslouches, I.A. Gonzalez, D. DeAlmeida, K. Islam, C. Steele, R.C. Montelaro T.A. Mietzner, De novo-derived cationic antimicrobial peptide activity in a murine model of Pseudomonas aeruginosa bacteraemia, J. Antimicrob. Chemother. 60 (2007) 669-672.

B. Deslouches, K. Islam, J.K. Craigo, S.M. Paranjape, R.C. Montelaro T.A. Mietzner, Activity of the de novo engineered antimicrobial peptide WLBU2 against Pseudomonas aeruginosa in human serum and whole blood: Implications for systemic applications, Antimicrob. Agents Chemother. 49 (2005) 3208-3216.

B. Deslouches, S.M. Phadke, V. Lazarevic, M. Cascio, K. Islam, R.C. Montelaro, T.A. Mietzner, De novo generation of cationic antimicrobial peptides: Influence of length and tryptophan substitution on antimicrobial activity, Antimicrob. Agents Chemother. 49 (2005) 316-322.

B. Rubinov, N. Wagner, H. Rapaport, G. Ashkenasy, Self-replicating amphiphilic beta-sheet peptides. Angew. Chem. Int. Ed. Engl. 48 (2009) 6683-6686.

C. Calonder, Y. Tie, P.R. Van Tassel, History dependence of protein adsorption kineticsProc, Natl. Acad. Sci. U. S. A. 98 (2001) 10664-10669.

D.S. Mantus, B.D. Ratner, B.A. Carlson, J.F. Moulder, Static secondary ion mass spectrometry of adsorbed proteins. Anal. Chem. 65 (1993) 1431-1438.

D.A.D. Parry, R.D.B. Fraser, J.M. Squire, Fifty years of coiled-coil and α-helical bundles: A close relationship between sequence and structure, J. Struct. Biol. 163 (2008) 258-269.

E. Dickinson, Mixed biopolymers at interfaces: Competitive adsorption and multilayer structures, Food Hydrocolloid. 25 (2011), 1966-1983.

E.K. Asciutto, I.J. General, K. Xiong, S.A. Asher, J.D. Madura, Sodium perchlorate effects on the helical stability of a mainly alanine peptide, Biophys. J. 98 (2010) 186-196.

F. Costa, I.F. Carvalho, R.C. Montelaro, P. Gomes, M.C.L. Martins, Covalent immobilization of antimicrobial peptides (AMPs) onto biomaterial surfaces, Acta Biomater. 7 (2011) 1431-1440.

F. Fang, J. Satulovsky, I. Szleifer, Kinetics of protein adsorption and desorption on surfaces with grafted polymers, Biophys. J. 89 (2005) 1516-1533.

F. Fiumara, L. Fioriti, E.R. Kandel, W.A. Hendrickson, Essential role of coiled coils for aggregation and activity of Q/N-rich prions and polyQ proteins, Cell 143 (2010) 1121-1135.

F. Höök, B. Kasemo, T. Nylander, C. Fant, K. Sott, H. Elwing, Variations in Coupled Water, Viscoelastic Properties, and Film Thickness of a Mefp-1 Protein Film during Adsorption and Cross-Linking: A Quartz Crystal Microbalance with Dissipation Monitoring, Ellipsometry, and Surface Plasmon Resonance Study, Anal. Chem. 73 (2001) 5796-5804.

F. Höök, J. Vörös, M. Rodahl, R. Kurrat, P. Böni, J.J. Ramsden, M. Textor, N.D. Spencer, P. Tengvall, J. Gold B. Kasemo, A Comparative Study of Quantitative Protein Adsorption on Titanium Oxide Surfaces Using in situ Ellipsometry, Optical Waveguide Lightmode Spectroscopy, and Quartz Crystal Microbalance Techniques, Colloids Surf. B. Biointerfaces 24 (2002) 155-170.

G. Grigoryan, A.E. Keating, Structural specificity in coiled-coil interactions, Curr. Opin. Struc. Biol. 18 (2008) 477-483.

H. Lee, D.H. Kim, K.N. Witte, K. Ohn, J. Choi, B. Akgun, S. Satija Y.-Y. Won, Water is a poor solvent for densely grafted poly (ethylene oxide) chains: A conclusion drawn from a self-consistent field theory-based analysis of neutron reflectivity and surface pressure–area isotherm data, J. Phys. Chem. B 116 (2012) 7367-7378.

H. Noh, E.A. Vogler, Volumetric interpretation of protein adsorption: competition from mixtures and the Vroman effect, Biomaterials 28 (2007) 405-422.

H. Salmio, D. Brühwiler, Distribution of amino groups on a mesoporous silica surface after submonolayer deposition of aminopropylsilanes from an anhydrous liquid phase, The Journal of Physical Chemistry C 111 (2006) 923-929.

I.A. Gonzalez, X.X. Wong, D. De Almeida, R. Yurko, S. Watkins, K. Islam, R.C. Montelaro, A. El-Ghannam T.A. Mietzner, Peptides as potent antimicrobials tethered to a solid surface: Implications for medical devices, Nat. Precedings (2008).

J.E. Baio, T. Weidner, G. Interlandi, C. Mendoza-Barrera, H.E. Canavan, R. Michel, D.G. Castner, Probing albumin adsorption onto calcium phosphates by x-ray photoelectron spectroscopy and time-of-flight secondary ion mass spectrometry, J. Vac. Sci. Technol. B 29 (2011), 04D113 1-6.

J.J Grigsby, H.W. Blanch, J.M. Prausnitz, Effect of secondary structure on the potential of mean force for poly-lysine in the α-helix and β-sheet conformations, Biophys. Chem. 99 (2002) 107-116.

J.K. Dill, J.A. Auxier, K.F. Schilke, J. McGuire, Quantifying nisin adsorption behavior at pendant PEO layers, J. Colloid Interface Sci., 395 (2013) 300-305.

J.M. Rifkind, Helix–coil transition of poly-*L*-arginine: A comparison with other basic polypeptides, Biopolymers 8 (1969) 685-688.

J.P. Schneider, J.W. Kelly, Templates that induce α-helical, β-sheet, and loop conformations, Chem. Rev. 95 (1995) 2169-2187.

K.F. Schilke, J. McGuire, Detection of nisin and fibrinogen adsorption on poly (ethylene oxide) coated polyurethane surfaces by time-of-flight secondary ion mass spectrometry (TOF-SIMS), J. Colloid Interface Sci. 358 (2011) 14-24.

K. Wang, J.D. Keasling, S.J. Muller, Effects of the sequence and size of non-polar residues on self-assembly of amphiphilic peptides, Int. J. Biol. Macromol. 36 (2005) 232-240.

L. Baugh, T. Weidner, J.E. Baio, P.C.T. Nguyen, L.J. Gamble, P.S. Stayton, D.G. Castner, Probing the orientation of surface-immobilized protein G B1 using ToF-SIMS, sum frequency generation, and NEXAFS spectroscopy. Langmuir, 26 (2010), 16434-16441.

L. Whitmore, B.A. Wallace, Dichroweb, an online server for protein secondary structure analyses from circular dichroism spectroscopic data, Nucleic Acids Res. 32 (2004) W668-W673.

L. Whitmore, B.A. Wallace, Protein secondary structure analyses from circular dichroism spectroscopy: Methods and reference databases, Biopolymers 89 (2008) 392-400.

M. Binazadeh, H. Zeng, L.D. Unsworth, Effect of peptide secondary structure on adsorption and adsorbed film properties, Acta Biomater. 9 (2013) 6403-6413.

M. Rabe, D. Verdes, S. Seeger, Understanding protein adsorption phenomena at solid surfaces, Adv. Colloid. Interfac. 162 (2011), 87-106.

M.C. Lampi, X. Wu, K.F. Schilke, J. McGuire, Structural attributes affecting peptide entrapment in PEO brush layers, Colloids Surf. B. Biointerfaces 106 (2013) 79-85.

M.C. Skinner, A.O. Kiselev, C.E. Isaacs, T.A. Mietzner, R.C. Montelaro M.F. Lampe, Evaluation of WLBU2 peptide and 3-O-octyl-sn-glycerol lipid as active ingredients for a topical microbicide formulation targeting Chlamydia trachomatis, Antimicrob. Agents Chemother. 54 (2010) 627-636.

M.L. Tiffany, S. Krimm, Circular dichroism of the “random” polypeptide chain, Biopolymers 8 (1969) 347-359.

M.P. Ryder, J. McGuire K.F. Schilke, Cleaning requirements for silica-coated sensors used in optical waveguide lightmode spectroscopy, Surf. Interface Anal. 45 (2013) 1805-1809.

M.P. Ryder, K.F. Schilke, J.A. Auxier, J. McGuire, J.A. Neff, Nisin adsorption to polyethylene oxide layers and its resistance to elution in the presence of fibrinogen, J. Colloid Interface Sci. 350 (2010) 194-199.

M.V. Voinova, M. Jonson, B. Kasemo, 'Missing mass' effect in biosensor's QCM applications. Biosens. Bioelectron. 17(2002): 835-841.

N.D. Lazo, D.T. Downing, Circular dichroism of model peptides emulating the amphipathic α-helical regions of intermediate filaments, Biochemistry 36 (1997) 2559-2565.

N.E. Zhou, C.M. Kay, R.S. Hodges, Synthetic model proteins: position effects of interchain hydrophobic interactions on stability of two-stranded α-helical coiled-coils, J. Biol. Chem. 267 (1992) 2664-2670.

N.E. Zhou, C.M. Kay, R.S. Hodges, Synthetic model proteins: The relative contribution of leucine residues at the nonequivalent positions of the 3-4 hydrophobic repeat to the stability of the two-stranded α-helical coiled-coil, Biochemistry 31 (1992) 5739-5746.

N.J. Greenfield, Methods to estimate the conformation of proteins and polypeptides from circular dichroism data, Anal. Biochem. 235 (1996) 1-10.

N.J. Greenfield, G.D. Fasman, Computed circular dichroism spectra for the evaluation of protein conformation, Biochemistry (Mosc). 8 (1969) 4108-4116.

N.T. Samuel, M.S. Wagner, K.D. Dornfeld, D.G. Castner, Analysis of poly (amino acids) by static time-of-flight secondary ion mass spectrometry (TOF-SIMS), Surf. Sci. Spectra 8 (2001) 163-184.

R. Cukalevski, M. Lundqvist, C. Oslakovic, B. Dahlback, S. Linse, T. Cedervall, Structural changes in apolipoproteins bound to nanoparticles, Langmuir, 27 (2011) 14360-14369.

R.W. Woody, Theory of circular dichroism of proteins, in: G.D. Fasman (Ed.) Circular dichroism and the conformational analysis of biomolecules, Plenum Press, New York, 1996, pp. 25-30.

S.A. Onaizi, S.S.J. Leong, Tethering antimicrobial peptides: Current status and potential challenges, Biotechnol. Adv. 29 (2011) 67-74.

S.A. Potekhin, T.N. Melnik, V. Popov, N.F. Lanina, A.A. Vazina, P. Rigler, A.S.Verdini, G. Corradin, A.V. Kajava, De novo design of fibrils made of short α-helical coiled coil peptides, Chem. Biol. 8 (2001) 1025-1032.

S.L. Hirsh, D.R. McKenzie, N.J. Nosworthy, J.A. Denman, O.U. Sezerman, M.M.M. Bilek, The Vorman effect: Competitive protein exchange with dynamic multilayer protein aggregates, Colloids Surf. B. Biointerfaces 103 (2013) 395-404.

S.R. Sheth, D. Leckband, Measurements of attractive forces between proteins and end-grafted poly(ethylene glycol) chains, Proc. Natl. Acad. Sci. U.S.A. 94 (1997) 8399-8404.

S.Y. Jung, S.M. Lim, F. Albertorio, G. Kim, M.C. Gurau, R.D. Yang, M.A. Holden, P.S Cremer, The Vroman effect: A molecular level description of fibrinogen displacement, J. Am. Chem. Soc. 125 (2003), 12782-12786.

T.B. McPherson, H.S. Shim, K. Park, Grafting of PEO to glass, nitinol, and pyrolytic carbon surfaces by γ irradiation, J. Biomed. Mater. Res. 38 (1997) 289-302.

T.C. Terwilliger, The helical hydrophobic moment: a measure of the amphiphilicity of a helix. Nature, 299 (1982), 371-374.

T.M. Cooper, R.W. Woody, The effect of conformation on the CD of interacting helices: a theoretical study of tropomyosin, Biopolymers 30 (1990) 657-676.

V. Puddu, C.C. Perry, Peptide adsorption on silica nanoparticles: Evidence of hydrophobic interactions, ACS Nano 6 (2012) 6356-6363.

W.H. De Jong, P.J. Borm, Drug delivery and nanoparticles: Applications and hazards, Int. J. Nanomed. 3 (2008) 133.

W.T.E. Bosker, P.A. Iakovlev, W. Norde, M.A. Cohen Stuart, BSA adsorption on bimodal PEO brushes, J. Colloid Interface Sci. 286 (2005) 496-503.

X. Wu, M.P. Ryder, J. McGuire, K.F. Schilke, Adsorption, structural alteration and elution of peptide from pendant PEO layers, Colloids Surf. B. Biointerfaces 112 (2013) 23-29.

X. Wu, M.P. Ryder, J. McGuire, K.F. Schilke, Concentration effects on peptide elution from pendant PEO layers, submitted to Colloids Surf. B. Biointerfaces.

Y. Takechi, C. Mizuguchi, M. Tanaka, T. Kawakami, S. Aimoto, E. Okamura, H. Saito, Physicochemical mechanism for the lipid membrane binding of polyarginine: The favorable enthalpy change with structural transition from random coil to a-helix, Chem. Lett. 41 (2012) 1374-1376.

Y.-C. Tai, J. McGuire, J.A. Neff, Nisin antimicrobial activity and structural characteristics at hydrophobic surfaces coated with the PEO–PPO–PEO triblock surfactant Pluronic® F108, J. Colloid Interface Sci. 322 (2008) 104-111.

Y.-C. Tai, P. Joshi, J. McGuire, J.A. Neff, Nisin adsorption to hydrophobic surfaces coated with the PEO–PPO–PEO triblock surfactant Pluronic® F108, J. Colloid Interface Sci. 322 (2008) 112-118.

Y.-C. Tseng, T. McPherson, C.S. Yuan, K. Park, Grafting of ethylene glycol-butadiene block copolymers onto dimethyl-dichlorosilane-coated glass by γ-irradiation, Biomaterials 16 (1995) 963-972.

APPENDICES

STRUCTURAL ATTRIUTES AFFECTING PEPTIDE ENTRAPMENT IN PEO BURSH LAYERS

Marsha C. Lampi, Xiangming Wu, Karl F. Schilke, Joseph McGuire

School of Chemical, Biological and Environmental Engineering, Oregon State University, Corvallis, OR 97331

Colloids and Surfaces B: Biointerfaces
http://www.sciencedirect.com/science/journal/09277765
Volume 106, Pages 79-85

APPENDIX A

STRUCTURAL ATTRIBUTES AFFECTING PEPTIDE ENTRAPMENT IN PEO BRUSH LAYERS

Abstract

A more quantitative understanding of peptide loading and release from polyethylene oxide (PEO) brush layers will provide direction for development of new strategies for drug storage and delivery. In this work we recorded selected effects of peptide structure and amphiphilicity on adsorption into PEO brush layers based on covalently stabilized Pluronic® F108. Optical waveguide lightmode spectroscopy and circular dichroism measurements were used to characterize the adsorption of poly-*L*-glutamic acid, poly-*L*-lysine, and the cationic amphiphilic peptide WLBU2, to the brush layers. The structure of WLBU2 as well as that of the similarly-sized homopolymers was controlled between disordered and more ordered (helical) forms by varying solution conditions. Adsorption kinetic patterns were interpreted with reference to a simple model for protein adsorption, in order to evaluate rate constants for peptide adsorption and desorption from loosely and tightly bound states. While more ordered peptide structure apparently promoted faster adsorption and elution rates, resistance to elution while in the PEO layer was dependent on peptide amphiphilicity. The results presented here are compelling evidence of the potential to create anti-fouling surface coatings capable of storing and delivering therapeutics.

Key Words: PEO brush layer; peptide structure; peptide entrapment; peptide adsorption kinetics; OWLS; WLBU2

Introduction

The adsorption of the antimicrobial peptide nisin and various aspects of its behavior at PEO-coated surfaces have been examined through ellipsometry [1], circular dichroism and assays of antibacterial activity [2], zeta potential [3], and TOF-SIMS [4]. In this paper we complete the first step in describing the effects of peptide structure and amphiphilicity on adsorption into PEO brush layers. Optical waveguide lightmode spectroscopy (OWLS) was used to record the adsorption of poly-*L*-glutamic acid, poly-*L*-lysine, and the cationic amphiphilic peptide WLBU2 to PEO brush layers based on covalently stabilized Pluronic® F108. The structure of the homopolymers as well as that of WLBU2 was controlled between disordered and more ordered (helical) forms by varying solution conditions (Figure A.1).

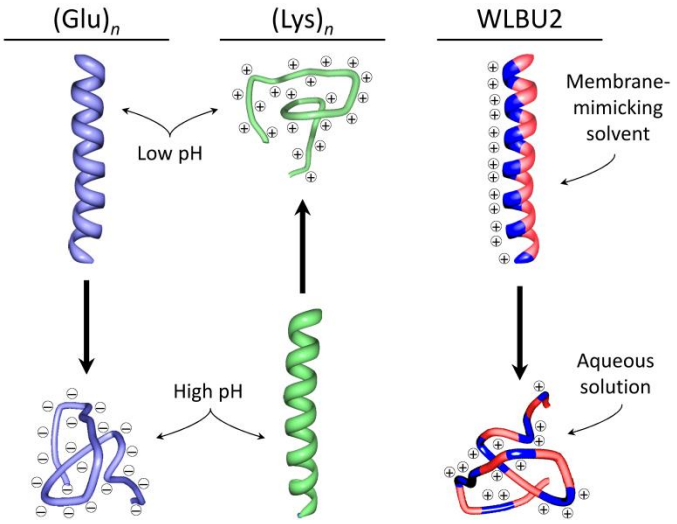

Figure A.1. Poly-*L*-glutamic acid and poly-*L*-lysine will adopt compact α-helical forms or disordered, highly-charged conformations depending on solution conditions. WLBU2 is an amphiphilic cationic peptide that is α-helical in membrane mimetic solvents and disordered in aqueous solution.

Poly-*L*-glutamic acid (PLG) and poly-*L*-lysine (PLL) are homopolymers of amino acids, with regular structure that can extend the full length of the peptide [5]. As with natural proteins, the solution pH, ionic strength, polarity, and peptide concentration can be modulated to adjust the structural conformation from compact α-helix to a variety of "disordered" states [6, 7]. WLBU2 is an engineered, cationic amphiphilic peptide (CAP) with 13 positively-charged arginine residues, and 11 hydrophobic valine or tryptophan residues. It shows substantial promise for clinical applications, due to its wide spectrum antimicrobial activity against both Gram-negative and Gram-positive bacteria under physiological conditions [8-11]. Segregation of the positively-charged and hydrophobic groups onto opposing faces of an α-helix confers the ability to disrupt bacterial cell membranes, killing the bacteria. Moreover, in addition to its high, broad-spectrum potency in blood, it has been shown to retain its antimicrobial activity when immobilized by a number of methods at solid surfaces [12-15].

While it shows no appreciable stable structure in water, WLBU2 exhibits high α-helix content in membrane-mimetic solvents (e.g., 81% α-helix in 30% trifluoroethanol in phosphate buffer) [10]. Finally, while WLBU2 is highly amphiphilic, neither PLG nor PLL is amphiphilic. Thus, WLBU2 serves both as a good control for the effects of amphiphilicity on peptide integration into brush layers, and as a clinically-relevant application for this research. There is great potential for biocompatible surface coatings based on entrapment of bioactive agents, for relatively short-term medical device applications (e.g., anti-infective coatings for acute hemodialysis catheters) as well as blood treatment applications featuring high surface-to-volume ratio, high flow rate,

extracorporeal microfluidic devices. Any among a range of microfluidic device architectures (e.g., microchannels, micropost arrays) can accommodate the high blood flow rates necessary for applications such as sepsis treatment, or the chemical processing of blood for transfusions. Strategies featuring drug-loaded but otherwise nonfouling coatings for blood contact hold promise for enhancing the performance of such devices.

Materials and Methods

Peptide preparation. Lyophilized 20-residue average, 3.0 kDa molecular weight poly(*L*-glutamic acid sodium salt, PLG) was purchased from Alamanda Polymers (Huntsville, AL), and was used as supplied. PLG was dissolved at 1.0 mg/mL in HPLC water, and separated into 1.0 mL aliquots that were frozen and thawed prior to each experiment. The 1.0 mg/mL PLG (pI ~ 2.5) was diluted to 0.1 mg/mL in either 1.0 N HCl (EMD Chemicals) or a dilute HCl aqueous solution, pH 4.7, to invoke either helical or disordered conformations, respectively. Similarly, a 4.2 kDa 21-residue poly-*L*-lysine hydrobromide (PLL, Almanda Polymers) was dissolved at 1.0 mg/mL in HPLC water, and separated into 1.0 mL aliquots that were frozen and then thawed prior to each experiment. The 1.0 mg/mL PLL (pI ~ 11.8) solution was diluted to 0.10 mg/mL in either 1.0 N NaOH or HPLC water to invoke either helical or disordered conformations, respectively. Lyophilized WLBU2 (GenScript,) was dissolved at 5.0 mg/mL in HPLC water and frozen in 200 μL aliquots. Prior to use, the WLBU2 stock solution was thawed and diluted to 0.1 mg/mL in HPLC water, 10 mM sodium phosphate with 150 mM NaCl, pH 7.4 (PBS), or alternatively, with PBS with additional salt. All 0.1 mg/mL peptide solutions were degassed for 40 min under vacuum immediately before use.

Preparation of OWLS sensor chips. OWLS waveguide sensor chips with a ~10 nm surface silica thin film coating (MicroVacuum Ltd.) were cleaned by immersing in chromosulfuric acid (ACROS Organics) for 10 min at room temperature, rinsed with HPLC water, and dried with nitrogen gas. After cleaning, the sensors were immersed in molecular sieve-dried absolute ethanol, and dried with a stream of nitrogen to remove bulk moisture. Silanization was performed by chemical vapor deposition at room temperature [16]. For this purpose sensors were placed in a sealed reaction chamber with the waveguide surface facing up. Argon gas was used for 20 min to purge the system, creating an environment devoid of moisture. 0.20 mL of trichlorovinylsilane (TCVS, TCI America) was then injected into the system, vaporized, and delivered to the waveguide surfaces using the argon carrier gas. After 1 h of vapor deposition, a second 0.2 mL aliquot of TCVS was injected into the system and allowed to react for 1 h. The waveguides were then removed and cured at 150 ℃ for 1 h.

Self-assembled F108 brush layers were formed on the silanized waveguide surfaces by incubating overnight with 5% Pluronic® F108 (BASF) in HEPES (Gibco BRL), pH 7.4. The brush layers were then gamma irradiated at 0.3 Mrad to covalently attach the F108 to the surface. The PEO functionalized OWLS sensors were dried with N_2 gas and stored until use in the dark to prevent oxidation of the vinyl moieties. Hydrophobic control sensors were prepared as described above, but in the absence of F108.

Measurement of peptide adsorption kinetics. Buffer solutions were prepared to match the composition of the 0.1 mg/mL peptide solutions and degassed for 5 h. The buffer for helical PLG was prepared at 0.9 N HCl to account for dissolving the peptide in HPLC

water prior to diluting to 0.1 mg/mL in 1.0 N HCl. Based on similar reasoning, the solution used for the disordered form of PLG was prepared by adding 10% HPLC water to the HCl solution originally used to dissolve the peptide. The buffer for helical PLL was prepared at 0.9 N NaOH, and HPLC water was used for experiments with the disordered form. The buffers for WLBU2 testing were 10 mM sodium phosphate including 150 mM NaCl, pH 7.4 (PBS), or PBS with salt added to 400 or 600 mM NaCl.

Waveguide sensors were equilibrated overnight in the appropriate buffer and the refractive index of the HCl solutions were calculated using linear interpolation of tabulated values [17]. At the start of each experiment, the sensor was allowed to equilibrate within the system for 40-60 min. OWLS Relative Intensity Mode (RIM) with buffer introduced at 50.0 μL/min (OWLS^{TM} 210-SIS) was used. When the baseline slopes were on the order of 1.0×10^{-9}, about 4 mL of 0.10 mg/mL peptide solution was introduced to the system and adsorption to the sensor was allowed to occur for 30 min. Adsorption was followed by a 30 min rinse where peptide-free buffer was introduced. The adsorption-rinse cycle was then repeated. Each cyclic, adsorption-elution experiment was performed at least twice on each type of surface. At the conclusion of each test, the flow cell was cleaned with HPLC water and 0.1 N HCl.

Peptide structural evaluation. Hydrophobic silica nanoparticles (Product R816, Degussa, 190 m^2/g, 10-12 nm), were coated with F108 by suspension in HPLC water for 10 h on a rotator. The amount of F108 used for this purpose was sufficient to cover the surface presented by the silica nanoparticles in suspension (about 3.3 mg/m^2) [2]. F108-coated silica nanoparticles were then incubated with PLL or WLBU2 at 0.20 mg/mL for a

desired period of time (2 h to 7 d) at room temperature. The amount of nanoparticles (10 mg/mL) selected was based on OWLS results and provided 5 times more surface area than would be required for complete adsorption.

Peptide structure in the presence or absence of nanoparticles was evaluated by circular dichroism (CD) using a Jasco J-815 spectropolarimeter (0.1 cm path length, cylindrical cuvette) at 25 ℃. The instrument was calibrated using 0.6 mg/mL *D*(+) – camphorsulfonic acid. Spectra were recorded from 260 to 195 nm in 0.5 nm increments and digitally stored. In each case 10 scans were recorded and averaged in order to increase the signal-to-noise ratio. The 0.10 mg/mL (without nanoparticles) and 0.20 mg/ml (with nanoparticles) peptide samples prepared as outlined above were filtered (PVDF 0.20 μm filter) prior to recording CD spectra. CD spectra were recorded along with peptide-free reference samples in each case in order to subtract background signals and ensure the measurement of peptide properties only. Peptide-nanoparticle suspensions were then washed by centrifugation (10,000 rpm, 20 min), and resuspended in water. CD spectra were then recorded again, under the same conditions outlined above. All experiments were performed in triplicate.

Results and Discussion

Adsorption of WLBU2. Figure A.2 shows representative results for adsorption from a solution of WLBU2 dissolved in PBS at uncoated and PEO-coated surfaces. The peptide adsorbed with high affinity to the uncoated surface and showed substantial resistance to elution, owing to its highly cationic, amphiphilic character. A TCVS-treated silica surface

has a negative zeta potential but is otherwise hydrophobic [3]. The high level of adsorption at the uncoated surface may be indicative of multilayer adsorption, presumably involving electrostatic association with the surface and hydrophobic association between adsorbed peptide layers. Adsorption of WLBU2 was also evident at the PEO layer, however in much lower amounts as compared to the uncoated surface. While an appreciable fraction of the amount present at the end of a 30 min adsorption cycle was elutable, an elution plateau attained after each cycle indicates the presence of a peptide population entrapped in a fashion irreversible to elution by peptide-free buffer.

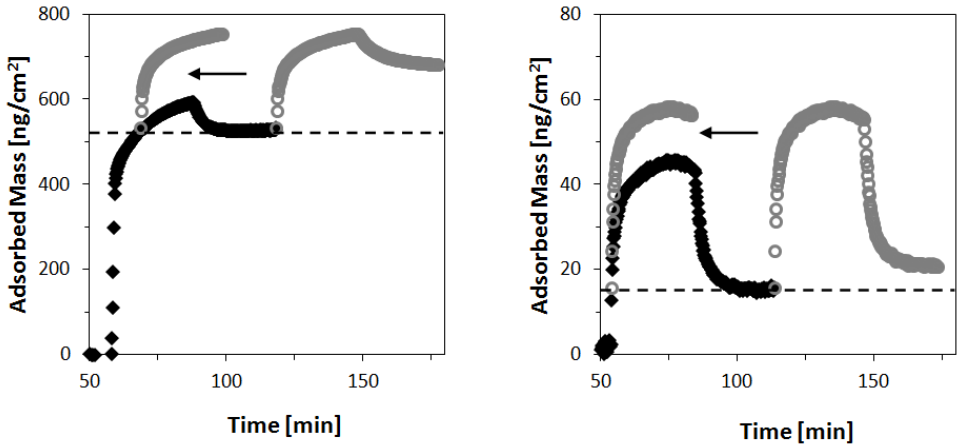

Figure A.2. Cyclic adsorption and elution of WLBU2 at (left) an uncoated, silanized, γ-irradiated surface and (right) a PEO layer. The initial rate of adsorption in the second cycle is shifted back for illustrative purposes, to allow comparison of adsorption rates at equal surface coverages in each cycle.

While disordered in water, WLBU2 shows high α-helix content in membrane-mimetic solvents. Such solvents were not used in this study, as the pendant PEO configuration present in water and aqueous buffers would be significantly compromised. However, in aqueous solution it is fair to expect that the presence of added salt may shield the charged groups on the peptide that prohibit adoption of secondary structure. In fact the CD spectra

of Figure A.3 show WLBU2 to be disordered in water, but increasingly helical in PBS with the addition of salt [18, 19]. The amount of α-helical structure in a peptide can be calculated as proportional to the molar ellipticity at 222 or 208 nm [20-22]. A greater magnitude of ellipticity at either wavelength indicates greater α-helical structure. The representative spectra of Figure A.3 indicate that salt increases the fraction of helical structure in WLBU2, being 9.3, 15.8, 16.2, or 17.8% α-helix when dissolved in water, PBS, PBS + 250 mM NaCl, or PBS + 450 mM NaCl, respectively. In summary the peptide structure tends to be more ordered as the amount of salt in the aqueous solvent is increased.

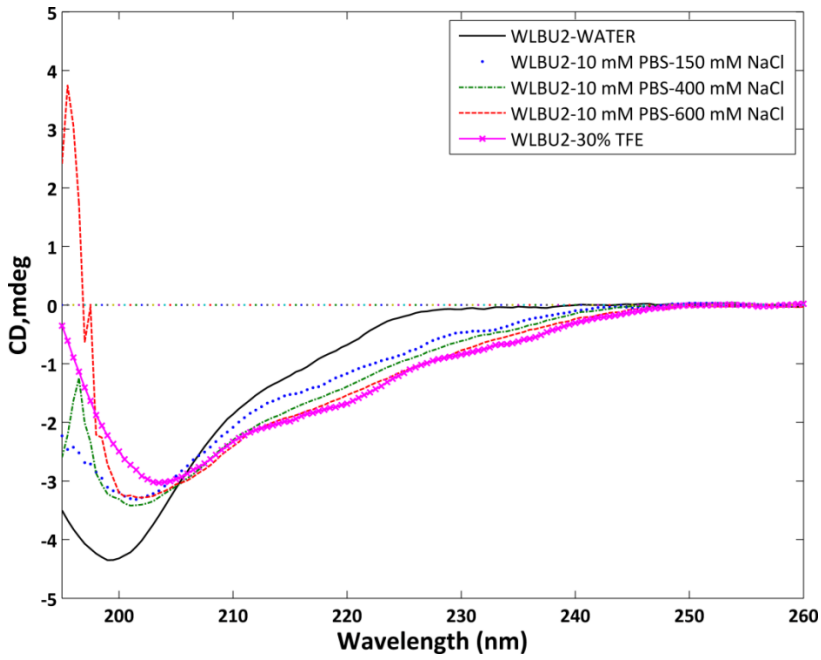

Figure A.3. CD spectra of WLBU2 in water, PBS, PBS + 250 mM NaCl, and PBS + 450 mM NaCl.

Figure A.4 shows representative results for WLBU2 adsorption from pure water in comparison to WLBU2 adsorption from PBS at PEO-coated surfaces. Adsorption was

slower and less extensive in water than in PBS, but the elution plateaus were similar. Slower adsorption in water is consistent with the peptide having no stable secondary structure in that solvent. The peptide is small enough to become entrapped independent of its secondary structure, but its entry into the PEO layer is apparently facilitated by adoption of a more ordered conformation.

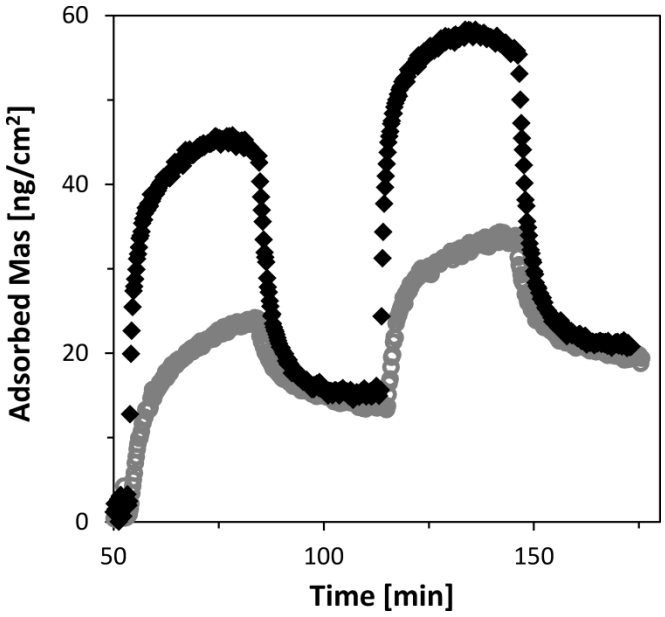

Figure A.4. Adsorption of WLBU2 from water at a PEO layer (gray symbols). WLBU2 adsorption from PBS at a PEO layer (black symbols) is replotted from Figure A.2 for comparison.

Adsorption of PLG and PLL. The carboxylic acid side-chains of PLG are protonated (–COOH) at low pH, and unprotonated ($–COO^-$) at higher pH. CD studies of its secondary structure in aqueous NaCl show a sharp transition in conformation from α-helix to random coil as the solution pH is increased [5, 23]. This loss of orderly structure at higher pH was attributed to electrostatic repulsion between the negatively-charged (unprotonated) carboxylic side-chains. Cations from salts (e.g. Ca^{2+} or Na^+) may also

shield the net negative charge of unprotonated PLG, causing similar conformational changes.

Unprotonated (disordered) PLG in dilute HCl (pH 4.7) was found to adsorb to both the uncoated surface and the PEO brush layer, albeit in small amounts (Figure A.5).

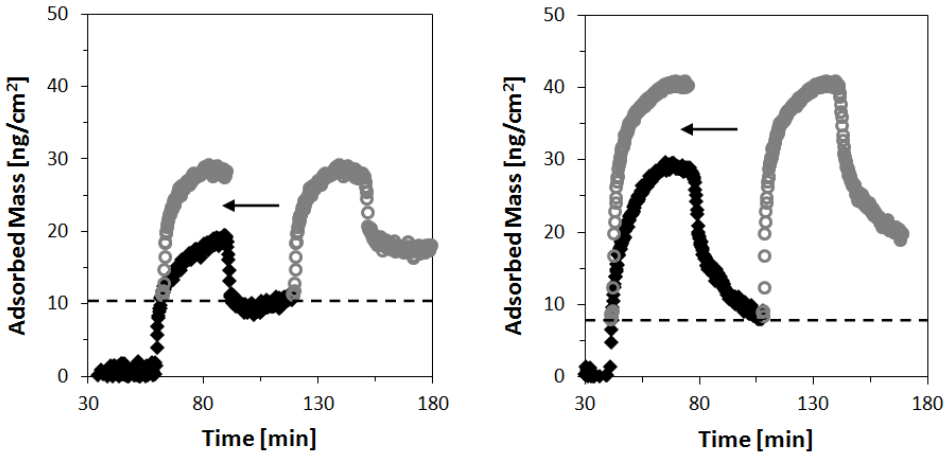

Figure A.5. Cyclic adsorption and elution of poly-*L*-glutamic acid (dilute HCl, pH 4.7) at (left) an uncoated, silanized, γ-irradiated surface and (right) a PEO layer. The initial rate of adsorption in the second cycle is shifted back for illustrative purposes, to allow comparison of adsorption rates at equal surface coverages in each cycle.

Being at once negatively charged and non-amphiphilic, PLG would be expected to show little affinity for the uncoated surface. The flat elution plateaus recorded at that surface (Figure A.5, left panel) indicate a population of peptide that is irreversibly bound, presumably localized at defects (e.g., asperities, other physical heterogeneities) on the surface. While in a disordered form, as observed for WLBU2 in water, PLG is apparently small enough to enter the PEO layer (Figure A.5, right panel). But the absence of an elution plateau suggests the adsorbed peptide is entirely elutable.

The representative results of Figure A.5 also indicate that, with comparable amounts of adsorption recorded at each surface, peptide adsorption to a PEO brush was still distinctly different than that observed at the surface not coated with PEO. Visual inspection of the elution patterns indicates that there is no irreversibly bound peptide at the PEO layer. This suggests the peptide is (reversibly) located within the PEO brush itself, and not associating with the underlying surface. If peptide was associating with the underlying surface, we would expect an elution plateau similar to that seen at the uncoated surface (Figure A.5, left panel). Moreover, there is an obvious history dependence on adsorption recorded with the uncoated surface that is not apparent with the PEO layer. In particular, with adsorption to the uncoated surface, the initial adsorption rate during the second adsorption step is substantially greater than that observed at the same surface coverage during the first step. This behavior was not observed at the PEO layer, suggesting again that peptide association with the underlying surface does not play a significant role in adsorption in that case.

No appreciable adsorption to either the uncoated surface or the PEO brush layer was recorded by OWLS for the protonated, helical (ordered) form of PLG. Similarly, no evidence of PLL adsorption in either form was detected by OWLS. While it is entirely reasonable to expect insignificant adsorption by the homopolymers, we applied CD to the evaluation of PLL structure in the presence and absence of uncoated and F108-coated nanoparticles. The representative results shown in Figure A.6 (top panel) indicate that spectra recorded for PLL are similar, independent of the presence of F108-coated nanoparticles. Moreover, after the F108-coated nanoparticles (suspended in PLL solution)

are washed with water, Figure A.6 (top panel) indicates that peptide was substantially removed from the sample. These results are consistent with no obvious location of PLL within the PEO brush. On the other hand, Figure A.6 (bottom panel) shows that relatively little peptide is removed upon washing a suspension of WLBU2 and F108-coated particles. This result is indicative of peptide entrapment and is consistent with the outcome of OWLS detection of WLBU2 adsorption and elution from PBS (Figure A.4). These spectra also show WLBU2 gains considerable α-helix content after entrapment within the F108 layer from PBS (increasing from 15.8 to 24.9% α-helix after entrapment). Induction of α-helix in this way is owing to the hydrophobicity of the PEO layer (below). Contrary to OWLS detection of WLBU2 adsorption from HPLC water (Figure A.4), CD spectra provided no corroborating evidence of WLBU2 entrapment from this solvent by F108-coated nanoparticles (data not shown). In particular, spectra recorded for the disordered form of WLBU2 in HPLC water with and without F108-coated nanoparticles were similar, and after washing with water the peptide was substantially removed from suspension with the coated nanoparticles. This finding suggests some degree of structural order may be necessary for entry into the brush. We have completed a comprehensive CD investigation of this possibility that will be described in a separate report.)

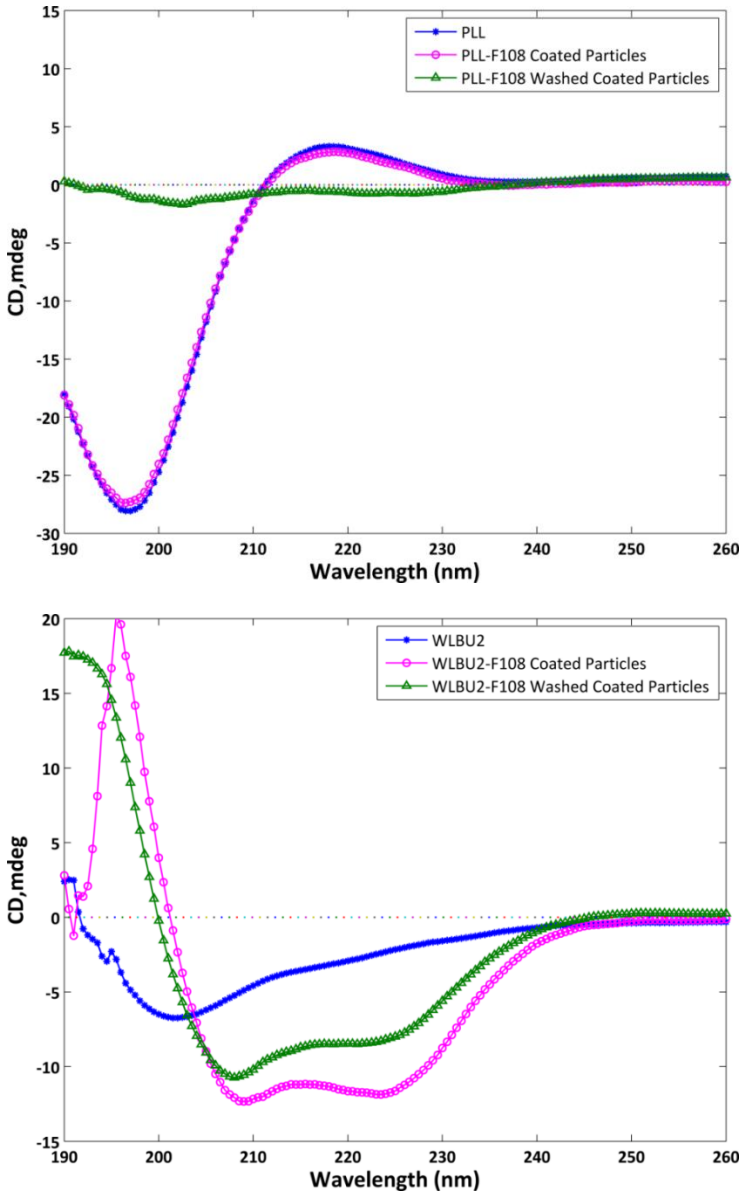

Figure A.6. CD spectra of: (top) poly-*L*-lysine in water, and in suspension with F108-coated nanoparticles before and after washing, and (bottom) WLBU2 in PBS, and in suspension with F108-coated nanoparticles before and after washing.

It is reasonable to expect based on Figures A.4-A.6 that any peptide retention in the PEO layer is owing to its amphiphilicity. Theoretical and experimental evidence suggests that below the hydrophilic outer region of a PEO brush there exists a hydrophobic region that

is favorable for protein adsorption [24, 25]. In particular, using surface force measurements, Sheth and Leckband adsorption [25] provided direct evidence for the formation of strong attractive forces between PEO and protein (streptavidin). Forces were repulsive on approach, but became attractive when the proteins were pressed into the PEO layer. They rationalized this in relation to the competitive interactions between solvent as well as proteins for the chain segments, and to the ability of PEO to adopt higher order intrachain structures. Lee et al. [26] demonstrated that PEO chains are not hydrophilic when they are arranged in the polymer brush configuration. They indicated that at the high PEO chain concentrations consistent with brush formation, the specific configuration of the polymer that enables hydrophilic interaction with water may become disrupted, rendering the polymer less soluble (or even insoluble) in water. Others had in fact predicted theoretically [27, 28] and shown experimentally [29] that beyond some threshold PEO chain density the PEO brush would "collapse" owing to this effect. While increasing chain density within a brush layer might eventually favor lateral compression, Lee et al. concluded that the widely observed, steric-repulsive character of PEO brushes is retained because the hydrophobicity of the brush (which favors compression) is not sufficient to overcome the opposing force of the chain conformational entropy (which resists compression) [26].

We have used OWLS to record changes in adsorbed mass during cyclic adsorption-elution experiments with the cationic, amphiphilic peptide nisin, at uncoated and PEO-coated surfaces (Dill et al., 2013). PEO layers in that work were prepared by radiolytic grafting of F108 as well as Pluronic® surfactant F68 to silanized waveguides, producing

long- or short-chain PEO layers (141 vs. 80 EO units), respectively. As recorded here with WLBU2, nisin adsorption to the uncoated surface showed history dependence while nisin adsorption to the F108-coated surface did not show history dependence. While nisin entry into the F68 brush was observed during the adsorption step, it was completely eluted upon introduction of peptide-free buffer, indicating that the peptide did not associate with the underlying surface. The lack of stable surface contact in that case suggested nisin entrapment within (the longer PEO chains of) F108 involved its location within the hydrophobic inner region, without contacting the underlying surface. In summary, while peptide adsorption in a fashion resistant to elution (entrapment) within the PEO brush was not detected with OWLS or CD in the case of the homopolymers, entrapment was evident in the case of WLBU2. Thus we conclude entrapment of peptide in PEO is explainable by its association with the inner, hydrophobic region of the PEO brush, and the lack of retention of peptide is explainable by its inability to take part in such association.

Comparison to a model for protein adsorption. It is instructive to interpret the adsorption-elution patterns recorded with OWLS at F108-coated surfaces with reference to a simple model for protein adsorption and desorption [30]. When a peptide solution is introduced to the PEO layer, the change in adsorbed amount as a function of time, $d\Gamma/dt$, may be written as $d\Gamma/dt = k_a c_b \Phi - \sum_i k_{d,i}\Gamma_i$, where $k_a c_b$ is the intrinsic adsorption rate, Φ is the cavity function, $k_{d,i}$ is the desorption rate constant for peptide adsorbed in state i, and Γ_i is the amount of peptide adsorbed in state i. These adsorption "states" represent

different peptide conformations, etc., that result in different resistances to elution. The cavity function is defined as the fraction of the surface on which the center of an incoming molecule could adsorb without overlapping a previously adsorbed molecule [1, 30-33]. During elution, when the contacting peptide solution is replaced by a peptide-free solution, peptide concentration in the bulk goes to zero, and a net desorption from the surface occurs, such that $d\Gamma/dt = \sum_i k_{d,i}\Gamma_i$.

Estimation of the rate constants from experimental data is straightforward based on the above. The lumped adsorption rate constant ($k_a c_b$) was obtained by using the data of Figures A.4 and A.5 to generate plots of $d\Gamma/dt$ *vs.* Γ. Linear regression of the early kinetics and extrapolation to $\Gamma = 0$ approaches a condition where desorption does not occur and $\Phi = 1$, such that the "y-intercept" is $k_a c_b$, i.e., $\left.\frac{d\Gamma}{dt}\right|_{\Gamma=0} = k_a c_b$.

The desorption rate constants were estimated using the elution profiles, assuming the existence of two desorbable states, one that is less tightly bound (state 1) and one that is more tightly bound (state 2), and one irreversibly bound state (state 3). The values of k_{d_1} and k_{d_2} were found using the slopes of a plot of $d\Gamma/dt$ *vs.* Γ during the first rinse cycle. From this plot, two distinct linear regions could be identified, with k_{d_1} characterizing the slope of the line at high surface coverages and k_{d_2} characterizing the slope of the line at lower surface coverages.

The amount of peptide adsorbed in each state at the onset of rinsing, Γ_1, Γ_2, and Γ_3, is also easily determined from the same plot of $d\Gamma/dt$ *vs.* Γ. The value of Γ at the intercept of the

two lines was taken as equal to $\Gamma_2 + \Gamma_3$, i.e., the surface concentrate on after all peptide in state 1 had been eluted. Γ_1 was thus determined by a simple mass balance. The value of Γ corresponding to the "x-intercept" of the second linear region (i.e., of slope k_{d_2}) was taken as Γ_3, and Γ_2 was then also determined by a mass balance. (If the plot of $d\Gamma/dt$ *vs.* Γ during elution showed only a single linear region, then Γ_2 was set equal to zero.) The kinetic parameters and surface coverages in each state for peptide adsorption to PEO (as recorded by OWLS) are summarized in Table A.1.

Table A.1. Adsorption and desorption kinetic parameters, and surface coverages in each state estimated for peptide adsorption to PEO.

Parameter	WLBU2 in water (disordered)	WLBU2 in PBS (more ordered)	Poly-*L*-glutamic acid (disordered)
$k_a c_b$ [ng·(cm^2·min)$^{-1}$]	0.11	1.0	0.16
$k_{d,1}$ [min^{-1}]	0.0054	0.0069	0.012
$k_{d,2}$ [min^{-1}]	—	—	0.00061
Γ_1 [ng/cm^2]	8.0	25	11
Γ_2 [ng/cm^2]	—	—	18
Γ_3 [ng/cm^2]	16	18	0.62

As discussed by Calonder et al. [31], in order to compare independent OWLS data sets in a quantitative way, it is vital to use the same waveguiding surface each time. Without repositioning the waveguide in a given OWLS experiment, the reproducibility between any two adsorption experiments (separated by a cleaning step, *in situ*) is very high. However, in order to avoid artifacts introduced by incomplete washing of the PEO brush layers used here, independent experiments were performed with a new, repositioned waveguide each time. Thus the entries in Table A.1 simply offer a quantitative representation of the adsorption and elution trends revealed by Figures A.4 and A.5, as opposed to absolute rate constants and surface coverages. Consistent with earlier visual inspection of peptide adsorption at the F108-coated surfaces, this analysis shows the intrinsic adsorption rate constant is greater for the more ordered form of WLBU2 than for the disordered WLBU2 or the disordered PLG. In addition, the desorption rate constants are lower for the amphiphilic WLBU2 than for the non-amphiphilic PLG. The amphiphilic WLBU2 also showed a substantially greater proportion of irreversibly entrapped peptide than did the non-amphiphilic PLG.

Conclusions

We have seen for a peptide of a size allowing adsorption to a PEO layer, that peptide structure and amphiphilic character will affect the adsorption affinity. In particular the results reported here direct us to expect that a more ordered, compact peptide will enter the PEO phase more readily than a peptide of similar size that adopts a less ordered, less compact form. We also expect amphiphilicity will promote peptide retention, by

association with the inner region of the PEO layer. An experimentally based, quantitative understanding of the adsorption and function of peptides at otherwise protein-repellent PEO layers does not currently exist, and these results provide a rationale for hypotheses to drive further discovery and understanding in this important area.

Acknowledgments

The authors would like to thank Dr. Kerry McPhail of the OSU College of Pharmacy for use of her CD instrument. This work was supported in part by the National Institute of Biomedical Imaging and Bioengineering (NIBIB, grant no. R01EB011567). The content is solely the responsibility of the authors and does not necessarily represent the official views of NIBIB or the National Institutes of Health.

References

[1] Y.-C. Tai, P. Joshi, J. McGuire and J.A. Neff, Nisin adsorption to hydrophobic surfaces coated with the PEO–PPO–PEO triblock surfactant Pluronic® F108, J. Colloid Interface Sci., 322 (2008) 112-118.

[2] Y.-C. Tai, J. McGuire and J.A. Neff, Nisin antimicrobial activity and structural characteristics at hydrophobic surfaces coated with the PEO–PPO–PEO triblock surfactant Pluronic® F108, J. Colloid Interface Sci., 322 (2008) 104-111.

[3] M.P. Ryder, K.F. Schilke, J.A. Auxier, J. McGuire and J.A. Neff, Nisin adsorption to polyethylene oxide layers and its resistance to elution in the presence of fibrinogen, J. Colloid Interface Sci., 350 (2010) 194-199.

[4] K.F. Schilke and J. McGuire, Detection of nisin and fibrinogen adsorption on poly(ethylene oxide) coated polyurethane surfaces by time-of-flight secondary ion mass spectrometry (tof-sims), J. Colloid Interface Sci., 358 (2011) 14-24.

[5] S.P. Adiga and D.W. Brenner, Designing smart nanovalves: Modeling of flow control through nanopores via the helix-coil transition of grafted polypeptide chains, Macromolecules, 40 (2007) 1342-1348.

[6] J.M. Finke, P.A. Jennings, J.C. Lee, J.N. Onuchic and J.R. Winkler, Equilibrium unfolding of the poly(glutamic acid)$_{20}$ helix, Biopolymers, 86 (2007) 193-211.

[7] L. Ma, Z. Ahmed and S.A. Asher, Ultraviolet resonance raman study of side chain electrostatic control of poly-*L*-lysine conformation, J. Phys. Chem. B, 115 (2011) 4251-4258.

[8] B. Deslouches, I.A. Gonzalez, D. DeAlmeida, K. Islam, C. Steele, R.C. Montelaro and T.A. Mietzner, *De novo*-derived cationic antimicrobial peptide activity in a murine model of *pseudomonas aeruginosa* bacteraemia, J. Antimicrob. Chemother., 60 (2007) 669-672.

[9] B. Deslouches, K. Islam, J.K. Craigo, S.M. Paranjape, R.C. Montelaro and T.A. Mietzner, Activity of the *de novo* engineered antimicrobial peptide wlbu2 against *pseudomonas aeruginosa* in human serum and whole blood: Implications for systemic applications, Antimicrob. Agents Chemother., 49 (2005) 3208-3216.

[10] B. Deslouches, S.M. Phadke, V. Lazarevic, M. Cascio, K. Islam, R.C. Montelaro and T.A. Mietzner, *De novo* generation of cationic antimicrobial peptides: Influence of length and tryptophan substitution on antimicrobial activity, Antimicrob. Agents Chemother., 49 (2005) 316-322.

[11] M.C. Skinner, A.O. Kiselev, C.E. Isaacs, T.A. Mietzner, R.C. Montelaro and M.F. Lampe, Evaluation of wlbu2 peptide and 3-*o*-octyl-*sn*-glycerol lipid as active ingredients for a topical microbicide formulation targeting *chlamydia trachomatis*, Antimicrob. Agents Chemother., 54 (2010) 627-636.

[12] F. Costa, I.F. Carvalho, R.C. Montelaro, P. Gomes and M.C.L. Martins, Covalent immobilization of antimicrobial peptides (amps) onto biomaterial surfaces, Acta Biomater., 7 (2011) 1431-1440.

[13] I.A. Gonzalez, X.X. Wong, D. De Almeida, R. Yurko, S. Watkins, K. Islam, R.C. Montelaro, A. El-Ghannam and T.A. Mietzner, Peptides as potent antimicrobials tethered to a solid surface: Implications for medical devices, Nature Precedings, (2008).

[14] R.C. Montelaro and T.A. Mietzner, Virus derived antimicrobial peptides, in, United States, 2005.

[15] S.A. Onaizi and S.S.J. Leong, Tethering antimicrobial peptides: Current status and potential challenges, Biotechnol. Adv., 29 (2011) 67-74.

[16] K.C. Popat, R.W. Johnson and T.A. Desai, Characterization of vapor deposited thin silane films on silicon substrates for biomedical microdevices, Surf. Coat. Technol., 154 (2002) 253-261.

[17] A.L. Olsen and E.R. Washburn, An interpolation table for refractive index-normality relationship for solutions of hydrochloric acid and sodium hydroxide, Trans. Kans. Acad. Sci., 40 (1937) 117-126.

[18] R.W. Woody, Theory of circular dichroism of proteins, in: G.D. Fasman (Ed.) Circular dichroism and the conformational analysis of biomolecules, Plenum Press, New York, 1996, pp. 25-30.

[19] J.W. Nelson and N.R. Kallenbach, Persistence of the a-helix stop signal in the s-peptide in trifluoroethanol solutions, Biochemistry (Mosc). 28 (1989) 5256-5261.

[20] N.J. Greenfield, Methods to estimate the conformation of proteins and polypeptides from circular dichroism data, Anal. Biochem., 235 (1996) 1-10.

[21] N.J. Greenfield and G.D. Fasman, Computed circular dichroism spectra for the evaluation of protein conformation, Biochemistry (Mosc). 8 (1969) 4108-4116.

[22] J.D. Morrisett, J.S.K. David, H.J. Pownall and A.M. Gotto, Interaction of an apolipoprotein (apolp-alanine) with phosphatidylcholine, Biochemistry (Mosc). 12 (1973) 1290-1299.

[23] K. Inoue, N. Baden and M. Terazima, Diffusion coefficient and the secondary structure of poly-*L*-glutamic acid in aqueous solution, J. Phys. Chem. B, 109 (2005) 22623-22628.

[24] A. Halperin, Polymer brushes that resist adsorption of model proteins: design parameters, Langmuir, 15 (1999) 2525-2533.

[25] S.R. Sheth and D. Leckband, Measurements of attractive forces between proteins and end-grafted poly(ethylene glycol) chains, Proceedings of the National Academy of Sciences, 94 (1997) 8399-8404.

[26] H. Lee, D.H. Kim, K.N. Witte, K. Ohn, J. Choi, B. Akgun, S. Satija and Y.-Y. Won, Water is a poor solvent for densely grafted poly(ethylene oxide) chains: A conclusion drawn from a self-consistent field theory-based analysis of neutron reflectivity and surface pressure–area isotherm data, J. Phys. Chem. B, 116 (2012) 7367-7378.

[27] A. Halperin, Compression induced phase transitions in PEO brushes: The *n*-cluster model, Eur. Phys. J. B, 3 (1998) 359-364.

[28] M. Wagner, F. Brochard-Wyart, H. Hervet and P. Gennes, Collapse of polymer brushes induced by n-clusters, Colloid & Polymer Science, 271 (1993) 621-628.

[29] T. Hu and C. Wu, Clustering induced collapse of a polymer brush, Phys. Rev. Lett., 83 (1999) 4105-4107.

[30] Y. Tie, C. Calonder and P.R. Van Tassel, Protein adsorption: Kinetics and history dependence, J. Colloid Interface Sci., 268 (2003) 1-11.

[31] C. Calonder, Y. Tie and P.R. Van Tassel, History dependence of protein adsorption kinetics, Proceedings of the National Academy of Sciences, 98 (2001) 10664-10669.

[32] C. Calonder and P.R. Van Tassel, Kinetic regimes of protein adsorption, Langmuir, 17 (2001) 4392-4395.

[33] J.C. Dijt, M.A. Cohen Stuart and G.J. Fleer, Kinetics of adsorption and desorption of polystyrene on silica from decalin, Macromolecules, 27 (1994) 3207-3218.

BINDING INTERACTIONS OF BACTERIAL LIPOPOLYSACCHARIDE AND THE CATIONIC AMPHIPHILIC PEPTIDES POLYMYXIN B AND WLBU2

Matthew P. Ryder, Xiangming Wu, Greg R. McKelvey, Joseph McGuire, Karl F. Schilke

School of Chemical, Biological and Environmental Engineering, Oregon State University, Corvallis, OR 97331

Submitted to Colloids and Surfaces B: Biointerfaces
www.elsevier.com/locate/colsurfb

APPENDIX B

BINDING INTERACTIONS OF BACTERIAL LIPOPOLYSACCHARIDE AND THE CATIONIC AMPHIPHILIC PEPTIDES POLYMYXIN B AND WLBU2

Abstract

Passage of blood through a sorbent device for removal of bacteria and endotoxin by specific binding with immobilized, membrane-active, bactericidal peptides holds promise for treating severe blood infections. Peptide insertion in the target membrane and rapid/strong binding is desirable, while membrane disruption and release of degradation products to the circulating blood is not. Here we describe interactions between bacterial endotoxin (lipopolysaccharide, LPS) and the membrane-active, bactericidal peptides WLBU2 and polymyxin B (PmB). Analysis of the interfacial behavior of mixtures of LPS and peptide using air-water interfacial tensiometry and optical waveguide lightmode spectroscopy strongly suggests insertion and stabilization of intact LPS vesicles by the peptide WLBU2. In contrast, dynamic light scattering (DLS) studies show that LPS vesicles appear to undergo peptide-induced destabilization in the presence of PmB. Circular dichroism spectra further confirm that WLBU2, which shows disordered structure in aqueous solution and substantially helical structure in membrane-mimetic environments, is stably located within the LPS membrane in peptide-vesicle mixtures. We therefore expect that presentation of WLBU2 at an interface, if tethered in a fashion which preserves its mobility and solvent accessibility, will enable the capture of bacteria and endotoxin without promoting reintroduction of endotoxin to the circulating blood,

thus minimizing adverse clinical outcomes. On the other hand, our results suggest no such favorable outcome of LPS interactions with polymyxin B.

Keywords: cationic amphiphilic peptides; WLBU2; polymyxin B; lipopolysaccharide; endotoxin; sepsis; interfacial tensiometry

Introduction

Severe sepsis is a blood infection that in the US alone affects about 750,000 people each year, killing 28-50% of them [1-3]. The number of sepsis-related deaths continues to increase, and is already greater than the annual number of deaths in the US from prostate cancer, breast cancer and AIDS combined. During bacterial growth or as a result of the action of antibacterial host factors, lipopolysaccharide (LPS, endotoxin) is released from the cell wall of Gram-negative bacteria. The high immunostimulatory potency of endotoxin causes dysregulation of the inflammatory response with elevated production and release of proinflammatory cytokines [4], leading to blood vessel damage and organ failure [1, 2].

Hemoperfusion, involving passage of blood through a sorbent device for the removal of selected targets, holds promise for treating sepsis [5-7]. Toraymyxin™, a commercial hemoperfusion device, has been used clinically in Japan since 1994 for removal of endotoxin by specific binding with the immobilized antimicrobial peptide polymyxin B (PmB), and was introduced to the European market in 2002 [8]. However, such devices have not been widely adopted elsewhere, as clinical trials have shown little significant change in either endotoxin or cytokine concentrations, or in incidence of mortality [7, 9]. Several studies further indicated that hemoperfusion results in significant depletion of both white blood cells and platelets [10, 11]. PmB is covalently attached to a polystyrene fiber matrix within such devices, and it is fair to expect that immobilization in that way would strongly inhibit peptide mobility, accessibility, and activity [12-14]. In addition, nonspecific loss of blood protein, platelets and cells through interaction with the

otherwise unprotected polystyrene surface is likely. The clinical utility of PmB itself has been limited due to nephrotoxicity and neurotoxicity, monocyte stimulation (IL-1 release), and substantial blood protein losses can occur during operation of devices with immobilized PmB [5, 6, 15, 16]. In addition, PmB resistance among common pathogens is not rare [17]. Successful hemoperfusion for sepsis treatment will require surface modification that will ensure highly selective capture of bacteria and endotoxin that reach the interface. In addition, surface coatings must provide pathogen binding functionality without evoking a host cell response, without nonspecific adsorption of protein, and without platelet activation and blood cell damage caused by cell-surface interactions.

Cationic amphiphilic peptides (CAPs) constitute a major class of antimicrobials that allow neutrophils and epithelial surfaces to rapidly inactivate invading pathogens [18, 19]. A number of CAPs have been shown to bind LPS with affinities comparable to PmB [20, 21]. For example, the CAP human cathelicidin peptide LL-37 has been shown to neutralize the biological activity of LPS and to protect rats from lethal endotoxin shock, revealing no statistically significant differences in antimicrobial or anti-endotoxin activities between LL-37 and PmB [22]. Despite the broad activity of LL-37 and other natural CAPs, their potency is inhibited in the presence of physiological concentrations of NaCl and divalent cations. However the 24-residue, *de novo* engineered peptide WLBU2, a synthetic analogue of LL-37, shows highly selective, potent activity against a broad spectrum of Gram-positive and Gram-negative bacteria at physiologic NaCl and serum concentrations of Mg^{2+} and Ca^{2+} [23-26]. Moreover WLBU2 shows greater antimicrobial

activity than either LL-37 or PmB, and is active against a much broader spectrum of bacteria [27, 28].

A major distinguishing feature of CAPs is their capacity to adopt an amphiphilic secondary structure in bacterial membranes, typically involving segregation of their positively-charged and hydrophobic groups onto opposing faces of an α-helix [18]. The propensity for α-helix formation in cell membranes correlates positively with CAP activity and selectivity of bacterial over human cells, and WLBU2 has been optimized specifically for formation of an amphipathic α-helix conformation in cell membranes [23-25, 28]. Finally, in addition to its broad-spectrum antimicrobial activity in blood, WLBU2 retains potency while bound to solid surfaces [14, 26, 27, 29, 30] and importantly, shows high affinity for adhesion of susceptible bacteria [27].

In this paper we describe the outcomes of a comparative study of molecular interactions of WLBU2 and PmB with LPS. Analysis of the competitive adsorption behavior of peptide and LPS recorded with optical waveguide lightmode spectroscopy (OWLS) and interfacial tensiometry, and analysis of peptide structure and particle size distribution in peptide-vesicle suspensions with circular dichroism (CD) and dynamic light scattering (DLS), were used to evaluate differences in the stability of peptide-vesicle association, and hence the associated potential of each peptide for use in hemoperfusion for endotoxin removal.

Materials and Methods

Peptides and Lipopolysaccharides. Unless otherwise specified, all reagents were purchased from commercial vendors and were of analytical reagent or higher grade.

WLBU2 (RRWVRRVRRWVRRVVRVVRRWVRR, 3400.1 Da) was obtained from GenScript (Piscataway, NJ). Polymyxin B sulfate (PmB, 1385.6 Da) and purified *Pseudomonas aeruginosa* lipopolysaccharide (LPS) were purchased from Sigma-Aldrich (St Louis, MO). All solutions were prepared using HPLC-grade water, and all peptides and LPS were used as received, without further purification.

Stock solutions of WLBU2 were made in phosphate buffered saline (PBS, 10 mM sodium phosphate with 150 mM NaCl at pH 7.4), or in 0.5M $HClO_4$ for circular dichroism. Working solutions at 50 μM or 5 μM concentrations were prepared in degassed PBS, using the calculated molar extinction coefficient at 280 nm (16,500 M^{-1} cm^{-1}) of WLBU2 [31]. Similarly, 10 mg/mL stock solutions of PmB in degassed PBS were diluted to 50 μM or 5 μM. LPS was dissolved in PBS to 10 mg/mL, and diluted to 0.1 mg/mL in degassed PBS. All dilute peptide/LPS solutions were prepared and degassed under vacuum with sonication immediately before use.

Surface Modification of OWLS Sensors. SiO_2-coated OW2400c OWLS waveguides (MicroVacuum, Budapest, Hungary) were cleaned by submersion in 5% w/v sodium dodecyl sulfate (SDS) for thirty minutes, followed by 10 min at 80 ℃ in 5:1:1 H_2O:27% HCl:30% H_2O_2, then rinsed with HPLC H_2O and dried under a stream of N_2 [32]. Cleaned waveguide surfaces were modified with trichlorovinylsilane (TCVS, TCI America, Portland, OR) by a variation of the method of Popat [33-35]. Briefly, clean OWLS sensors were exposed to flowing dry N_2 in a sealed vessel for 1 hr to remove any residual surface moisture, after which 200 μL of was added and allowed to vaporize at 25 ℃, while flowing N_2 transported the TCVS vapor across the waveguide surfaces. The N_2

flow was maintained for three hours, after which the sensors were cured at 120 ℃ for 30 min to stabilize the vinylsilane layer. Cleaned and modified sensors were stored in 1.5 mL centrifuge vials under N_2 in the dark to prevent oxidation of the vinyl moieties.

Optical Waveguide Lightmode Spectroscopy. Silanized waveguides were equilibrated prior to use by incubation overnight in PBS [36], then rinsed with HPLC H_2O, dried with N_2, and immediately installed in the flow cell (4.8 uL total volume) of a MicroVacuum OWLS 210 instrument (Budapest, Hungary) equipped with a 4 mL narrow-bore Tygon® flow loop in line with the flow cell. Incoupling peak angles (±TE and TM) were recorded about four times per minute at 20 ℃, and a stable baseline was achieved with PBS prior to the injection of peptide or LPS. Unless otherwise indicated, flow rates were maintained at 50 µL/min during adsorption and elution steps. Peptides or LPS were either introduced singly (sequential adsorption) for 40 min, with a PBS rinse for 40 min between analytes, or as mixtures (competitive adsorption) for 40 minutes followed by a 40 minute PBS rinse.

Interfacial tensiometry. A FTÅ model T10 (First Ten Ångstroms, Portsmouth, VA) equipped with a Du Nuöy ring (CSC Scientific Co, Fairfax, VA) was used to measure the baseline surface tension of 6.5 mL of PBS, after which 500 µL of peptide or LPS stock solution was injected to reach final concentrations of 5 or 50 µM WLBU2 or PmB in PBS, with or without 0.1 mg/mL LPS. Data was collected for at least 20 min to determine the steady state surface tension of the resulting peptide and/or LPS solutions. The platinum ring was flamed to remove contaminants between experiments.

***Dynamic Light Scattering*.** Apparent particle sizes of peptide and LPS solutions and mixtures were measured at 20 ℃ by dynamic light scattering (DLS) at 635 nm, using a Brookhaven Instruments 90 Plus Particle Size Analyzer (Holtsville, NY). Ten 1-minute scans were averaged for each sample, and cumulative size distributions extracted from the multimodal size distribution data.

***Circular Dichroism*.** Peptide secondary structure in the presence or absence of LPS was evaluated in triplicate by circular dichroism (CD) using a Jasco J-815 spectropolarimeter (Easton, MD) at 25 ℃. Spectra were recorded in a cylindrical cuvette (0.1 cm pathlength) from 185 to 260 nm in 0.5 nm increments after calibration with 0.6 mg/mL *D*(+)-camphorsulfonic acid, and 10 scans/sample were averaged to increase the signal-to-noise ratio. All concentrations of peptides and LPS were the same as for tensiometry and OWLS. The spectra from each of the three replicates for each sample differed only slightly (~5%) in signal intensity; representative spectra are shown throughout. Peptide α-helix content was estimated from CD spectra using DichroWeb [37, 38].

Results and Discussion

Competitive adsorption of peptides and LPS at the air-water interface. Surface tension depression was recorded for mixtures of LPS (0.1 mg/mL) and peptide at high (50 μM) or low (5 μM) peptide concentrations in buffer (Figures B.1 and B.2). In the absence of peptide, LPS vesicles decreased surface tension to a steady value of about 40 mN/m. In contrast, while 50 μM PmB slightly reduced surface tension, PMB had almost no effect

on surface tension at 5 μM (Figure B.1, top). However, when PmB is mixed with LPS, a faster rate of surface tension decrease is observed at each concentration, and, in the case of 50 μM PmB, the surface tension is reduced to a greater extent than observed with LPS alone (Figure B.1, bottom).

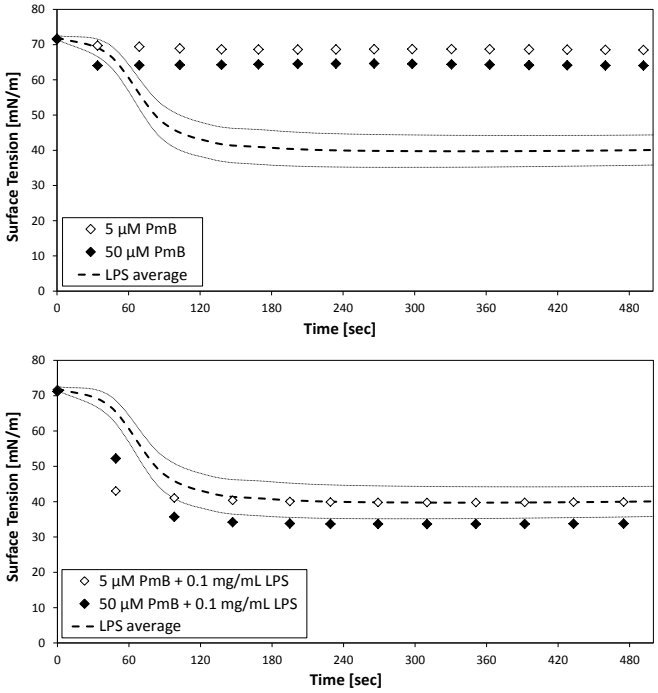

Figure B.1. Air-water tensiometry of suspensions of 5 or 50 μM PmB and 1.0 mg/mL LPS in PBS, as individual species (top) and as mixtures of peptide and LPS (bottom). Average values (- - -) and standard deviation (n = 5, gray lines) are shown for LPS.

As with PmB, WLBU2 in the absence of LPS did not substantially decrease surface tension at either concentration (Figure B.2, top). However, unlike PmB, the similarity in the rate and extent of surface tension depression at each WLBU2 concentration suggests that monolayer coverage of the interface is achieved in each case.

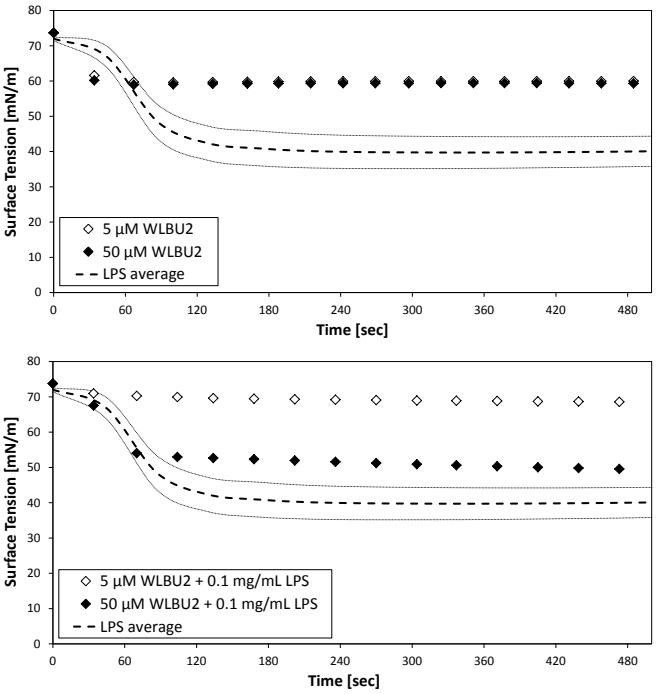

Figure B.2. Air-water tensiometry of suspensions of 5 or 50 µM WLBU2 and 1.0 mg/mL LPS in PBS, as individual species (top) and as mixtures of peptide and LPS (bottom). Average values (- - -) and standard deviation (*n* = 5, gray lines) are shown for LPS.

The dimensions of the peptides were determined using the open-source viewer Jmol™ [39] from structures of PmB from the NCBI PubChem repository (CID 49800003), and a helical structure ofWLBU2 predicted using PEP-Fold [40, 41] (Figure B.3). From those dimensions, the expected surface concentrations of PmB and WLBU2 peptides adsorbed in a monolayer in a "side-on" or "end-on" conformation were estimated, assuming a footprint of the solution dimensions and close-packed rectangular (side-on) or hex-packed circular (end-on) configurations (Table B.1). The ratio of the surface tension depression for WLBU2 relative to PmB (Figure B.1 and Figure B.2, top panels) is about 3.23 at 5 µM peptide, and about 1.55 at 50 µM peptide. These values fall within limits based on expectations for monolayer coverage.

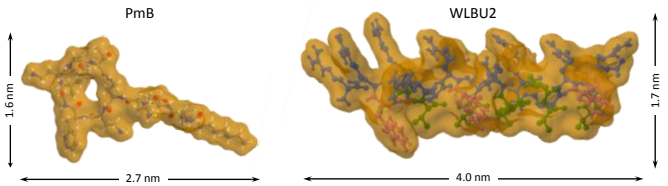

Figure B.3. Molecular structure and approximate dimensions of PmB (left) and helical form of WLBU2 (right) peptide.

Mixtures of LPS and WLBU2 behave quite differently from the mixtures of PmB and LPS (Figure B.1 and Figure B.2, bottom panels). In particular, the presence of WLBU2 with LPS results in appreciably reduced surface tension depression when compared to LPS alone (Figure B.2, bottom). At the low (5 μM) concentration of WLBU2, the surface tension depression is nearly negligible compared to that associated with either WLBU2 or LPS alone. At higher (50 μM) WLBU2 concentrations in an LPS-WLBU2 mixture, the surface tension was depressed substantially, but did not reach that of LPS alone.

These results strongly suggest that suspensions of LPS with WLBU2 are more stable than similar suspensions of LPS with PmB. In particular, suspensions of LPS with WLBU2 show substantially less surface activity (e.g., vesicle adsorption and spreading at the interface) than is exhibited by LPS alone (Figure B.2, bottom). In contrast, suspensions of LPS with polymyxin B show greater surface activity than is observed for LPS alone (Figure B.1, bottom).

These findings are potentially consistent with the notion that peptide insertion (into the vesicle membrane) and stabilization of intact LPS vesicles occurs in the case of WLBU2, while peptide-induced destabilization of LPS vesicles occurs in the case of PmB. We further tested this hypothesis by evaluating the adsorption behavior of peptide-LPS mixtures at a hydrophobic solid surface, and observation of peptide 2 °structure and particle size distributions in such mixtures.

Table B.1: Size and estimated packing density of PmB and WLBU2 adsorbed "side-on" and "end-on" at an interface. Dimensions were estimated from published (PmB) or predicted (WLBU2) molecular structures.

Peptide	MW (Da)	Length (nm)	Width (nm)	"Side-On" Monolayer (ng/cm^2)	"End-On" Monolayer (ng/cm^2)
PmB	1385.6	2.7	1.6	53	86
WLBU2	3400.1	4.0	1.7	83	180

Competitive adsorption of peptides and LPS at a hydrophobic solid surface. Fig shows the adsorption and elution kinetics recorded with mixtures of LPS (0.1 mg/mL) and peptide at high (50 μM) or low (5 μM) peptide concentrations. The total mass remaining after elution was similar for both mixtures containing PmB, with final adsorbed masses of 74 or 55 ng/cm^2, respectively. The adsorption kinetics of LPS in the presence of PmB (Figure B.4) are also consistent with the tensiometry results of Figure B.1, and suggest that destabilized LPS vesicles adsorb and spread at the interface.

In contrast, the final adsorbed masses after elution for mixtures containing 0.1 mg/mL LPS and 5 or 50 μM WLBU2 were substantially different. The final adsorbed mass was nearly zero at the low peptide concentration, but reached 590 ng/cm^2 with 50 μM

WLBU2. The observation of extremely low surface activity (i.e. adsorbed amounts) in WLBU2-LPS mixtures at low peptide concentration is consistent with the tensiometry results (Figure B.2, bottom). It also suggests formation of LPS vesicles which are stabilized against spreading at the hydrophobic surface under these conditions, presumably due to their association with the membrane-active peptide WLBU2. The reason for the high value of adsorbed mass remaining after elution in the case of the 50 μM WLBU2-LPS mixture is not obvious. With reference to Figure B.2 (bottom), however, the high adsorption would not be consistent with any enhancement of LPS vesicle spreading at the interface. Rather, it is possible that WLBU2-stabilized LPS vesicles locate at the interface under this condition.

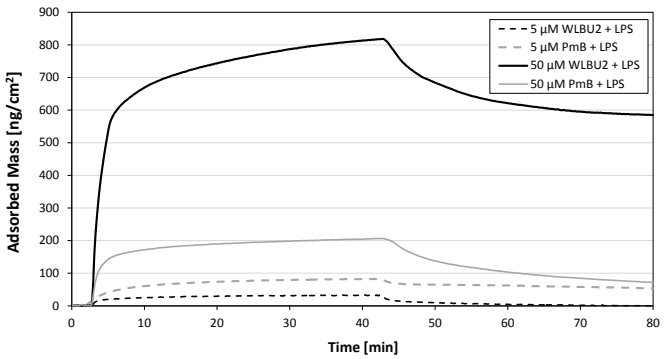

Figure B.4. OWLS kinetic data for competitive adsorption from mixtures of LPS (0.1 mg/mL) and peptide at low (5 μM) and high (50 μM) peptide concentrations.

Peptide structure in peptide-LPS mixtures. WLBU2 structure is substantially disordered in aqueous solution, but becomes increasingly helical in the presence of certain anions (e.g. ClO_4^-) [42], membrane-mimetic solvents, or bacterial membranes. For example, Deslouches et al. (2005b) showed that WLBU2 has no appreciable stable structure in

water, but reaches 81% α-helix content in an ideal membrane mimetic solvent (30% trifluoroethanol in phosphate buffer) [25]. Circular dichroism shows that WLBU2 gains substantial helicity when mixed with LPS (Figure B.5, left), reaching 78% α-helix content. This strongly suggests that the peptide is located almost exclusively within the membranes of the LPS vesicles. Due to its rigid, cyclic structure, PmB would not be expected to become substantially α-helical, and in fact shows no appreciable helical structure under any conditions (Figure B.5, right). The CD spectrum from the PmB-LPS mixture appears to be primarily the sum of the CD signal from PmB and LPS alone.

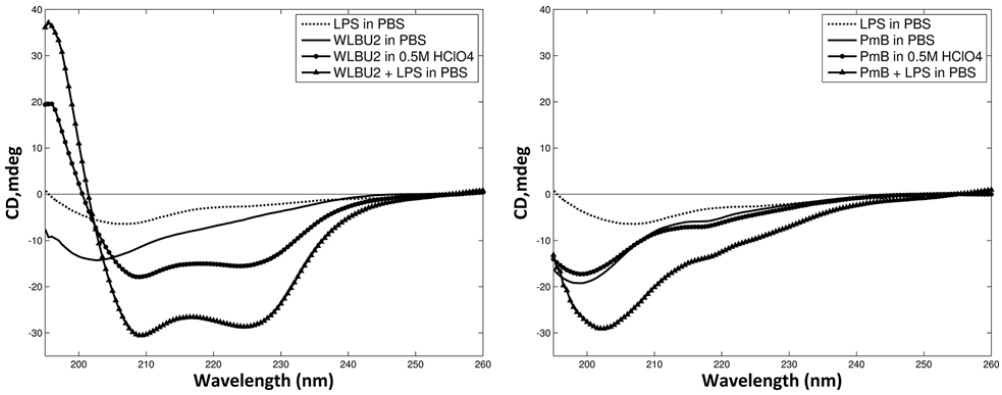

Figure B.5. Circular dichroism (CD) spectra of WLBU2 (left) and PmB (right) in PBS, with helix-inducing perchlorate ions, or in the presence of LPS vesicles.

Vesicle size distribution in peptide-LPS mixtures. Dynamic light scattering analysis of peptide-LPS mixtures and peptide-free LPS suspensions are presented in Figure B.6 as the cumulative oversize distribution of particle diameter. The particle size distribution was bimodal in all cases. At the lower mode, the presence of WLBU2 increased the apparent particle diameter of LPS, from 95 ±11 nm to 195 ±13 nm (mean ± standard deviation, n = 3), while addition of PmB had very little effect on particle size in the lower

mode (89 ±19 nm). At the upper mode, however, the presence of PmB decreased the mean particle diameter from 408 ±56 nm to 262 ±26 nm, consistent with disruption of the LPS vesicles. In contrast, the presence of WLBU2 greatly increased both the mean and the range of particle sizes, with a mean diameter of 909 ±204 nm. This increase in particle size and polydispersity suggests that WLBU2 induces aggregation of LPS vesicles.

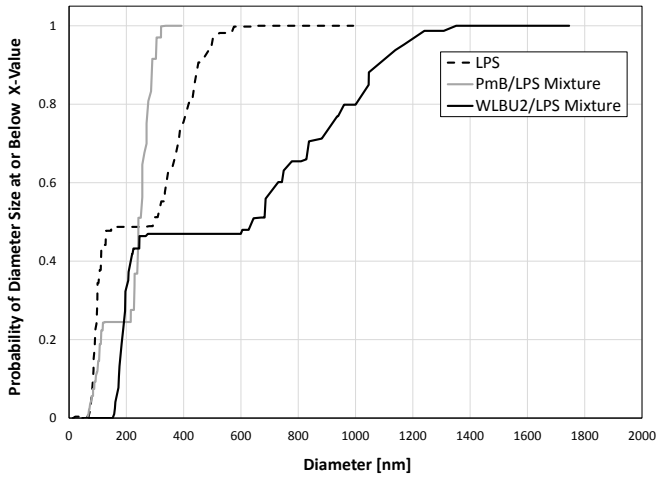

Figure B.6. Cumulative oversize distribution of particle diameter in peptide-LPS suspensions from dynamic light scattering (DLS).

Anecdotal evidence recorded during preparation of peptide-LPS suspensions at high concentrations (700 μM peptide and 1.4 mg/mL LPS) suggest that the increase in LPS particle diameter in the presence of WLBU2 is not caused by an increase in the individual vesicle size, but rather is due to large-scale aggregation of vesicles (Figure B.7). While there is a slight increase in turbidity of LPS suspensions when PmB is added, aggregation is not visible in either the PmB-LPS or peptide-free LPS suspensions.

Figure B.7. Visible aggregation rapidly occurs in concentrated mixtures of WLBU2 and LPS (top), but not in PmB-LPS (middle) or peptide-free LPS suspensions (bottom).

Taken together, the results described above strongly support the hypothesis that peptide insertion and stabilization of intact LPS vesicles occurs in the case of WLBU2, while PmB causes peptide-induced destabilization and disruption of LPS vesicles. Moreover, they suggest that the high value of adsorbed mass for WLBU2-LPS mixtures at high peptide concentration (Figure B.7) can be attributed to location of intact WLBU2-LPS vesicles or vesicle aggregates at the interface. We are currently evaluating the feasibility of endotoxin capture using membrane-active peptides which have been covalently tethered to surfaces by short and long hydrophilic linkers, and results from that work will contribute to the subject of a future report.

Conclusions

Analysis of the interfacial behavior of mixtures of LPS and peptide using interfacial tensiometry as well as OWLS, evaluation of peptide structure in such mixtures using CD, and determination of the particle size distributions in such mixtures using DLS, all

strongly suggest peptide insertion and stabilization of intact LPS vesicles in the case of WLBU2, while PmB appears to cause peptide-induced destabilization and disruption of LPS vesicles. In the context of blood purification with hemoperfusion, the most desired outcome is insertion and tight binding of the peptide in the bacterial membrane or LPS vesicle, without destabilizing the membrane. Disruption and concomitant lysis of the membrane could cause the return of LPS or cellular degradation products to the circulating blood, and is not desirable. Thus, we expect that presentation of WLBU2 at an interface, tethered in a fashion preserving its solvent accessibility and mobility, may promote the capture of pathogens or endotoxin that reach the surface without destabilizing or disrupting the captured vesicle or pathogen. Based on the results provided here, there is no reason to expect a similar outcome with PmB.

Acknowledgments

The authors thank Dr. Kerry McPhail and Dr. Jeff Nason for the use of their CD and DLS instruments, respectively. This work was supported in part by the National Institute of Biomedical Imaging and Bioengineering (NIBIB, grant no. R01EB011567). The content is solely the responsibility of the authors and does not necessarily represent the official views of NIBIB or the National Institutes of Health.

References

[1] D.C. Angus R.S. Wax, Epidemiology of sepsis: An update, Crit. Care Med. 29 (2001) S109-S116.

[2] J. Cohen, The immunopathogenesis of sepsis, Nature 420 (2002) 885-891.

[3] K. Wood D. Angus, Pharmacoeconomic implications of new therapies in sepsis, Pharmacoeconomics 22 (2004) 895-906.

[4] N. Matsuno, T. Ikeda, K. Ikeda, K. Hama, H. Iwamoto, M. Uchiyama, K. Kozaki, Y. Narumi, K. Kikuchi, H. Degawa T. Nagao, Changes of cytokines in direct endotoxin adsorption treatment on postoperative multiple organ failure, Ther. Apher. 5 (2001) 36-39.

[5] F.B. Anspach, Endotoxin removal by affinity sorbents, J. Biochem. Biophys. Methods 49 (2001) 665-681.

[6] K. Buttenschoen, P. Radermacher H. Bracht, Endotoxin elimination in sepsis: Physiology and therapeutic application, Langenbeck's Archives of Surgery 395 (2010) 597-605.

[7] B. Davies J. Cohen, Endotoxin removal devices for the treatment of sepsis and septic shock, The Lancet Infectious Diseases 11 (2011) 65-71.

[8] H. Shoji, Extracorporeal endotoxin removal for the treatment of sepsis:Endotoxin adsorption cartridge (Toraymyxin), Theor. Apheresis Dial. 7 (2003) 108-114.

[9] J.-L. Vincent, P.-F. Laterre, J. Cohen, H. Burchardi, H. Bruining, F.A. Lerma, X. Wittebole, D. De Backer, S. Brett, D. Marzo, H. Nakamura S. John, A pilot-controlled study of a polymyxin B-immobilized hemoperfusion cartridge in patients with severe sepsis secondary to intra-abdominal infection, Shock 23 (2005) 400-405.

[10] T. Ikeda, Hemoadsorption in critical care, Ther. Apher. 6 (2002) 189-192.

[11] T. Ueno, M. Sugino, H. Nemoto, H. Shoji, A. Kakita M. Watanabe, Effect over time of endotoxin adsorption therapy in sepsis, Theor. Apheresis Dial. 9 (2005) 128-136.

[12] V. Hlady J. Buijs, Protein adsorption on solid surfaces, Curr. Opin. Biotechnol. 7 (1996) 72-77.

[13] J.A. Neff, P.A. Tresco K.D. Caldwell, Surface modification for controlled studies of cell–ligand interactions, Biomaterials 20 (1999) 2377-2393.

[14] S.A. Onaizi S.S.J. Leong, Tethering antimicrobial peptides: Current status and potential challenges, Biotechnol. Adv. 29 (2011) 67-74.

[15] F.B. Anspach O. Hilbeck, Removal of endotoxins by affinity sorbents, J. Chromatogr. 711 (1995) 81-92.

[16] J. Li, R.L. Nation, J.D. Turnidge, R.W. Milne, K. Coulthard, C.R. Rayner D.L. Paterson, Colistin: The re-emerging antibiotic for multidrug-resistant gram-negative bacterial infections, The Lancet Infectious Diseases 6 (2006) 589-601.

[17] M. Hogardt, S. Schmoldt, M. Götzfried, K. Adler J. Heesemann, Pitfalls of polymyxin antimicrobial susceptibility testing of Pseudomonas aeruginosa isolated from cystic fibrosis patients, J. Antimicrob. Chemother. 54 (2004) 1057-1061.

[18] R.E.W. Hancock, Cationic peptides: Effectors in innate immunity and novel antimicrobials, The Lancet Infectious Diseases 1 (2001) 156-164.

[19] R.E.W. Hancock A. Rozek, Role of membranes in the activities of antimicrobial cationic peptides, FEMS Microbiol. Lett. 206 (2002) 143-149.

[20] M. Gough, R. Hancock N. Kelly, Antiendotoxin activity of cationic peptide antimicrobial agents, Infect. Immun. 64 (1996) 4922-4927.

[21] M.G. Scott, H. Yan R.E.W. Hancock, Biological properties of structurally related a-helical cationic antimicrobial peptides, Infect. Immun. 67 (1999) 2005-2009.

[22] O. Cirioni, A. Giacometti, R. Ghiselli, C. Bergnach, F. Orlando, C. Silvestri, F. Mocchegiani, A. Licci, B. Skerlavaj, M. Rocchi, V. Saba, M. Zanetti G. Scalise, LL-37 protects rats against lethal sepsis caused by gram-negative bacteria, Antimicrob. Agents Chemother. 50 (2006) 1672-1679.

[23] B. Deslouches, I.A. Gonzalez, D. DeAlmeida, K. Islam, C. Steele, R.C. Montelaro T.A. Mietzner, De novo-derived cationic antimicrobial peptide activity in a murine model of Pseudomonas aeruginosa bacteraemia, J. Antimicrob. Chemother. 60 (2007) 669-672.

[24] B. Deslouches, K. Islam, J.K. Craigo, S.M. Paranjape, R.C. Montelaro T.A. Mietzner, Activity of the de novo engineered antimicrobial peptide WLBU2 against Pseudomonas aeruginosa in human serum and whole blood: Implications for systemic applications, Antimicrob. Agents Chemother. 49 (2005) 3208-3216.

[25] B. Deslouches, S.M. Phadke, V. Lazarevic, M. Cascio, K. Islam, R.C. Montelaro T.A. Mietzner, De novo generation of cationic antimicrobial peptides: Influence of

length and tryptophan substitution on antimicrobial activity, Antimicrob. Agents Chemother. 49 (2005) 316-322.

[26] R.C. Montelaro T.A. Mietzner, Virus derived antimicrobial peptides, U.S. Patent 6,887,847, 2005.

[27] I.A. Gonzalez, X.X. Wong, D. De Almeida, R. Yurko, S. Watkins, K. Islam, R.C. Montelaro, A. El-Ghannam, T.A. Mietzner, Peptides as potent antimicrobials tethered to a solid surface: Implications for medical devices, Nature Precedings (2008).

[28] M.C. Skinner, A.O. Kiselev, C.E. Isaacs, T.A. Mietzner, R.C. Montelaro M.F. Lampe, Evaluation of WLBU2 peptide and 3-O-octyl-sn-glycerol lipid as active ingredients for a topical microbicide formulation targeting Chlamydia trachomatis, Antimicrob. Agents Chemother. 54 (2010) 627-636.

[29] F. Costa, I.F. Carvalho, R.C. Montelaro, P. Gomes M.C.L. Martins, Covalent immobilization of antimicrobial peptides (AMPs) onto biomaterial surfaces, Acta Biomater. 7 (2011) 1431-1440.

[30] J.R. McClanahan, R. Peyyala, R. Mahajan, R.C. Montelaro, K.F. Novak D.A. Puleo, Bioactivity of WLBU2 peptide antibiotic in combination with bioerodible polymer, Int. J. Antimicrob. Agents 38 (2011) 530-533.

[31] C.N. Pace, F. Vajdos, L. Fee, G. Grimsley T. Gray, How to measure and predict the molar absorption coefficient of a protein, Protein Sci. 4 (1995) 2411-2423.

[32] M.P. Ryder, J. McGuire K.F. Schilke, Cleaning requirements for silica-coated sensors used in optical waveguide lightmode spectroscopy, Surf. Interface Anal. 45 (2013) 1805-1809.

[33] K.C. Popat, R.W. Johnson T.A. Desai, Characterization of vapor deposited thin silane films on silicon substrates for biomedical microdevices, Surf. Coat. Technol. 154 (2002) 253-261.

[34] J.K. Dill, J.A. Auxier, K.F. Schilke J. McGuire, Quantifying nisin adsorption behavior at pendant PEO layers, J. Colloid Interface Sci. 395 (2013) 300-305.

[35] M.C. Lampi, X. Wu, K.F. Schilke J. McGuire, Structural attributes affecting peptide entrapment in PEO brush layers, Colloids Surf. B. Biointerfaces 106 (2013) 79-85.

[36] J.J. Ramsden, Porosity of pyrolysed sol-gel waveguides, J. Mater. Chem. 4 (1994) 1263-1265.

[37] L. Whitmore B.A. Wallace, Dichroweb, an online server for protein secondary structure analyses from circular dichroism spectroscopic data, Nucleic Acids Res. 32 (2004) W668-W673.

[38] L. Whitmore B.A. Wallace, Protein secondary structure analyses from circular dichroism spectroscopy: Methods and reference databases, Biopolymers 89 (2008) 392-400.

[39] A. Herráez, Biomolecules in the computer: Jmol to the rescue, Biochemistry and Molecular Biology Education 34 (2006) 255-261.

[40] J. Maupetit, P. Derreumaux P. Tuffery, Pep-fold: An online resource for de novo peptide structure prediction, Nucleic Acids Res. 37 (2009) W498-W503.

[41] P. Thévenet, Y. Shen, J. Maupetit, F. Guyon, P. Derreumaux P. Tufféry, Pep-fold: An updated de novo structure prediction server for both linear and disulfide bonded cyclic peptides, Nucleic Acids Res. 40 (2012) W288-W293.

[42] X. Wu, M.P. Ryder, J. McGuire, K.F. Schilke, Adsorption, structural alteration and elution of peptides at pendant PEO layers, Colloids Surf. B. Biointerfaces 112 (2013) 23-29.

BINDING OF BACTERIAL LIPOPOLYSACCHARIDE BY THE CATIONIC AMPHIPHILIC PEPTIDE WLBU2 AT INTERFACES

Matthew P. Ryder, Xiangming Wu, Miranda Raper, Joseph McGuire, Karl F. Schilke

School of Chemical, Biological and Environmental Engineering, Oregon State University, Corvallis, OR 97331

For submission to Biomaterials Literature

APPENDIX C

BINDING OF BACTERIAL LIPOPOLYSACCHARIDE BY THE CATIONIC AMPHIPHILIC PEPTIDE WLBU2 AT INTERFACES

Abstract

Passage of blood through a sorbent device for removal of bacteria and endotoxin by specific binding with immobilized, membrane-active, bactericidal peptides holds promise for treating severe blood infections. Peptide insertion in the target membrane and rapid/strong binding is desirable, while competing interactions with blood proteins is not. Here we describe interactions between bacterial endotoxin (lipopolysaccharide, LPS) and the bactericidal peptide WLBU2 in a myriad of surface proximal motifs, i.e. surface bound, PEG entrapped, and PEG tethered. Analysis of the interactions using QCM-D, and CD, as well as the effects of γ-irradiation on PEGylated WLBU2 using UV/Vis spectroscopy and NMR, all reveal that WLBU2 can interact with LPS in a manner keeping with its purpose whether irradiated, PEGylated, or tethered. Further, interactions between LPS and WLBU2 in these motifs in the presence of fibrinogen reveal a complicated interaction between fibrinogen and LPS, and between fibrinogen and WLBU2, but data analysis suggests that WLBU2 may still preferentially capture LPS over interactions with fibrinogen. We therefore expect that tethered WLBU2 in an engineered hemoperfusive devise will enable the capture of bacteria and endotoxin without promoting reintroduction of endotoxin to the circulating blood, minimized blood protein interaction, and minimal adverse clinical outcomes.

Introduction

Severe sepsis is a blood infection that in the US alone affects about 750,000 people each year, killing 28-50% of them [1-3]. The number of sepsis-related deaths continues to increase, and is already greater than the annual number of deaths in the US from prostate cancer, breast cancer and AIDS combined. During bacterial growth or as a result of the action of antibacterial host factors, lipopolysaccharide (LPS, endotoxin) is released from the cell wall of Gram-negative bacteria. The high immunostimulatory potency of endotoxin causes dysregulation of the inflammatory response with elevated production and release of proinflammatory cytokines [4], leading to blood vessel damage and organ failure [1, 2].

Hemoperfusion, involving passage of blood through a sorbent device for the removal of selected targets, holds promise for treating sepsis [5-7]. Successful hemoperfusion for sepsis treatment will require surface modification that will ensure highly selective capture of bacteria and endotoxin that reach the interface. In addition, surface coatings must provide pathogen binding functionality without evoking a host cell response, without nonspecific adsorption of protein, and without platelet activation and blood cell damage caused by cell-surface interactions.

In a previous paper we demonstrated that WLBU2 inserts into, and stabilizes, the membrane of LPS. This was done in comparison to polymyxin B (PmB), a peptide used clinically for hemoperfusion in Japan [7, 8]. PmB appeared to cause peptide-induced destabilization and disruption of LPS vesicles. That work was accomplished by analysis of the interfacial behavior of mixtures of LPS and peptide using interfacial tensiometry as

well as OWLS, evaluation of peptide structure in such mixtures using CD, and determination of the particle size distributions in such mixtures using DLS. In the context of blood purification with hemoperfusion, peptide insertion in the susceptible membrane and tight binding is desired, while membrane disruption, concomitant lysis and return of degradation products to the circulating blood is not desired. In this work, we take the next step toward a prototype device, providing evidence that presentation of WLBU2 at an interface, tethered in a fashion preserving its solvent accessibility and mobility, can promote the capture of endotoxin that enters the interface. Tethered and entrapped peptide motifs (Figure C.1) are compared.

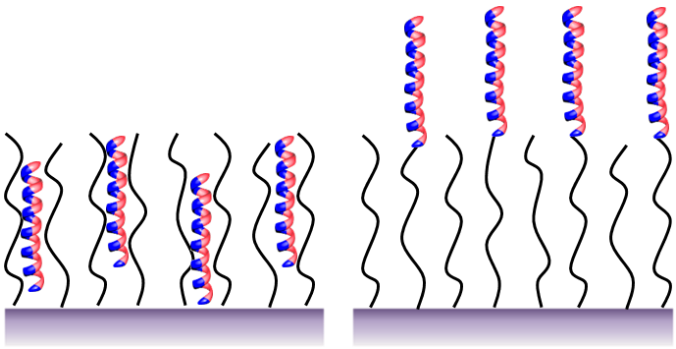

Figure C.1: Cartoon illustration of WLBU2 at an interface in an entrapped (left) or tethered (right) motif. Image is not to scale.

Materials and Methods

Proteins, Surfactants, and Lipopolysaccharide. Unless otherwise specified, all reagents were purchased from commercial vendors and were of analytical reagent or higher grade. WLBU2 (RRWVRRVRRWVRRVVRVVRRWVRR, 3.4 kDa), CysWLBU2 ,and WLBU2Cys were obtained from GenScript (Piscataway, NJ). The latter peptides are

structurally identical to the original WLBU2 except for an additional cysteine at the N-terminus and C-terminus, respectively. All peptides were used at 50 μM in phosphate buffered saline (10 mM PBS, 150 mM NaCl) unless otherwise noted. Fibrinogen from bovine plasma (Fib, 340 kDa), and purified *Pseudomonas aeruginosa* lipopolysaccharide (LPS) were purchased from Sigma-Aldrich (St Louis, MO). LPS was used at 0.1 mg/mL in PBS in all cases. All solutions were prepared using HPLC-grade water, and all peptides and LPS were used as received, without further purification. Fibrinogen was prepared in HPLC, incubated at 37 °C for 2 hr, and 0.45 μm filtered prior to use [9]. Fibrinogen was used at 2 mg/mL in all cases.

Self-assembled PEO brush layers were formed by suspension of hydrophobic silica nanoparticles (R816, Degussa, 190 m^2/g, 10-12 nm) in Pluronic® F127 (PEO_{101}-PPO_{56}-PEO_{101}, ≈12.6 kDa, BASF) in HPLC water (1 % wt/v) overnight on a rotator. F127 was also used in conjunction with QCM-D sensors, described later. End Group Activated F127 Pluronic, activated with pyridyl disulfide (EGAP-PDS) was obtained from Allvivo Vascular, Inc. EGAP-PDS was incubated with CysWLBU2 in equimolar concentrations for 8 hr at room temperature (EGAP-WLBU2) before use similar to F127. F127 was used instead of F108, as in previous chapters, because the EGAP from Allvivo is based on the F127 triblock.

Surface Modification of QCM-D sensors. QSX303 silicon dioxide QCM-D sensors were purchased from Biolin (Linthicum, MD) and were cleaned by 15 min UV/O_3 clean followed by 1 hr in 5 % w/v sodium dodecyl sulfate (SDS) and then another 15 min in UV/O_3. Cleaned sensor surfaces were modified with trichlorovinylsilane (TCVS, TCI

America, Portland, OR) by a variation of the method of Popat [10-12]. Briefly, clean QCM-D sensors were exposed to flowing dry N_2 in a sealed vessel for 1 hr to remove any residual surface moisture, after which 200 µL of TCVS was added and allowed to vaporize at 25 ℃, while flowing N_2 transported the TCVS vapor across the sensor surfaces. The N_2 flow was maintained for three hours, after which the sensors were cured at 120 ℃ for 30 min to stabilize the vinylsilane layer. Cleaned and modified senors were stored in 1.5 mL centrifuge vials under N_2 in the dark until further use. All silanized sensors were submerged in 1% w/v F127 or EGAP-WLBU2 and exposed to γ-radiation from a ^{60}Co source (Oregon State University Radiation Center) for a total dose of 0.3 Mrad to achieve polymer grafting [13]. Sensors were used immediately after surface preparation.

Au coated QCM-D sensors (Biolin, Linthicum, MD) were cleaned by 15 min UV/O_3 clean followed by 10 min in 5:1:1 H_2O:30% H_2O_2:27% NH_4OH solution at 80 ℃, followed by another 15 min UV/O_3 clean. These sensors were used immediately after cleaning.

Quartz Crystal Microbalance with Dissipation. All modified sensors were submerged in HPLC water for 1 hr prior to instrument use to remove residual F127 or EGAP. The adsorption and elution of peptides, LPS, and Fibrinogen were measured with a Q-Sense E4 QCM-D (Q-Sense, Linthicum, MD). QCM-D allows simultaneous measurement of changes in resonance frequency (Δf) and energy dissipation (ΔD) caused by adsorbed mass on QCM-D sensors. For rigid layers, changes in mass can be directly calculated by the Sauerbrey equation [14]:

$$\Delta m = -C\frac{1}{n}\Delta f$$

Where Δm is the change in adsorbed mass, Δf is the change in frequency, n is the frequency overtone, and C is a constant parameter characteristic to the quartz crystal, very commonly 17.7 ng/cm^2 s.

A high precision peristaltic pump was used to flow sample solutions over QCM-D sensors. Flow rates were maintained at 50 μL/min, and solution temperature was maintained at 20 ℃. QCM-D experiments began by collecting baseline data of a peptide free phosphate buffered saline solution (10 mM PBS, 150 mM NaCl) followed by introduction of WLBU2, or variant, followed by rinse with PBS, a subsequent challenge with LPS, Fibrinogen, or a mixture of both, and a final rinse with PBS. All adsorption and elution steps proceeded for 40 min. In all QCM-D data presented, the Δf is from the 5th overtone. All QCM-D data on surfaces containing pre-adsorbed triblock was baseline adjusted using MatLab prior to use. In brief, this was accomplished by modeling the baseline assuming a simple kinetic model for the removal of excess triblock, suggested by an initial increase in frequency. The model was fit to the baseline by minimizing the residual between the model and the data, and the model was subtracted from the whole subset of data.

Circular Dichroism. Peptide secondary structure in the presence or absence of LPS was evaluated by circular dichroism (CD) using a Jasco J-815 spectropolarimeter (Easton, MD) at 25 ℃. Spectra were recorded in a cylindrical cuvette (0.1 cm pathlength) from 185 to 260 nm in 0.5 nm increments after calibration with 0.6 mg/mL *D*(+)-

camphorsulfonic acid, and 10 scans/sample were averaged to increase the signal-to-noise ratio. All concentrations of solutions were the same as QCM-D. Representative spectra are shown throughout. Peptide helicity was estimated from representative CD spectra using DichroWeb [15-16].

UV/Vis Spectroscopy. Peptide concentration, as well as the extent of WLBU2 attachment to EGAP-PDS was assessed using a Thermo-Electron Genesys 6 UV-Vis spectrophotometer (Madison, WI). Concentration of WLBU2 and variants was assessed using the calculated molar extinction coefficient at 280 nm (16,500 M^{-1} cm^{-1}) of WLBU2 [17]. The extent of covalent attachment was assessed at 343 nm by the increase in pyridine-2-thione (P2T) concentration (8080 M^{-1} cm^{-1}) [18].

Nuclear Magnetic Resonance. Proton nuclear magnetic resonance (^{1}H-NMR) spectra were taken using a Brüker (Billerica, MA) Robinson 400 MHz NMR spectrometer with TopSpin 2.1 software at room temperature (25 °C) using ~1000 μM WLBU2 and γ-WLBU2 in D_2O. Each sample was measured using 128 scans. The spectra were post processed by setting the line broadening factor to 0.8 Hz.

Results and Discussion

***Interaction between LPS and surface bound peptide*.** The interaction between LPS (0.1 mg/mL) and surface bound WLBU2, and WLBU2 variants recorded by QCM-D are presented in Figure C.2 and Figure C.3. If a given system shows small or insignificant changes in dissipation, QCM-D data can be modeled using the Sauerbrey model [14], which directly relates (negative) changes in frequency to changes in adsorbed mass. If

the change in dissipation is large, modeling becomes more complex, requiring the Voigt model of viscoelasticity in fluids [19, 20]. Adsorbed mass of WLBU2, CysWLBU2, and WLBU2Cys prior to LPS adsorption was ~300 ng/cm^2, ~425 ng/cm^2, and 400 ng/cm^2, respectively, calculated by the Sauerbrey equation [14]. Figure C.2 shows that adsorption to a peptide coated surface is similar for all WLBU2 variants and is greater than adsorption of LPS to a bare gold surface. The enhanced adsorption of LPS vesicles at the peptide-coated surface is likely caused primarily by electrostatic interaction between the negatively charge LPS vesicle with WLBU2, which carries an out of balance charge of +13 at physiologic pH. WLBU2 with a cysteine added to either the amine- (CysWLBU2) or carboxy-terminated (WLBU2Cys) end is expected to adsorb "end-on" to the gold surface mediated by the high-avidity gold-thiol association. Chemical bonding energies can vary greatly, with hydrophobic association at ~0.8 kcal/mol [21], common hydrogen bonds ranging from 2 to 7 kcal/mol [22, 23], C-C bonds at 83 kcal/mol [24], and gold-thiol bonds at 45 kcal/mol [25, 26]. As thiol-gold interactions approximate covalent attachment (45 v 83 kcal/mol, compared to 7 for H-bonding), it is expected that WLBU2 associated in this manner will not be replaced by LPS. On the other hand, WLBU2 randomly associated to a surface may be removable. As seen in the QCM-D data (Figure C.2), adsorption of LPS to each of the three WLBU2-variant coated surfaces is similar. LPS association to end-on oriented WLBU2 molecules, presenting either the amine or carboxy end, behaves substantially the same as to randomly adsorbed WLBU2, suggesting that LPS association to each of these layers is likely electrostatic, and not indicative of higher order interaction. Since the orientation of WLBU2 does not seem to change the adsorption of LPS, and modifying peptides at the N-terminus is more

straightforward than the C-terminus, only the CysWLBU2 variant was used for further experimentation.

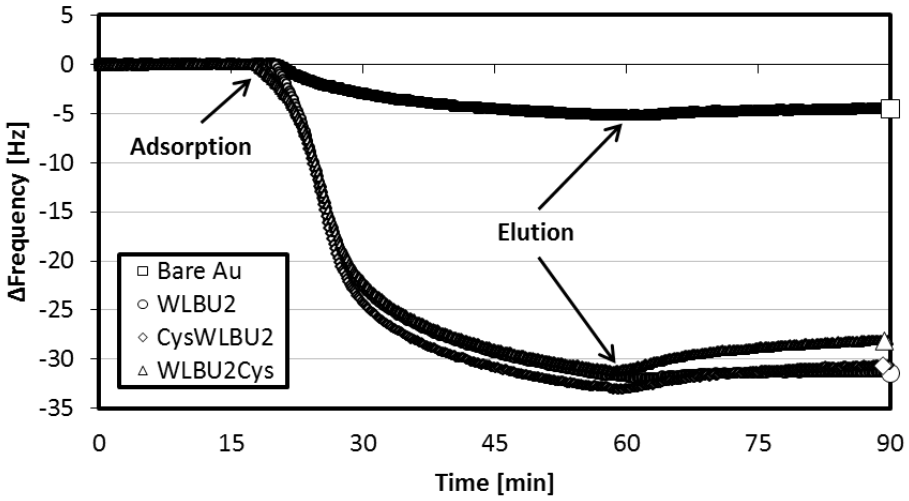

Figure C.2: ΔFrequency for LPS on a bare Au surface (□), on a Au surface coated with WLBU2 (○), CysWLBU2 (◇), and WLBU2Cys (△).

Figure C.3 shows dissipation vs frequency curves for each experiment. Data in this format allows visual inspection of the quality of the adsorbed layer. In particular, if the data shows hysteresis effects, adsorption is likely changing the structure of the adlayer. More generally, data displayed in this manner describes the comparable rigidity of a layer changing with adsorption and elution; as the slope decreases, the rigidity increases. The data shown in Figure C.3 nearly overlap for each of the LPS on peptide experiments, with hysteresis ranging from 0.4 – 1.9%. This strongly suggests the structure of LPS does not change upon adsorption to a WLBU2 coated surface, whether adsorbed randomly or end on. For LPS adsorbed to Au, the slope of the dissipation versus frequency is greater than any of the LPS on peptide experiments, suggesting a much more rigid layer, and this

curve shows hysteresis upon elution, with a change of nearly 18%. Taken together, this strongly suggests that LPS vesicles unfold at a gold surface, but remain largely intact and electrostatically adsorbed to a peptide coated surface.

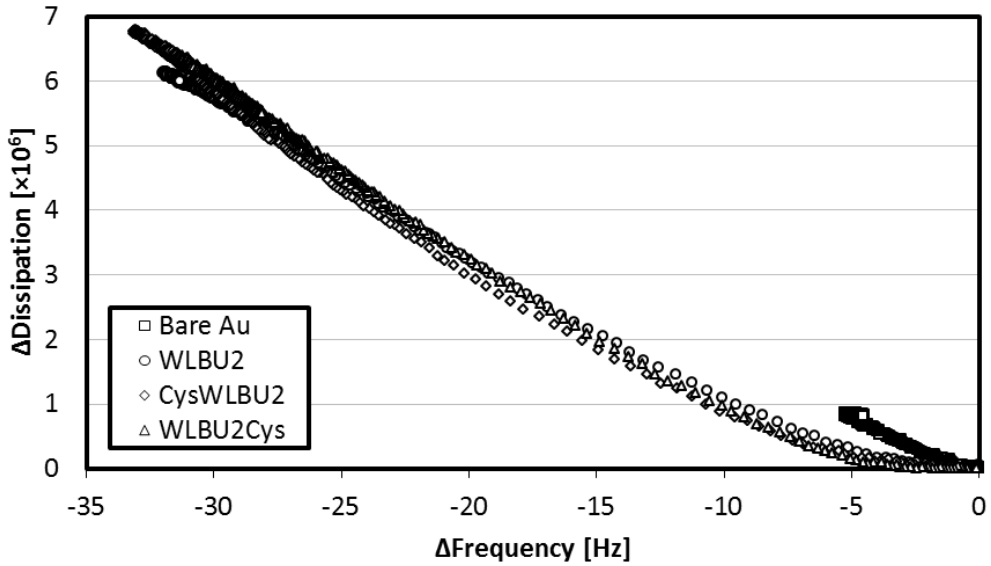

Figure C.3: ΔDissipation vs ΔFrequency for LPS on a bare Au surface (□), on a WLBU2 coated Au surface (○), on a CysWLBU2 coated Au surface (◇), and on a WLBU2Cys coated Au surface (△).

Figure C.4 shows CD spectra for WLBU2 in suspension with hydrophobic nanoparticles with and without LPS. The α-helicity changes from 10% on the bare particle without LPS to 23% with LPS included. This data supports the hypothesis drawn from the QCM-D data that surface bound WLBU2 does not substantially interact with LPS in a meaningful way.

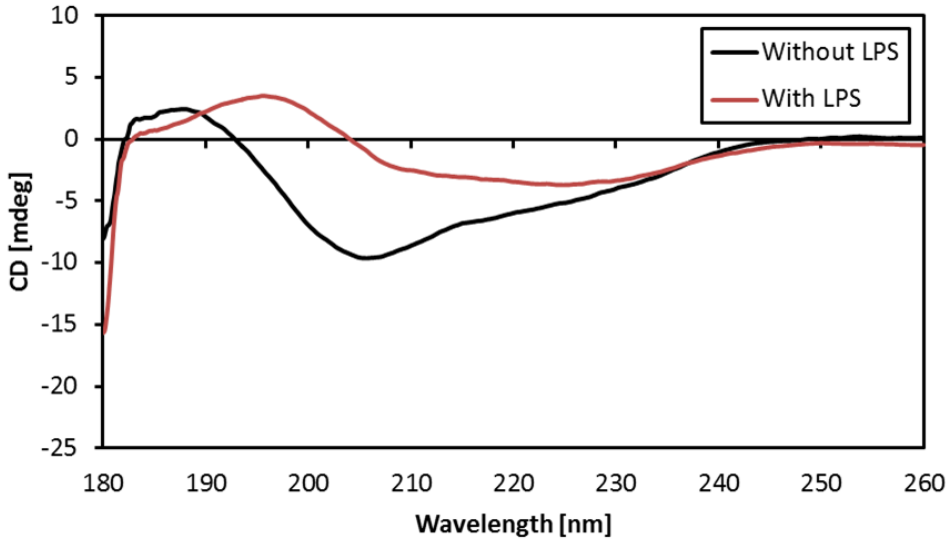

Figure C.4: CD spectra of WLBU2 non-specifically bound to a hydrophobic surface before and after LPS interaction.

Interaction between LPS and PEO layers. PEO layers are commonly considered to be nonfouling. As such, we expect no irreversible location of LPS at pendent PEO layers. Figure C.5 shows that this is indeed the case as change in both the frequency and dissipation returns to the original baseline upon elution.

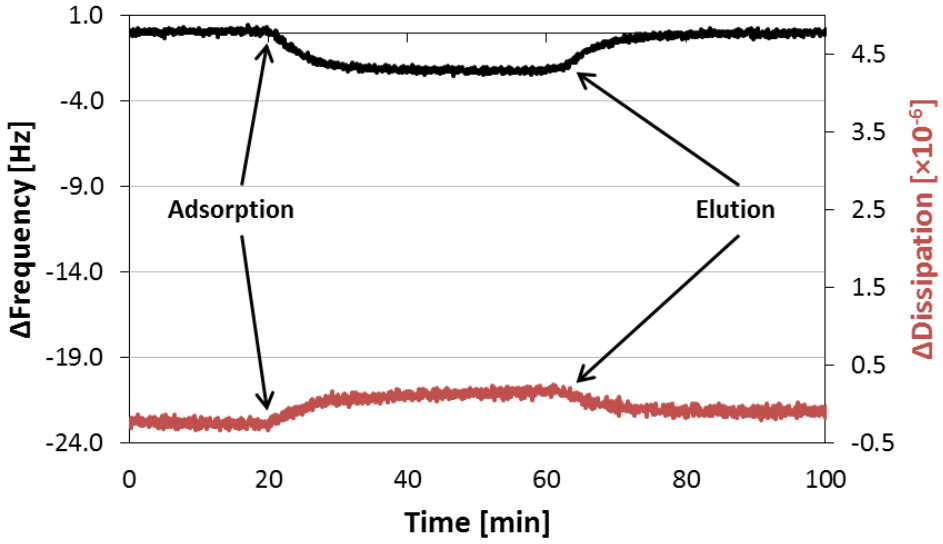

Figure C.5: ΔFrequency (black line, primary y-axis) and ΔDissipation (red line, secondary y-axis) for LPS on a surface containing covalently attached F127 only.

Interaction between LPS and peptide at PEO layers

LPS at peptide entrapped layers. In previous work, we have demonstrated that WLBU2, among other peptides, is able to penetrate PEO brush layers. This tendency toward small peptide entrapment requires that, for the purposes of peptide tethering, EGAP-WLBU2 constructs must be prepared in advance of adsorption to a surface. If attachment were to be conducted *in situ*, location of WLBU2, either entrapped or tethered would not be discernable. Figure C.6 shows QCM-D data for LPS association at peptide entrapped PEO layers. For the concentration used, we expect a maximum loading of WLBU2 to be around 0.2 molecules/nm^2 (~120 ng/cm^2) for entrapped peptide in membrane mimetic solvents, which would encourage α-helicity. Because the manner in which WLBU2 entrapment was conducted, i.e. in PBS rather than perchloric acid, it is expected that the actual amount of WLBU2 will be substantially less than that seen in Wu *et al*. In fact,

when calculating the concentration of WLBU2 in solution by UV/Vis spectroscopy for entrapped WLBU2 on nanoparticles for CD analysis (Figure C.10), the apparent concentration of WLBU2 was below the detectable limit. Figure C.7 shows that for entrapped peptide, there is very little initial peptide present, but upon introduction of LPS, the α-helicity increases from 3% to 8%.

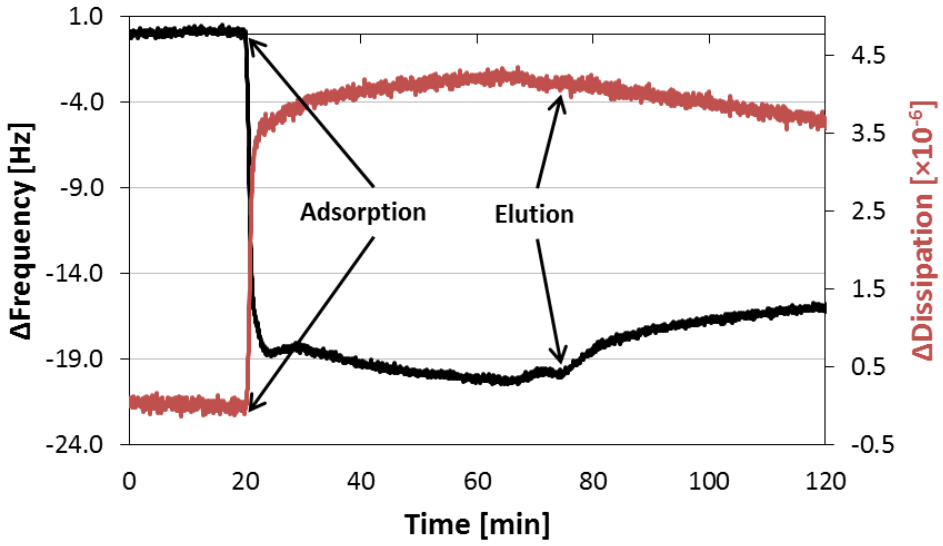

Figure C.6: ΔFrequency (black line, primary y-axis) and ΔDissipation (red line, secondary y-axis) for LPS on a surface containing covalently attached F127 and entrapped WLBU2 peptide.

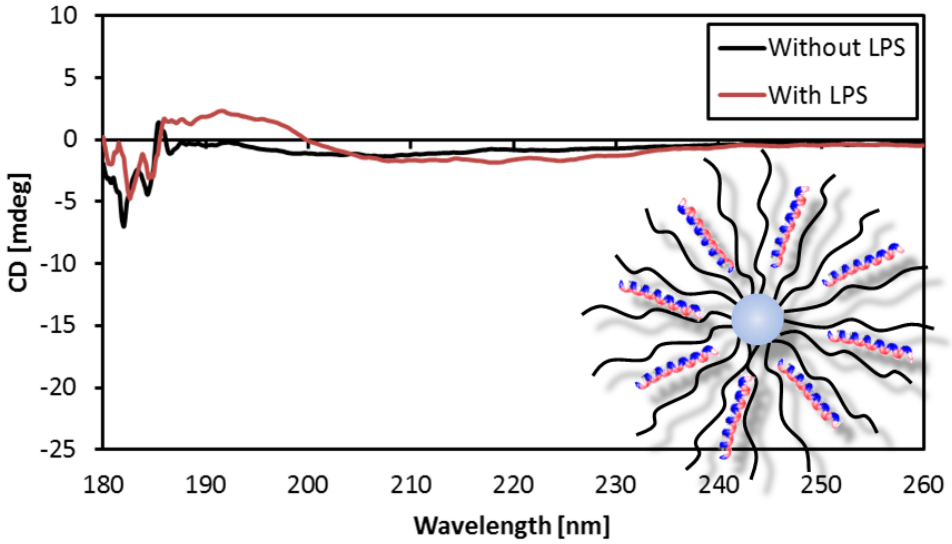

Figure C.7: Evaluation of entrapped WLBU2 on hydrophobic nanoparticles mixed with 0.1 mg/mL LPS. α-helicity increases from 3% to 8% after introduction of LPS. Note-graphic is representative only, and not to scale.

LPS at peptide tethered PEO layers. In the context of LPS capture in a hemoperfusion device, it is paramount to retain the mobility and solvent accessibility of the active capture agent, in this case WLBU2. Further, management of peptide density and distance from the primary interface requires more control than peptide entrapment allows. Thus, the peptide must be tethered to the surface, and to avoid convolution with potential entrapment of the peptide, it is important to build the tethered-WLBU2 construct prior to surface immobilization. In our work, we have commonly used γ-irradiation to covalently attach triblocks to our surfaces. It is therefore important to first investigate the effect of both a tether and γ-irradiation on the structure and function of WLBU2. Covalent attachment of WLBU2 with EGAP-PDS occurs spontaneously at room temperature according to the reaction scheme presented in Figure C.8. Constructs were prepared by mixing equimolar quantities of EGAP-PDS and CysWLBU2, average total conversion

was greater than 50% as evaluated by the evolution of pyridine-2-thione (P2T) absorption at 343 nm ($\varepsilon = 8080\ M^{-1}\ cm^{-1}$).

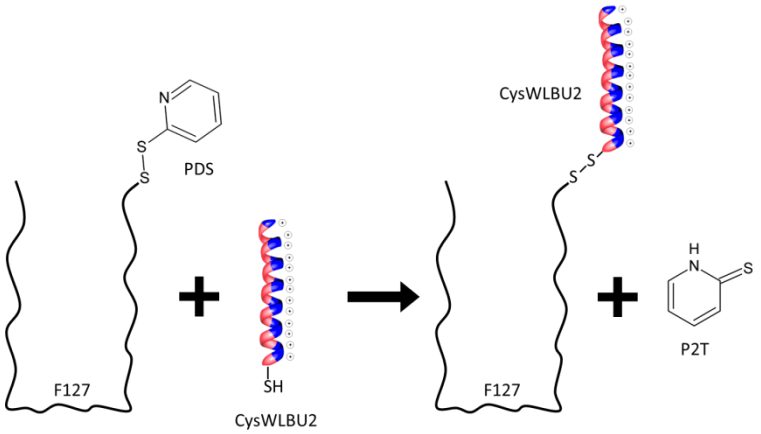

Figure C.8: Covalent association of CysWLBU2 with EGAP-PDS to create EGAP-WLBU2. Release of P2T allows the direct calculation of total amount of construct produced. Note- schematic is not to scale.

Unmodified WLBU2 shows a substantial increase in α-helicity upon exposure to LPS, increasing in helicity from ~0 to 78%, illustrated in Figure C.9.

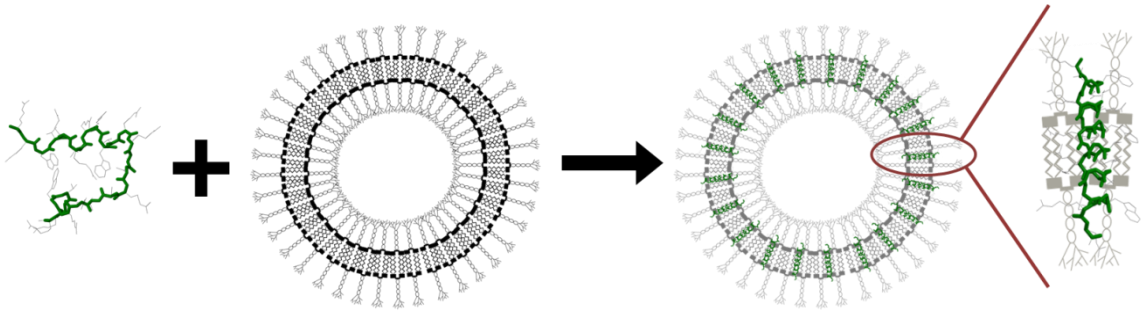

Figure C.9: Cartoon schematic of WLBU2 interaction with LPS vesicles. Disordered WLBU2 adopts an α-helical conformation by penetrating the LPS vesicle and integrating into the Lipid A region of LPS. Images are not to scale.

This is owing to the WLBU2 infiltrating the lipid A region of the LPS vesicle, a prerequisite for vesicle capture. EGAP-WLBU2 was evaluated in a similar manner;

results are shown in Figure C.10. The data show an increase in helicity from 2% in HPLC H_2O to 16% upon addition of LPS to 0.1 mg/mL.

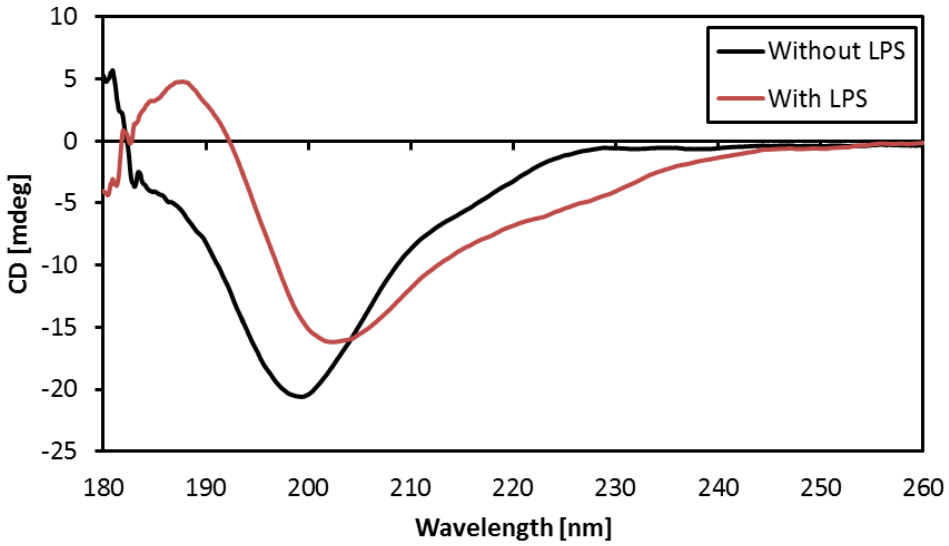

Figure C.10: CD spectra of EGAP-WLBU2 mixed with 0.1 mg/mL LPS. α-helicity increases from 2% to 16% after introduction of LPS.

Figure C.11 shows CD spectra of interaction of LPS with a tethered peptide associated with an interface. The data shows convincingly that WLBU2, when tethered to a surface retains its ability to adopt an α-helix upon introduction of LPS, changing from 2% helix without LPS to 17% including LPS.

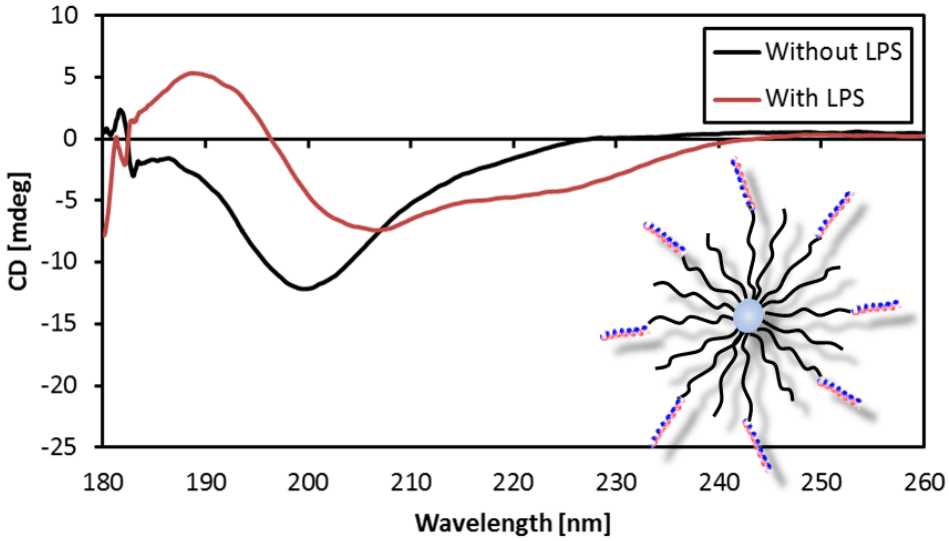

Figure C.11: Evaluation of EGAP-WLBU2 on hydrophobic nanoparticles mixed with 0.1 mg/mL LPS. α-helicity increases from 2% to 17% after introduction of LPS. Note-graphic is representative only, and not to scale.

These data clearly indicate that the inclusion of a covalent tether, on the order of 12.5 kDa, does not prevent WLBU2 from interacting with LPS in a manner keeping with that of unmodified WLBU2, and further suggests that WLBU2 covalently tethered to a surface will retain the ability to interact with LPS, and therefore capture vesicles from solution.

While the data shown in Figures Figure C.10 and Figure C.11 provide compelling evidence and support for the potential of tethered WLBU2 to capture LPS from solution, these systems had not been γ-irradiated. Figures Figure C.12 and Figure C.13 show the effects of comparable doses of γ-irradiation as used for covalent attachment of triblocks as evaluated by NMR (Figure C.12, ≈1000 μM WLBU2), and UV/Vis and CD (Figure C.13 ≈35 μM WLBU2).

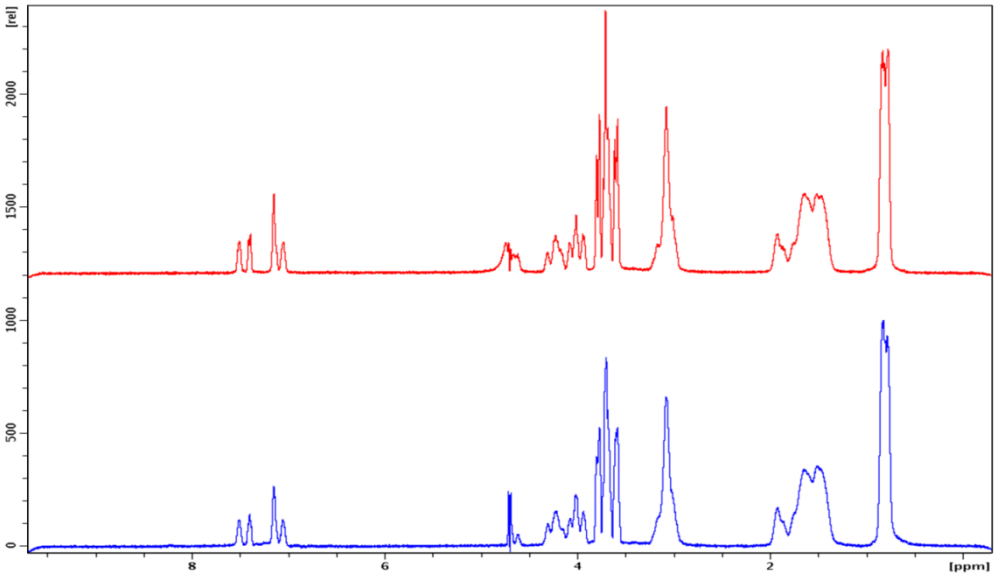

Figure C.12: NMR spectra of non-irradiated WLBU2 (red) and 0.3 Mrad γ-irradiated WLBU2. Data shown is at the same scale.

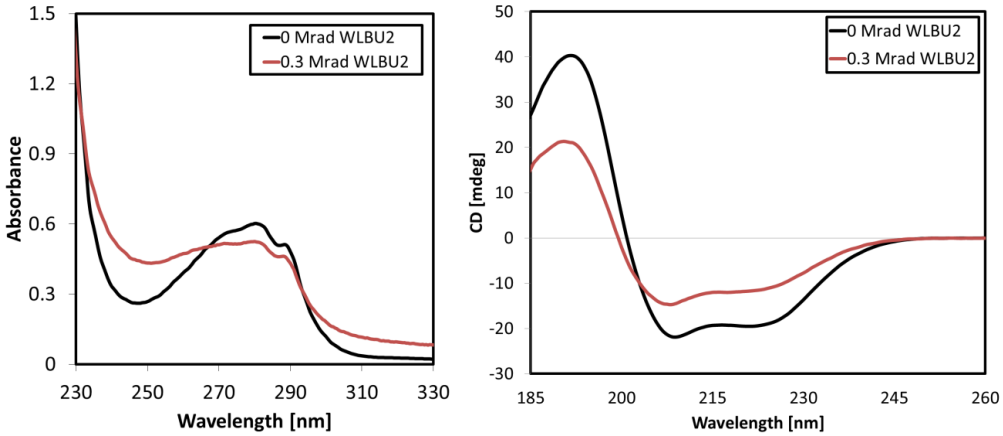

Figure C.13: UV/Vis (left) and CD spectra (right), of non-irradiated (black) and 0.3 Mrad γ-irradiated WLBU2. UV/Vis was done with peptide in PBS while CD was collected on WLBU2 in perchloric acid.

The NMR spectra shown in Figure C.12 show that the structure of WLBU2 remains intact upon irradiation, showing no significant difference in structure. Spectra recorded using UV/Vis spectroscopy (Figure C.13, left) shows more substantial change in the

characteristic curve, as the curve broadens, and its peak at 280 nm is reduced by 13%. Finally, in a helix inducing solvent (perchloric acid), WLBU2 is shown to decrease in α-helicity from 65% to 36% upon irradiation as indicated by the CD spectra shown in Figure C.13 (right).

With the effects of tethering and γ-irradiation understood, we can more appropriately evaluate the capture of LPS by tethered WLBU2 as witnessed in QCM-D and shown in Figure C.14. The QCM-D data presented shows clear evidence of LPS capture by tethered WLBU2 indicating that this system works.

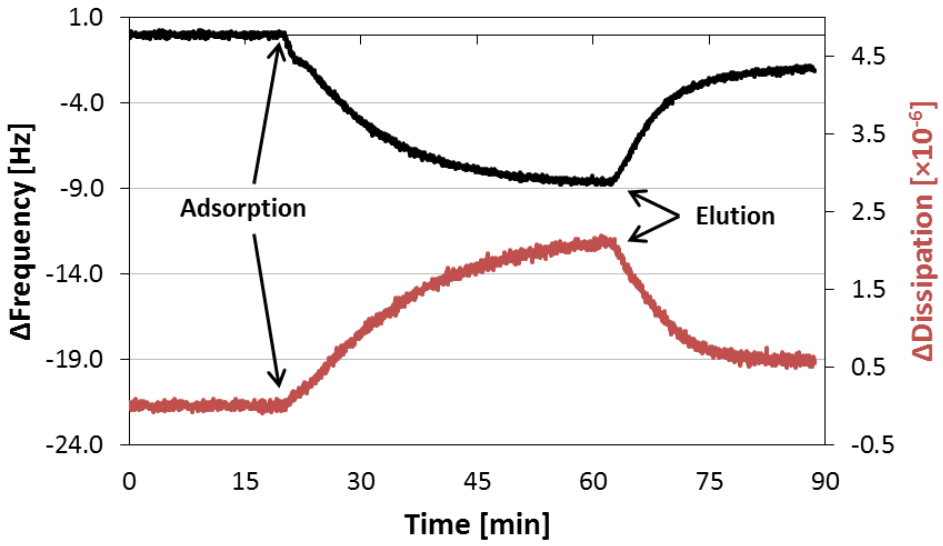

Figure C.14: ΔFrequency (black line, primary y-axis) and ΔDissipation (red line, secondary y-axis) for LPS on a surface containing covalently attached EGAP-WLBU2.

When comparing the capture of LPS between entrapped peptide PEO layers (Figure C.6) and tethered peptide PEO layers (Figure C.14), it seems that the entrapped peptide captures a greater amount of LPS than does the tethered peptide, as $\Delta F_{entrapped}/\Delta F_{tethered}$ = 2.3 at the end of the elution step, despite the lower surface concentration in the entrapped

case. This result, however, is consistent with the removal of WLBU2 from an entrapped motif and the creation of peptide bridges and LPS aggregation as shown in previous work. In this case, the resultant LPS-WLBU2 association may not indicate capture, but merely that the aggregates resist the flow parameters and do not leave the interface, illustrated in Figure C.15. This is further consistent with the very slow elution kinetics seen in Figure C.6 and the low elutability of only 24%. Because WLBU2 cannot participate in LPS bridging in the tethered motif, what remains at the surface upon elution (76% elutability) is likely due only to capture, and not convoluting complexes.

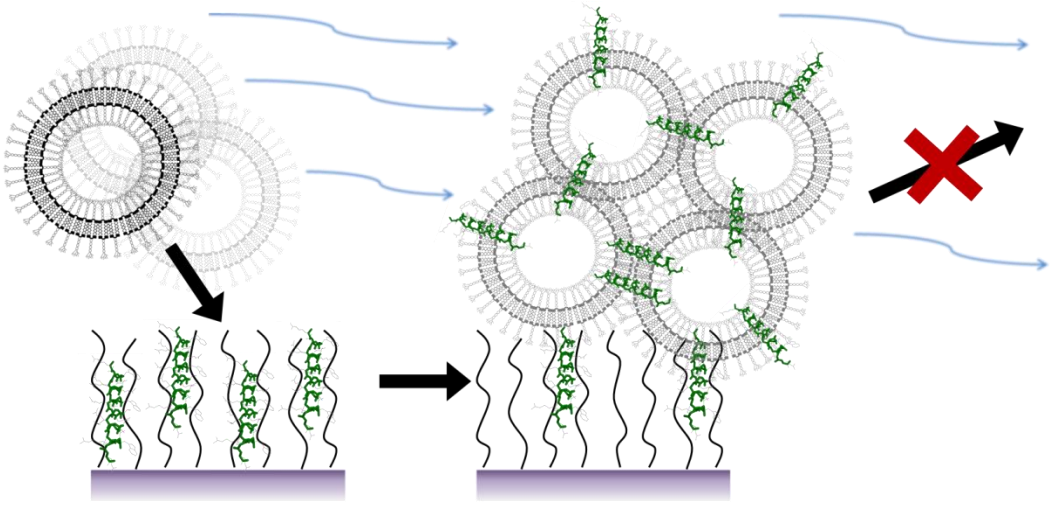

Figure C.15: Cartoon illustration of hypothesis for why entrapped WLBU2 is able to "capture" LPS. The LPS-WLBU2 association may not indicate capture, but merely that aggregates resist the flow (blue arrows, 50 µL/min) and do not leave the interface.

Effect of fibrinogen on LPS capture. A clinically relevant device must be able to capture LPS from whole blood in a hemoperfusive device. To that end, we must be able to demonstrate LPS capture from a complex milieu containing blood proteins. Figure C.16 shows QCM-D evidence that fibrinogen does not substantially adsorb or remain on a

surface containing only F127. Thus, any interaction described upon the inclusion of LPS and/or WLBU2 would suggest that location of fibrinogen is modulated by those excipients, and not by the PEO brush layer itself.

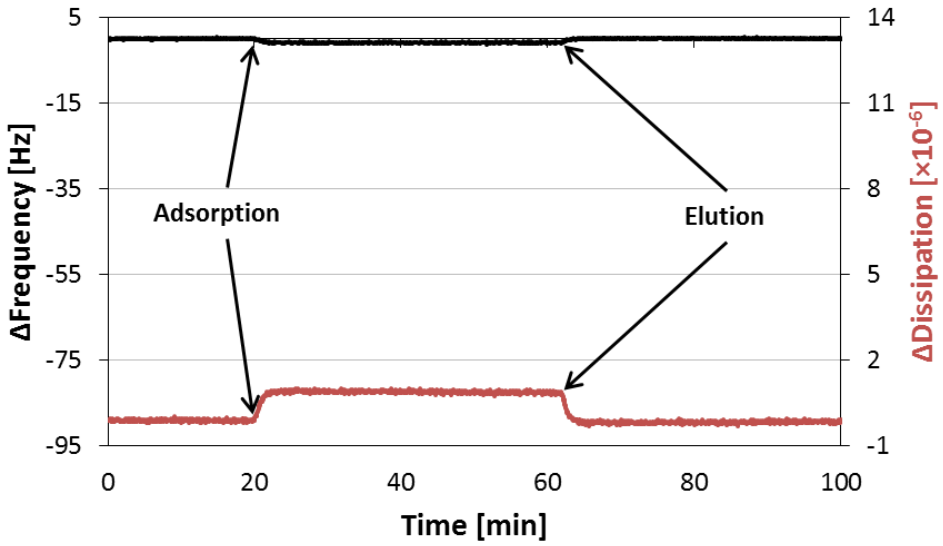

Figure C.16: ΔFrequency (black line, primary y-axis) and ΔDissipation (red line, secondary y-axis) for fibrinogen on a surface containing covalently F127 only.

Figures Figure C.17 and Figure C.18 show the adsorption and elution profiles, by Δ*f* and Δ*D*, of a mixture of fibrinogen and LPS on a surface containing entrapped WLBU2 (Figure C.17) and one with covalently attached EGAP-WLBU2 (Figure C.18). The concentration of fibrinogen is physiologically relevant, at 2 mg/mL, and LPS is at the same concentration for all other experiments, 0.1 mg/mL.

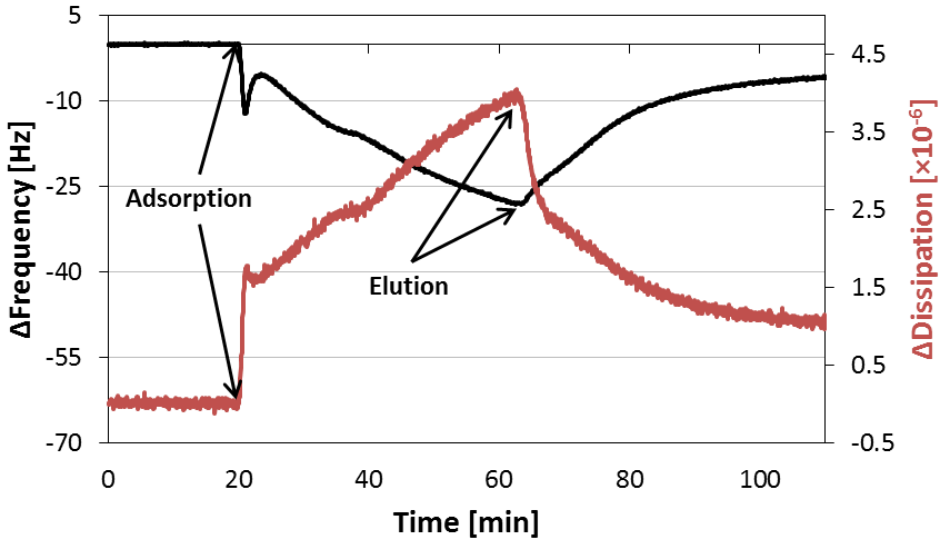

Figure C.17: ΔFrequency (black line, primary y-axis) and ΔDissipation (red line, secondary y-axis) for a mixture of fibrinogen and LPS on a surface containing entrapped WLBU2.

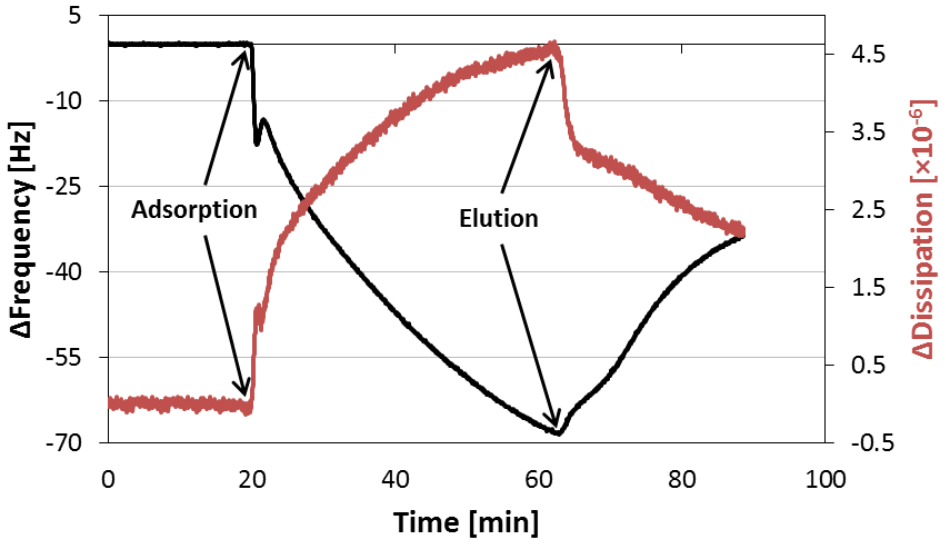

Figure C.18: ΔFrequency (black line, primary y-axis) and ΔDissipation (red line, secondary y-axis) for a mixture of fibrinogen and LPS on a surface containing covalently attached EGAP-WLBU2.

It is clear from the shape of these curves that the adsorption and elution of fibrinogen/LPS mixtures is complex. For both sets of data, the total adsorbed amount is higher ($-\Delta f \propto \Delta m$) at the end of both the adsorption and elution steps in the experiment than for LPS adsorption on respective surfaces alone. In the case of entrapped peptide contacted by the mixture (Figure C.17), 82% of the adsorbed mass is removed upon elution. For the EGAP-WLBU2 construct challenged by the mixture (Figure C.18), 51% of the mass is removed upon elution. Because the total adsorbed mass of both fibrinogen/LPS mixtures was greater than that for LPS alone, it is clear that fibrinogen itself interacts with WLBU2, interacts with LPS in a manner further encouraging location or capture at the interface, or some combination of the two.

Figure C.19 shows the comparison of Δf vs time for fibrinogen on an entrapped or tethered surface motif (Figure C.19, top), and the Δdissipation vs Δf for these same surfaces (Figure C.19, bottom).

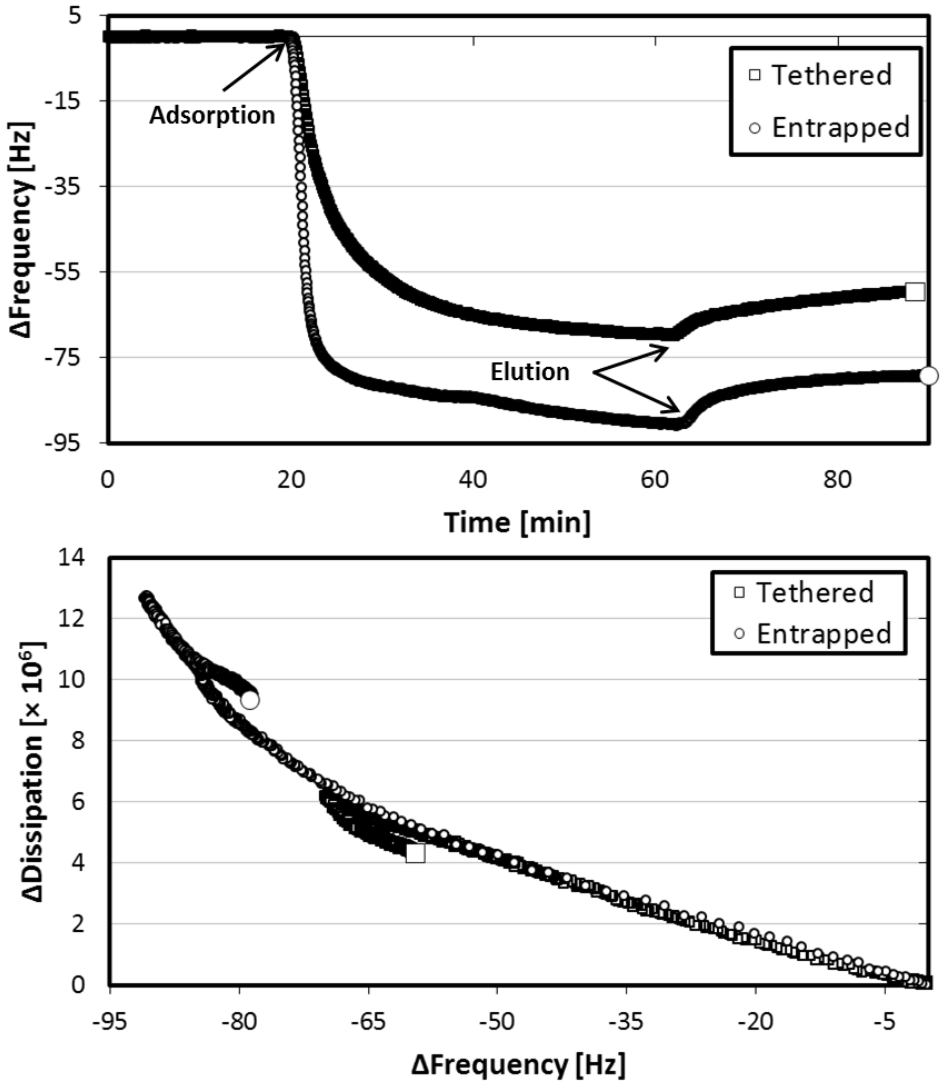

Figure C.19: ΔFrequency vs time (top) of fibrinogen challenge of entrapped WLBU2 (○) and tethered WLBU2 (□). The data shows similar curves, albeit different mass loadings in each case. The ΔDissipation vs ΔFrequency (bottom) is shown to largely overlap for each case.

It is clear from the data shown in Figure C.19 that fibrinogen does in fact interact with surfaces that contain WLBU2. The nature of this interaction appears not to depend on whether the surface contains entrapped or tethered WLBU2, as shown in Figure C.19 (bottom), despite overall mass loading being dissimilar (Figure C.19, top). Further

evidence of this is that the percent mass eluted is 14% and 15% for fibrinogen on the entrapped or tethered peptide, respectively. This interaction is directly related to the inclusion of WLBU2, as fibrinogen does not substantially adsorb or remain on a surface containing only F127, shown in Figure C.16.

The interaction between fibrinogen and WLBU2 associated surfaces is likely not due to a higher order interaction between the two proteins, but likely only suggestive of an electrostatic interaction between the two, as stated previously, WLBU2 contains an out of balance net positive charge of 13, while the outer regions of fibrinogen carry a net negative charge [27]. Interestingly, the adsorption and elution profile of fibrinogen as compared to fibrinogen/LPS mixtures adsorbs and retains more mass for both entrapped and tethered peptide. This strongly suggests that Fibrinogen/LPS mixtures exist as more than a binary mixture of discrete molecules, but rather as a fibrinogen-LPS complex. Further, although the experiments include a physiologically relevant concentration of fibrinogen, the concentration of LPS is well beyond what may be expected in a clinical setting; the 0.1 mg/mL used in this work corresponds to 500 g of LPS circulating in the human body. For this experimentation, using smaller concentrations of LPS may not be efficacious because the capture seen already by this non-optimized device analogue is rather low (Figure C.14). More direct investigation of the interactions of fibrinogen and LPS may be required to elucidate nuances shown in the data presented in this work, but for the purposes of a clinical device, it may be more worthwhile to continue investigations in other avenues.

Despite clear evidence that fibrinogen interacts with surfaces containing WLBU2, and that LPS and fibrinogen may create a complex structure, figures Figure C.20 and Figure C.21 suggest that WLBU2, whether entrapped or tethered may in fact preferentially capture LPS over fibrinogen. The data shown is of the ratio of Δf to ΔD vs time. Data shown in this manner allows for more direct comparison of surface characteristics with respect to adsorption and elution of various species, and time. Further, viewing the data in this manner reveals intricacies not captured by other graphical methods. For instance, as the ratio $-\Delta f/\Delta D$ increases, the adsorbed mass is changing more rapidly than is the dissipation, suggestive of increasing rigidity. Conversely, as this ratio decreases, the dissipation is increasing more rapidly than the frequency (or is decreasing less rapidly), indicating the overlayer becomes less rigid.

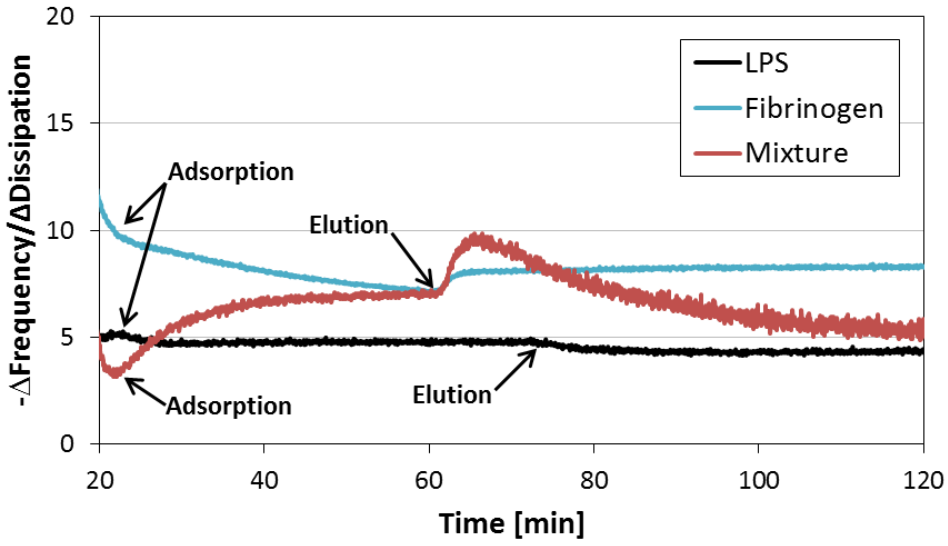

Figure C.20: -ΔFrequency/ΔDissipation of LPS (black), Fibrinogen (blue), and a Fibrinogen/LPS mixture (red) on surfaces with entrapped WLBU2. Data shown contains only adsorption and elution ratios. Mass loading was seen to decrease upon elution in all cases.

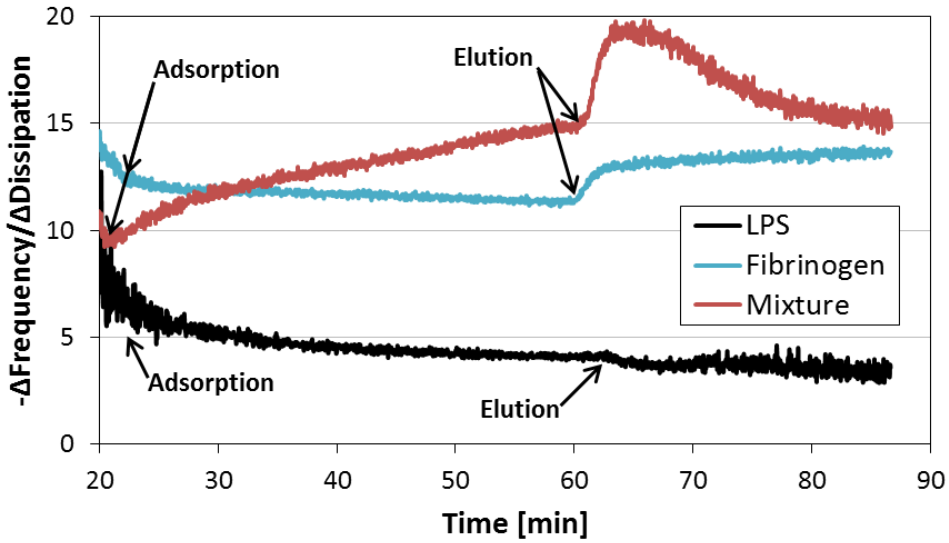

Figure C.21: -ΔFrequency/ΔDissipation of LPS (black), Fibrinogen (blue), and a Fibrinogen/LPS mixture (red) on surfaces with tethered WLBU2. Data shown contains only adsorption and elution ratios. Mass loading was seen to decrease upon elution in all cases.

In both Figure C.20 and Figure C.21, the overall shape of the curves is similar for each surface. For the surfaces challenged with LPS, the ratio, $-\Delta f/\Delta D$, does not appear to change much upon elution. This suggests that the overall structure of the LPS does not change upon elution, or more specifically, that there is unlikely to be an under layer of spread LPS. The slight decrease, in fact, indicates that the layer becomes less rigid, as mass was seen to decrease (frequency increases) upon elution in all figures showing ΔF vs time. For fibrinogen, the situation is quite the opposite, because the ratio of -ΔFrequency/ΔDissipation increases upon elution, and the mass decreased, the layer must (i) become rigid upon elution, or (ii) loosely bound fibrinogen is removed, revealing a rigid underlayer of associated protein. Finally, for the fibrinogen/LPS mixture on the entrapped WLBU2 surface, ratio of frequency to dissipation is nearly identical to that for

fibrinogen at the end of the adsorption cycle, but upon elution comes almost to the same point as that for LPS. This pattern is consistent with a system wherein a smaller molecule with slight affinity for the presented surface approaches that surface more quickly than its larger counterpart that has a higher affinity. Over time the larger, higher affinity molecule would replace the smaller one, resulting in a surface that initially behaves like one containing only the smaller molecule, but ends similarly to a system containing only the larger. As this pattern is seen in Figure C.20 and the pattern is similar, albeit not to the same extent in Figure C.21 it may be hypothesized that even in a complex milieu containing physiological quantities of fibrinogen, LPS capture is possible with both entrapped and tethered WLBU2.

Conclusions

Analysis of the interaction between surface immobilized, PEG chain entrapped, and PEG chain tethered WLBU2 with LPS using QCM-D, and CD, as well as the effects of γ-irradiation on PEGylated WLBU2 using UV/Vis spectroscopy and NMR, all reveal that WLBU2 can interact with LPS in a manner keeping with its purpose whether irradiated, PEGylated, or tethered. In this way, we have shown that WLBU2 holds promise for use in a hemoperfusive device for the capture of sepsis causing LPS. QCM-D data suggest that LPS capture by tethered WLBU2 likely retains its overall structure, meaning the LPS membranes do not rupture, which would pass LPS fragments back into the body after treatment. Introduction of a more complex milieu, i.e. fibrinogen and fibrinogen/LPS

mixtures, reveals that fibrinogen interacts with WLBU2, very likely by electrostatic association as WLBU2 carries a net positive charge, while fibrinogen carries a net negative charge. Furthermore, QCM-D reveals a possible complex between fibrinogen and LPS, rendering this system of less interest when considering the potential capture of LPS from whole blood. We are currently evaluating more relevant concentrations of LPS from solutions containing blood plasma, while also working toward an optimized surface concentration of presented WLBU2. Results from that work will contribute to the subject of a future report.

Acknowledgments

The authors thank Dr. Kerry McPhail for the use of her CD instrument. The authors also thank Greg McKelvey, Dan Cheung, and Miranda Raper for their contributions to this work by data collection in NMR, effects of γ-irradiation, and CD respectively, as well as Jennifer Neff and Allvivo Vascular Inc. for providing EGAP-PDS. This work was supported in part by the National Institute of Biomedical Imaging and Bioengineering (NIBIB, grant no. R01EB011567). The content is solely the responsibility of the authors and does not necessarily represent the official views of NIBIB or the National Institutes of Health.

References

[1] D.C. Angus, R.S. Wax, Epidemiology of sepsis: An update. Critical Care Medicine 2001;29(7):S109-S116.

[2] J. Cohen, The immunopathogenesis of sepsis. Nature 2002;420(6917):885-891.

[3] K. Wood, D. Angus, Pharmacoeconomic Implications of New Therapies in Sepsis. Pharmacoeconomics 2004;22(14):895-906.

[4] N. Matsuno, T. Ikeda, K. Ikeda, K. Hama, H. Iwamoto, M. Uchiyama, K. Kozaki, Y. Narumi, K. Kikuchi, H. Degawaand, Changes of Cytokines in Direct Endotoxin Adsorption Treatment on Postoperative Multiple Organ Failure. Therapeutic Apheresis 2001;5(1):36-39.

[5] F.B. Anspach, Endotoxin removal by affinity sorbents. Journal of Biochemical and Biophysical Methods 2001;49(1–3):665-681.

[6] K. Buttenschoen, P. Radermacher, H. Bracht, Endotoxin elimination in sepsis: physiology and therapeutic application. Langenbeck's Archives of Surgery 2010;395(6):597-605.

[7] B. Davies, J. Cohen, Endotoxin removal devices for the treatment of sepsis and septic shock. The Lancet Infectious Diseases 2011;11(1):65-71.

[8] H. Shoji, Extracorporeal endotoxin removal for the treatment of sepsis: endotoxin adsorption cartridge (Toraymyxin). Therapeutic Apheresis and Dialysis 2003;7(1):108-114.

[9] M. Bohner, T. Ring, N. Rapoport, K. Caldwell, Fibrinogen adsorption by PS latex particles coated with various amounts of a PEO/PPO/PEO triblock copolymer. Journal of Biomaterials Science, Polymer Edition 2002;13(6):732-745.

[10] K.C. Popat, R.W. Johnson, T.A. Desai, Characterization of vapor deposited thin silane films on silicon substrates for biomedical microdevices. Surface and Coatings Technology 2002;154(2-3):253-261.

[11] J.K. Dill, J.A. Auxier, K.F. Schilke, J. McGuire, Quantifying nisin adsorption behavior at pendant PEO layers. Journal of Colloid and Interface Science 2013;395(0):300-305.

[12] M.C. Lampi, X. Wu, K.F. Schilke, J. McGuire, Structural attributes affecting peptide entrapment in PEO brush layers. Colloids and Surfaces B: Biointerfaces 2013;106(0):79-85.

[13] T.B. McPherson, H.S. Shim, K. Park, Grafting of PEO to glass, nitinol, and pyrolytic carbon surfaces by γ irradiation. Journal of biomedical materials research 1997;38(4):289-302.

[14] G. Sauerbrey, Use of quartz vibration for weighing thin films on a microbalance. J. Physik 1959;155:206-212.

[15] L. Whitmore, B.A. Wallace, DICHROWEB, an online server for protein secondary structure analyses from circular dichroism spectroscopic data. Nucleic Acids Research 2004;32(suppl 2):W668-W673.

[16] L. Whitmore, B.A. Wallace, Protein secondary structure analyses from circular dichroism spectroscopy: Methods and reference databases. Biopolymers 2008;89(5):392-400.

[17] C.N. Pace, F. Vajdos, L. Fee, Grimsley G, Gray T. How to measure and predict the molar absorption coefficient of a protein. Protein Science 1995;4(11):2411-2423.

[18] G. Hermanson, Bioconjugate techniques 2nd ed. Academic Press; 2008.

[19] J.D. Ferry, Viscoelastic properties of polymers. Wiley New York; 1980.

[20] W. Philippoff, Relaxations in polymer solutions, liquids and gels. Physical acoustics: principles and methods 1965;2(part B):1-90.

[21] C. Pace, Evaluating contribution of hydrogen bonding and hydrophobic bonding to protein folding. Methods in enzymology 1995;259:538-554.

[22] J. Emsley, Very strong hydrogen bonding. Chemical Society Reviews 1980;9(1):91-124.

[23] J. Larson, T. McMahon, Gas-phase bihalide and pseudobihalide ions. An ion cyclotron resonance determination of hydrogen bond energies in XHY-species (X, Y= F, Cl, Br, CN). Inorganic Chemistry 1984;23(14):2029-2033.

[24] R. Sanderson, Chemical Bonds and Bonds Energy. Access Online via Elsevier; 1976.

[25] H. Grönbeck, A. Curioni, W. Andreoni, Thiols and disulfides on the Au (111) surface: The headgroup-gold interaction. Journal of the American Chemical Society 2000;122(16):3839-3842.

[26] R.G. Nuzzo, B.R. Zegarski, L.H. Dubois, Fundamental studies of the chemisorption of organosulfur compounds on gold (111). Implications for molecular self-assembly on gold surfaces. Journal of the American Chemical Society 1987;109(3):733-740.

[27] P. Bernabeu, A. Caprani, Influence of surface charge on adsorption of fibrinogen and/or albumin on a rotating disc electrode of platinum and carbon. Biomaterials 1990;11(4):258-264.